ERDC/CERL CR-06-2

US Army Corps of Engineers®
Engineer Research and Development Center

Fort Ord Groundwater Remediation Studies, 2002 – 2005

A. Russell Flegal, Patrick Mantey, Curt Oldenburg, and Paul Daley

August 2006

Construction Engineering Research Laboratory

ERDC/CERL CR-06-2
August 2006

Fort Ord Groundwater Remediation Studies, 2002–2005

A. Russell Flegal

Department of Environmental Toxicology, University of California
1156 High Street
Santa Cruz, CA 95064

Patrick Mantey

Department of Computer Engineering, University of California
1156 High Street
Santa Cruz, CA 95064

Curt Oldenburg

Earth Sciences Division, Lawrence Berkeley National Laboratory
1 Cyclotron Road
Berkeley, CA 94720

Paul Daley

Environmental Restoration Division, Lawrence Livermore National Laboratory
7000 East Avenue
Livermore, CA 94550

Final report

Prepared for U.S. Army Corps of Engineers

Under Work Unit

Monitored by Construction Engineering Research Laboratory
U.S. Army Engineer Research and Development Center
2902 Newmark Drive, Champaign, Illinois 61820

Abstract: This report presents the results of collaborative studies of groundwater contamination, remediation, and monitoring at the former Fort Ord Army Base in northern Monterey County, California. These complementary, integrated studies were conducted at the site by principal investigators from three different institutions: the Lawrence Livermore National Laboratory; Environmental Restoration Division, Physical and Biological Sciences Division at the University of California – Santa Cruz; and Earth Sciences Division, Lawrence Berkeley National Laboratory.

These collaborative studies resulted in assessments of groundwater flow monitoring technologies; analyses of aquifer response, groundwater flow, and plume evolution; simulation of in-situ permeable flow sensors for measuring groundwater velocity; and remote sampling and analyses of inorganic contaminants in the groundwater.

The first three assessments addressed concerns with organic contaminants previously detected at the site, while the fourth was designed to determine the applicability of the remote sampling system developed to monitor organic contaminants to the monitoring of inorganic contaminants that had also been detected at elevated levels in the general study area. Four separate reports were developed from this project and the results are combined in this integrated summary report.

Contents

Figures and Tables

Figures

Tables

Preface

This study was conducted by the University of California, Santa Cruz, in conjunction with their subcontractor-partners, Lawrence Livermore National Laboratory and Lawrence Berkeley National Laboratory, for the U.S. Army Engineer Research and Development Center – Construction Engineering Research Laboratory (ERDC/CERL) under Cooperative Agreement DACA42-02-2-0056. Funding was provided as part of an FY02 Congressional Appropriation to the Army for "Fort Ord Cleanup" under Program Element 643779, Environmental Quality Technology Demonstration/Validation. The proponent for this work was the Office of the Assistant Secretary of the Army for Installations and Environment (ASA (I&E)).

The research was supervised by the Materials and Structures Branch (CF-M) of the Facilities Division (CF), Construction Engineering Research Laboratory, U.S. Army Engineer Research and Development Center (ERDC-CERL) in Champaign, IL; and by the Environmental Engineering Branch (EP-E) of the Environmental Processes and Engineering Division (EP), Environmental Laboratory (ERDC-EL), in Vicksburg, MS. Richard Lampo (ERDC-CERL) was the primary Grant Officer's Technical Representative (GOTR) and Dr. Steven Larson (ERDC-EL) was the alternate GOTR.

At the time of publication Martin J. Savoie was Chief, CEERD-CF-M, and L. Michael Golish was Chief, CEERD-CF. The Acting Deputy Director of ERDC-CERL was Dr. Kumar Topudurti, and the Director was Dr. Ilker Adiguzel.

The Commander and Executive Director of ERDC was COL Richard B. Jenkins and the Director was Dr. James R. Houston.

Unit Conversion Factors

Multiply	By	To Obtain
degrees Fahrenheit	(F-32)/1.8	degrees Celsius
feet	0.3048	meters
gallons (U.S. liquid)	3.785412 E-03	cubic meters
inches	0.0254	meters
yards	0.9144	meters

1 Introduction

Overview

This report presents the results of collaborative studies of groundwater contamination, remediation, and monitoring at the former Fort Ord Army Base, located on Monterey Bay in northern Monterey County, California (Figure 1). These complementary, integrated studies were conducted at the Operable Unit 1 (OU 1) site by four principal investigators: Paul Daley, Russell Flegal, Patrick Mantey, and Curt Oldenburg, from three different institutions, the Lawrence Livermore National Laboratory; Environmental Restoration Division, Physical and Biological Sciences Division at the University of California - Santa Cruz; and Earth Sciences Division, Lawrence Berkeley National Laboratory.

These collaborative studies resulted in assessments of:

1. Groundwater flow monitoring technologies;
2. analyses of aquifer response, groundwater flow, and plume evolution;
3. simulation of in-situ permeable flow sensors for measuring groundwater velocity; and
4. remote sampling and analyses of inorganic contaminants in the groundwater.

The first three assessments addressed concerns with organic contaminants (e.g., trichloroethylene or TCE) previously detected at the site, while the fourth was designed to determine the applicability of the remote sampling system developed to monitor organic contaminants (e.g., TCE) to the monitoring of inorganic contaminants (e.g., chromium) that have also been detected at elevated levels in the general study area. Four separate reports were developed from this project (Daley et al. 2005; Johnson et al. 2005; Jordan et al. 2005; Su et al. 2005), and the results are combined in this integrated summary report.

Site Description

The study site, Operable Unit 1 (OU 1), is part of the former Fort Ord Army Base, located on Monterey Bay in northern Monterey County, California (Figure 1). It has been the site of ongoing studies by two of the investiga-

tors (Daley and Oldenburg), and has been extensively described in a previous report (Oldenburg et al. 2002). Consequently, the following description is abbreviated.

The OU 1 site is situated close to the Pacific coast in a sand dune area consisting of low hills and closed bowls vegetated by scrub oaks and coastal chapparal species. The unconsolidated dune sands extend from the surface to a depth of 90–130 ft (27–40 m); stabilization of the dunes with vegetation is thought to be relatively recent. The dune sands are bounded below by interbedded layers of clays and sands of varying thickness. The first water-bearing zone is the unconfined A-aquifer, which lies above the Fort Ord-Salinas Valley Aquitard (FO-SVA). The aquitard separates the A-aquifer consisting of dune sand from deeper, confined aquifers, the shallowest of which is called the 180-foot aquifer. The water table depth of the A-aquifer ranges from approximately 70 to 100 ft (21 to 30 m) below ground surface (bgs).

Figure 1. Location of the former Fort Ord, site of Operable Unit 1 (OU 1).

Problem statement

The former Fritzsche Army Airfield is located in the northernmost portion of the former Fort Ord Army Base. The airport fire department trained at a Fire Drill Area (FDA) adjacent to the airport. Fuels and solvents were placed in the burn pit and combusted for firefighter training from 1962 to 1985. Subsequently, soil and groundwater contamination was discovered in the A-aquifer, consisting of petroleum hydrocarbons, trichloroethylene (TCE), methylethylketone (MEK), 1,1,1-trichloroethane (1,1,1-TCA), cis-1,2-dichloroethylene (c-1,2-DCE), and minor amounts of related materials.

In the late 1980's, the area contaminated by these compounds was designated as Fort Ord's Operable Unit 1 (OU 1), and near-surface contaminated soil was excavated. Deeper contaminated soils in the FDA were bioremediated. Soil sampling confirmed that the surface soil cleanup was successful, and a groundwater extraction and treatment system was installed to capture and treat the residual contaminated groundwater. This system significantly reduced all of the contaminant concentrations. By the early 1990's, contaminants other than TCE were generally below the Maximum Contaminant Levels (MCLs) set by the U.S. Environmental Protection Agency (EPA) for drinking water. TCE, however, is still present at levels in the low tens of parts per billion, and is the target of continued remediation. Data obtained from drilling to the northwest of the original plume now indicate the TCE groundwater plume is 3000 ft (900 m) long, or approximately four times the originally characterized length.

In addition, public health concerns about chromium contamination in Monterey County aquifers were raised in 2001, when relatively high levels were detected in adjacent Santa Cruz County (Gonzalez et al. 2005). There, concentrations in the Aromas Red Sands aquifer were found to range from 2 to 40 μg/L, approaching the California MCL for chromium in drinking water (50 μg/L), as well as the MCL set by the U.S. EPA (100 μg/L). This public health concern was extended to Monterey County after it was determined that the elevated levels of chromium were due to naturally high levels in sediments within the aquifer, rather than industrial contamination (the Aromas Red Sands aquifer runs between the two counties).

Therefore, OU 1 was the focus of two concerns. The first, based on extensive measurements over the two preceding decades (Oldenburg et al. 2002), was that the contaminant TCE plume at the site was spreading and potentially contaminating the underlying aquifer which is used as a water

supply. The second was that the aquifer might also be contaminated with chromium, based in part on an anomalously high value (> 10 μg/L) previously measured at OU 1 in 1992.

In addition to these environmental and public health concerns, the site was considered an ideal location for research to investigate innovative methodologies to address groundwater contamination that might be applicable to other contaminated sites. On-site automatic sampling and analytical instrumentation had previously been installed at OU 1 to study movement of the TCE plume, and that instrumentation was available for upgrades and comparisons of different groundwater flow monitoring technologies. Complementary studies had provided a characterization of the TCE-contaminated aquifer, facilitating new analyses of aquifer response, groundwater flow, and plume evolution. That characterization also established the basis for simulation of in-situ permeable flow sensors for measuring groundwater velocity. Finally, the successful instrumentation and characterization of the movement of organics (i.e., TCE) in the aquifer provided the framework for testing the possibility of adapting that instrumentation to concurrently sample and trace the movement of inorganic contaminants (e.g., Cr) within the aquifer.

Objectives

Four main objectives were included in the proposal, which was written as a five-year program, but was only funded for year one. These were:

1. Develop real-time sampling, analysis, and data transmission for subsurface contaminants;
2. integrate real-time plume characterization into useful visualization tools for process engineering decision making;
3. explore the identification of source zone locations by using the combination of real-time measurement with process control; and
4. explore the expansion of technologies and processes to address contaminants from munitions and explore applications of technologies and processes to homeland security needs for water systems.

These objectives were placed in a chronological sequence, which extended over five years. As stated in the proposal, the “goal of the proposers is to address objectives 1 and 2 in the first year and, if sufficient funding is available, to begin work on objective 3. Continued work on 1, 2 and 3 and expansion to objective 4 is planned for subsequent years (2-5).” Although

the proposal was then funded for only one year, more progress was made in meeting the objectives than had been anticipated, as described in the following sections.

Approach

This study involved four Principal Investigators from three different institutions. The intent was to bring their complementary expertise together in collaborative groundwater studies, using the existing sampling system at the former Fort Ord site. The success of those collaborations is evidenced by the co-authored reports of those investigators (Daley et. al. 2005; Johnson et al. 2005; Jordan et al. 2005; and Su et al. 2005), as well as by the new proposal of the four investigators to continue those studies.

Deliverables for the first period of funding (and extended by no cost time extensions) included an annual operating report on the first three objectives. These included a summary data analysis and activities accomplished; proposed activities for succeeding year; and recommendations for ongoing remediation efforts.

These results were detailed in four individual reports, as follows:

- *Intercomparison of Groundwater Flow Monitoring Technologies at Site OU 1, Former Fort Ord, Californi*a. Daley, P.F., J. Jantos, W.H. Pedler and W.A. Mandell. 2005. Lawrence Livermore National Laboratory (LLNL).
- *Analysis of Aquifer Response, Groundwater Flow, and Plume Evolution at Site OU 1, Former Fort Ord, California*. Jordan, P.D., C.M. Oldenburg and G.W. Su. 2005. Lawrence Berkeley National Laboratory (LBNL).
- *Simulation of In-Situ Permeable Flow Sensors for Measuring Groundwater Velocity at OU 1, Former Fort Ord*, California. Su, G.W., B.M. Freifeld, C.M. Oldenburg, P.D. Jordan and P.F. Daley. 2005. Lawrence Berkeley National Laboratory.
- *Automated Water Sampling for Trace Metals in Response to Ephemeral Events*. Johnson, B., K. Ndung'u, J. Rybczynski, P. Mantey, A. Gonzalez, G. Scelfo and A. Flegal. 2005. University of California, Santa Cruz.

These reports were the result of sequenced studies, beginning with restarting and upgrading the groundwater sampling system by Daley and his as-

sociates (Daley et al. 2005). Oldenburg and his associates studied long-term quarterly TCE and water table elevation data to understand the evolution of the TCE plume (Jordan et al. 2005). Responses of the In-Situ Permeable Flow Sensors that are part of the groundwater sampling system were then simulated by Oldenburg and his associates to understand how heterogeneous formation properties affect measurements of groundwater flow velocity (Su et al. 2005). Daley concurrently worked with Flegal and Mantey and their associates (Johnson et al., 2005) to adapt his sampling system for collecting organic contaminants (e.g., TCE) to their needs for a comparable system for remotely collecting inorganic contaminants (e.g., Cr).

In addition to the work outlined above, we found that it was critical to have a network connection to the site to achieve our long-term goals of fully automating the sampling and analytical systems at OU 1 with a closed-loop operation. We therefore installed a radio link from the site to our relay station in the Santa Cruz Mountains and, from there, to the UC Santa Cruz campus, as well as a video camera at the site enabling researchers to view conditions at the site from remote locations (LLNL and LBNL). We also installed a meteorological data station at the site in order to correlate and coordinate measurements of the toxics in the groundwater with precipitation. This installation was made with a commercial quality meteorological station at the site that we linked via the network connection to our REINAS (Rosen et al. 1998) database at UCSC so real-time weather data (e.g., rainfall) were available at the site and also streamed to our real-time REINAS database for research use. This installation then enabled our plans for moving the data from the gas chromatograph (GC) at the site to the REINAS database in real time by linking the instrumentation computer with the REINAS computer at the Fort Ord site.

Summaries of the four reports

This report integrates the methodologies, results and discussions, conclusions, and recommendations from the four individual reports, which are briefly summarized below.

1. Groundwater flow monitoring technologies: The principal focus of this study was on the groundwater transport of TCE at OU 1, using three independent monitoring technologies (Figure 2). While all three technologies are designed to produce estimates of fluid flow rate, they differ in mode of installation, theory of operation, and types of data produced. Two

of the tools examined—the RAS Hydrophysical Logging tool (HPL), and the Lawrence Livermore National Laboratory Scanning Colloidal Borescope Flow Meter (SCBFM)—could be installed in existing boreholes to produce point estimates (in time), while the third employed permanently installed sensors for long-term logging of flow rate and direction, at the expense of portability (Hydrotechnics® In-Situ Permeable Flow Sensors [ISPFS]). The SCBFM and ISPFS produce estimates of both groundwater flow rate and direction, while the HPL produces flow rate estimates only. Although groundwater flow and azimuth data are crucial to the understanding of contaminant transport, determination of these parameters is often costly, indirect, and frequently difficult to verify. Many techniques have been developed to estimate flow in boreholes, but comparatively few studies have attempted to directly compare data from different groundwater flow monitoring tools (Wilson, et al. 2001). The present experiments were deployed at the OU 1 site to provide a nearly ideal, homogeneous hydrogeological environment in which tool performance could be compared.

2. Analyses of aquifer response, groundwater flow, and plume evolution: Data from the monitoring was then used in a continuation of analysis of the hydrogeology, ISPFS results, aquifer response, and changes in the TCE groundwater plume at OU 1. These analyses benefited from the availability in digital form of more recent, as well as older, groundwater chemistry records as well as treatment system totalizer data that were available at the time of Oldenburg et al. (2002).

3. Simulation of in-situ permeable flow sensors for measuring groundwater velocity: Data from the monitoring were also used to derive accurate estimates of groundwater flow velocities at the site. Those estimates are essential for a number of applications, including site characterization and monitoring, groundwater remediation, and water resources management. A number of technologies exist to measure groundwater flow velocities: the colloidal borescope (Kearl and Case 1992; Kearl and Roemer 1998), the horizontal heat-pulse flowmeter (Hess 1986; Young et al. 1991; Molz and Young 1993), the acoustic doppler velocimeter (SonTek 1996), and hydrophysical logging (Tsang, et al. 1990; Pedler et al. 1992; Tsang and Doughty 2003). A comparison of these technologies for measuring horizontal groundwater flow is detailed in Wilson et al. (1999). All of these techniques require measurements to be made in the screened interval of a borehole and only provide a snapshot in time of the flow velocities.

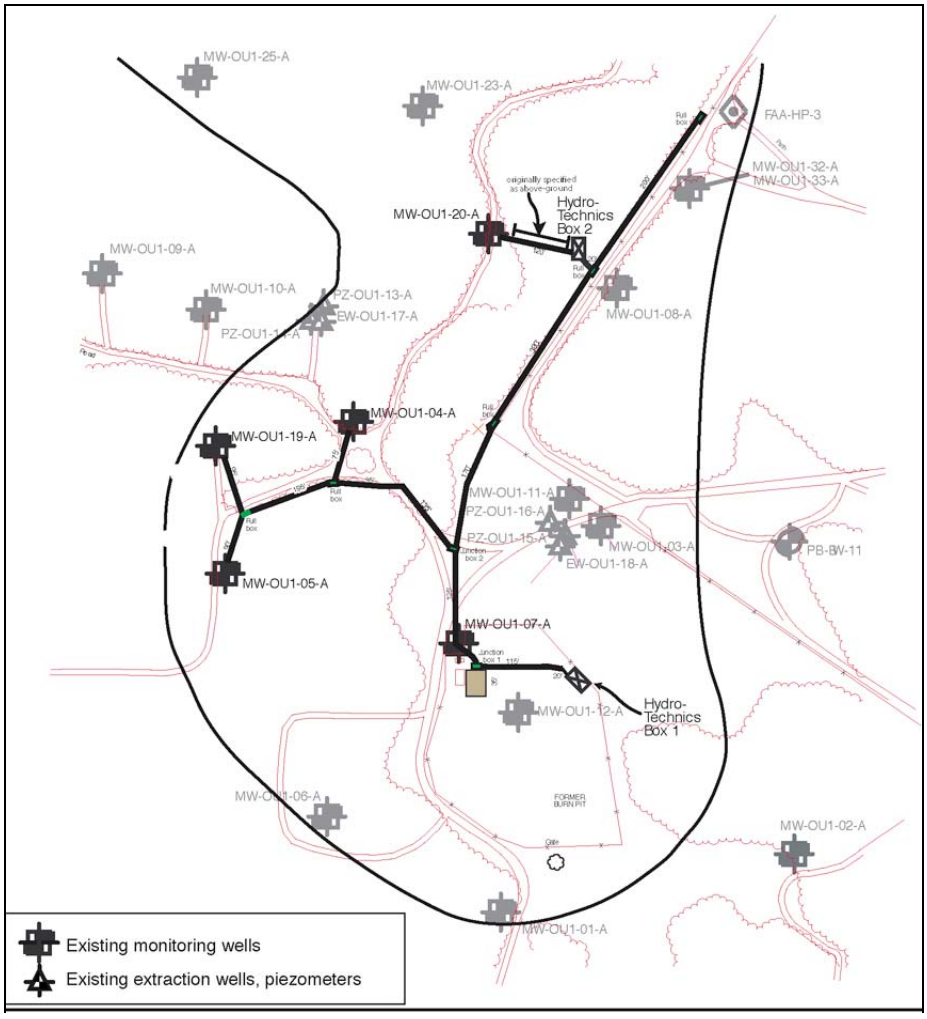

Figure 2. Fort Ord Operable Unit 1, Fire Drill Area (OU1-FDA). This map shows the distribution of new flow monitoring and groundwater sampling wells, and pre-existing groundwater monitoring wells.

4. Inorganic contaminant sampling and analysis in groundwater: Finally, the potential to conduct complementary analyses of inorganic contaminant concentrations and groundwater transport with the preceding sampling and modeling systems was investigated. The need for automated and remote sampling equipment and techniques is becoming necessary to rapidly and economically assess water quality due to increasing costs of personnel and threats to water supplies. Since organic and inorganic contaminants are typically sampled separately because of cross-contamination concerns, this research was designed to determine whether a single system could be used to collect both sets of samples–rather than installing two independent systems–and to remotely sample inorganic contaminants during ephemeral events using trace metal clean conditions.

2 Experimental Tasks

Groundwater flow monitoring technologies

Summary

Researchers installed a multipoint field chemical analysis and groundwater monitoring system at Operable Unit 1 (OU 1) at the former Fort Ord Army Base in California. In this installation, we buried stainless steel tubing to connect a network of ten wells located up to 1600 ft (480 m) from a control building. A subset of five wells has also been instrumented with In-Situ Permeable Flow Sensors (ISPFSs, Hydrotechnics, Inc.) to measure groundwater flow velocity and direction in the sandy unconfined aquifer. All ten wells are outfitted with dedicated micro-flow bladder pumps, with sample selection and processing hardware located at the analytical station and with a new version of pressure transducers to measure water table elevations. A dedicated low cost gas chromatograph in the control building provides on-line sample analysis and data.

The dedicated pumping system and associated instrumentation for the OU1 project was originally installed in the previous decade, was upgraded, and in operation until March 2004. At that time, operations were disrupted and suspended at the request of the Army Corps contractor, HydroGeoLogic, to allow them to install their permeation ("bag") samplers in those wells. Three of these samplers were removed, and the dedicated pumps in wells W-0U1-7a, W-OU1-36a, and W-OU1-37a were reinstalled by April 2005. The remaining wells at OU1 were reinstalled in June 2005. The entire system is back in operation. A new ASAP water sampler was also installed and plumbed at OU 2.

The data acquisition system at OU 1 was also expanded. This included data from the LLNL Colloidal Borescope, conductivity tool measurements that were made in parallel with HydroTechnics ISPFS flow monitoring, and continuous groundwater depth data from the OU 1 dedicated probes. Remote supervision of the real-time data acquisition was enabled with a radio link export of data from the GC at OU 1 to our measurement database at LLNL, via UCSC. As previously noted, a video camera was installed at OU 1 enabling researchers from remote locations (LLNL and LBNL) to view conditions at the site and a real-time meteorological data station was

also installed at the site in order to provide complementary data on factors influencing groundwater contaminant concentrations and flow (e.g., precipitation). Meteorological measurements from that installation were linked to the REINAS database at UCSC, which may also be used to link GC measurements from OU 1 and provide real-time data on organic contaminant concentrations to researchers at LLNL, LBNL, and UCSC.

The applicability of this remote sampling and analytical system was demonstrated. The real-time gas chromatograph was operated continuously for long periods, and calibration tests clearly demonstrated the feasibility of on-line instrumentation of the pumped water for trace organic analyses. The sampling system was also successfully tested for concurrent collections of inorganic contaminants, as discussed in a later section.

Background

Standard approaches to obtaining groundwater flow velocity information involve making hydraulic head measurements in screened boreholes across a site to determine hydraulic gradients. These are combined with hydraulic conductivity data to estimate the potential flow rate between the points sampled by the boreholes (Darcy's equation). This methodology will provide useful approximations in many instances, but it ultimately depends on the assumption that the available conductivity data accurately reflect the conditions throughout the target site. Moreover, hydraulic conductivity is generally determined by pumping or slug tests, which may undesirably average zones of preferential flow that are the main conduits of contaminant flow (Kearl and Case 1992; Kearl 1997), or generate problematic wastes in aquifers known or suspected to be contaminated. Sensors that do not depend on conductivity data can potentially provide useful flux data for modeling or remediation optimization without the drawbacks of traditional techniques, and provide a useful link between laboratory and field observations.

Alternative methods for determining flow across boreholes included tracer tests and borehole-dilution tests, which are often deployed with zone-isolating packers (Kearl and Case 1992). Spinner or impeller tools are sometimes used to estimate flows, but are most useful where vertical flow is suspected to be substantial; their use is limited by their relatively high stall speeds (Hess 1986; Molz et al. 1989). Hess (1986) and Kerfoot (1988, 1995) also presented development of heat-pulse flow meters that are designed to detect three dimensional flow vectors, although convective com-

ponents may complicate interpretation. Other physical methods include electromagnetic flowmeters (Young et al. 1991), acoustic (SonTek, Inc. 1996) and laser (Momii et al. 1993) Doppler velocimeters and use of radioisotopic tracers (Drost et al. 1968); in some cases tool intercomparisons have been performed (Molz et al. 1989, Wilson 2001). Clearly more studies of this kind are needed.

In-situ permeable flow sensor

The In-Situ Permeable Flow Sensor was developed in the early 1990s at Sandia National Laboratories in Albuquerque, NM,to directly measure groundwater flow vectors in unconsolidated, saturated, porous media (Ballard 1996; Ballard et al. 1996). The tool uses heat perturbation and advection from a cylindrical surface, which is in turn studded with an array of precision thermistors that measure heat dispersion around the tool due to groundwater flow. In theory, if a thin cylinder has uniform heat flux from its surface, the temperature distribution on the surface will vary as a function of the magnitude of groundwater flow past the surface. Relatively warmer temperatures will be sensed on the downstream side, and relatively cooler temperatures on the upstream side. Romero (1995) derived mathematical functions describing heat distribution of a finite-length heated cylinder in a permeable flow field (figure after Ballard 1996):

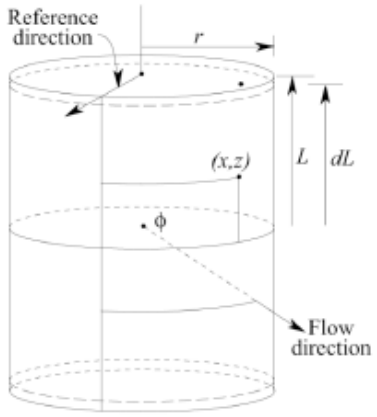

$$T(x,z) = Qr/K[1 + r/L\ Pe\ \cos(q - x)\ \sin\phi]$$

$$\left[ln[2L/r\ (d^2 - z^2)^{1/2}] - r/L\ Pe\ \cos(q - x)\ \sin\phi + 1/2 \int_{-\delta}^{\delta} \frac{e^{1/2Pe[(z-\xi)\cos\phi - |z-\xi|]}}{|z-\xi|}\, d\xi \right]$$

where T is the temperature at position x,z on the surface of the probe; x is the angular distance in the horizontal plane from the reference direction to the measurement point; z is the distance in the vertical from the midpoint of the probe (dimensionless, by dividing by the half-length of the tool, L); r is the tool radius; δ is the half-length of the heated region of the tool, again dimensionless by dividing by L; Q is the heat flux per unit area from the tool surface; K is thermal conductivity of the saturated porous medium; Pe is the dimensionless flow velocity, or Peclet number; θ is the angular distance in the horizontal plane from the reference direction, and ϕ is the angle between vertical and the flow velocity vector. The flow velocity, Pe is given by:

$$Pe = U_{\infty} L \rho c / K$$

where U_{∞} is the magnitude of the Darcy flow velocity far from the tool, ρ is the fluid density, and c is the fluid specific heat. In practice, the relative deviations of thermistor temperatures from the average for the entire tool temperature are used with a mathematical inversion algorithm to calculate flow vectors.

For this study, the ISPFS were installed approximately 30 in. above the surface of the FO-SVA clay layer, and a 2 in. monitoring well was placed adjacent to the thermal probe, with its deepest point approximately 15 in. above the uppermost part of the ISPFS (Figure 3). The normal practice for installation of these tools is to insert them through a hollow stem auger, and formation is allowed to collapse around the tool as the auger is withdrawn (Figure 4). Five of the tools were installed during installation of the integrated geochemical analysis station at the FDA. One of the tools suffered an electrical failure within the first few months of its operation (MW-OU1-40-A) and a second (MW-OU1-38-A) has not produced reliable data since its installation possibly due to incomplete collapse of the formation during installation. The remaining three devices have provided reliable data since that time, in good agreement with traditional gradient and conductivity analysis (Jordan et al. 2005). A detailed analysis and simulation of their performance in media with varying thermal properties is provided as part of this project by Su et al. (2005; in press).

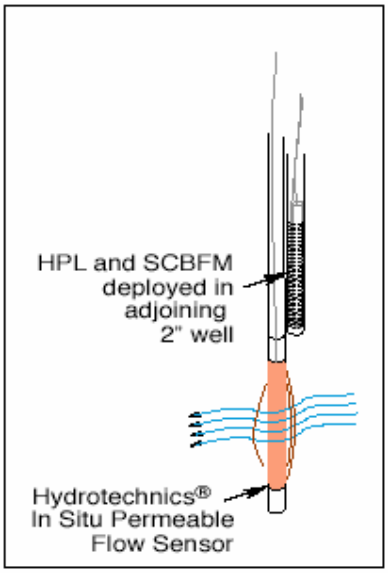

Figure 3. Schematic of an ISPFS and monitoring well installation.

Figure 4. Installation of ISPSF with adjacent hollow-stem auger at OU 1.

Hydrophysical logging tool

The hydrophysical logging tool (HPL) has been referred to as fluid-conductivity logging, fluid-electrical-conductivity logging, and ion logging (Cohen 1995). The HPL tool comprises a vertical array of electrical conductivity sensing electrodes and precision thermistors (Figure 5); wells under test are first scanned for ambient properties by recording signals from the sensing elements as the tool is lowered through the borehole fluid

(Figure 6). Then, the borehole fluid is slowly replaced with deionized water at a rate that does not change the pressure head. Finally, the fluid electrical conductivity and temperature of the borehole fluid is recorded through repeated vertical scanning over a period of many hours following emplacement of the low conductivity fluid, as formation water displaces fluids from the borehole. In essence the technique is a specialized instance of borehole tracer dilution where, in this case, the tracer is deionized water as described by Drost et al. (1968) and Tsang et al. (1990).

Figure 5. Calibration of the Hydrophysical logging tool with standardized salt solutions.

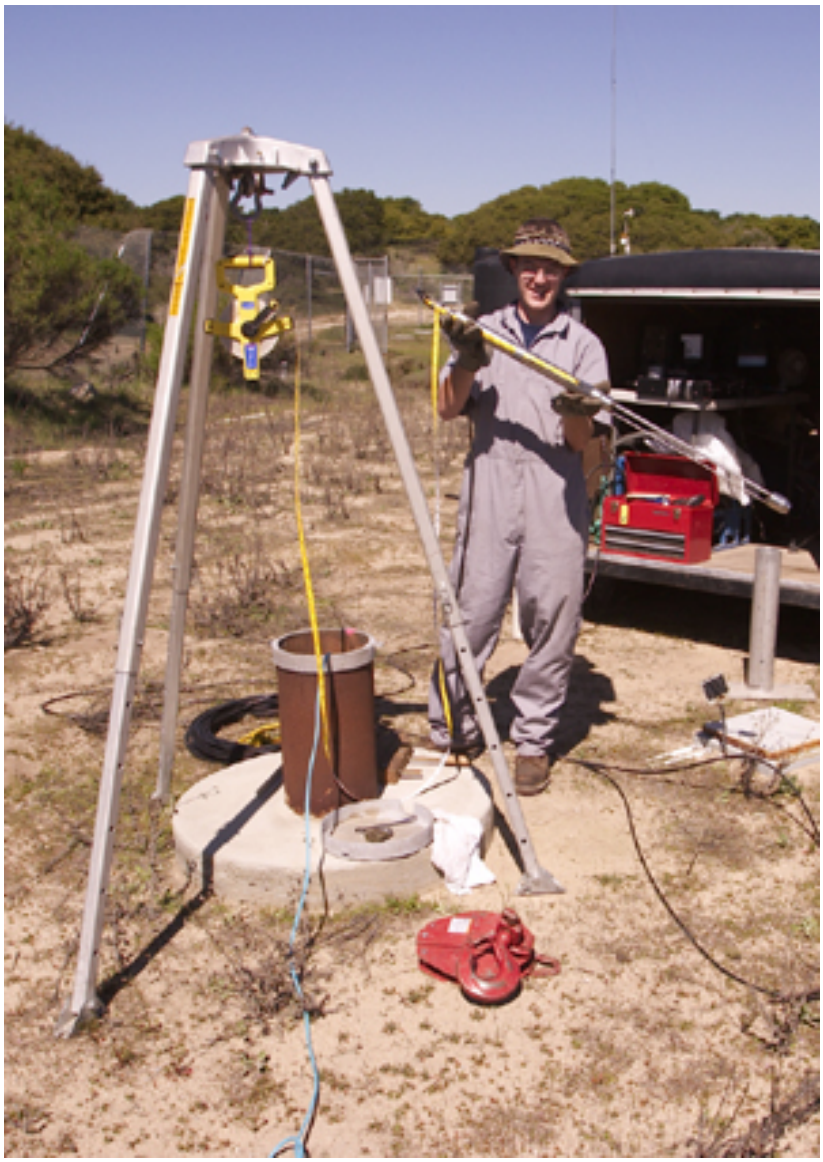

Figure 6. Preparing for installation of the LLNL Scanning Colloidal Borescope Flow Meter.

Inflow parameters are estimated following the general methods of Drost et al. 1968, although the application of dilution theory to borehole logging is innovative and has been shown to be practical for the identification of restricted infiltration zones (Tsang et al. 1990). The tracer is assumed to be uniformly placed in the borehole; its concentration, C_{obs}, is modified by influx of formation water at concentration C_f, flowing into the borehole at a velocity v^*, as shown below (after Wilson et al. 2001):

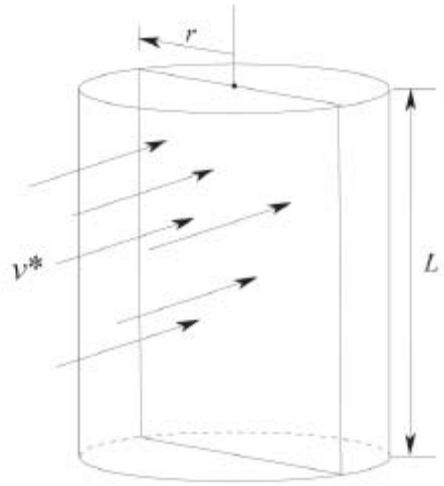

$$v^*C_f A - v^*C_{obs}A = W\frac{dC_{ob}}{dt}$$

where A is the borehole cross-sectional area ($A = 2rL$, r is the radius of the borehole, L is the length), and W is the corresponding volume ($W = \pi r2L$). If the substitution is made:

$$C = C_f - C_{obs}$$

equation can be rearranged:

$$v^*C = \frac{W}{A}\frac{dC}{dt}$$

that can be rearranged to solve for C:

$$C = C_0 \exp\left(-\frac{2t}{\pi r}v^*\right)$$

where C_0 is C at t = 0, or $C_f - C_{obs}$ at t = 0. Taking the natural logarithm of both sides gives:

$$\ln\left(\frac{C}{C_0}\right) = -\frac{2v^*}{\pi r}t$$

and the ratio C/C_0 should produce a linear semi-log plot, the slope of which is proportional to the velocity of fluid flowing through the well:

$$v^* = \frac{\pi r \ln\left(\frac{C_2}{C_1}\right)}{2(t_2-t_1)}$$

where t_1 and t_2 are the times corresponding to C_1 and C_2 on the semi-log plot. This velocity corresponds to the measured fluid velocity through the borehole. This may differ from the actual formation flow rate, as flow lines tend to converge toward the borehole, and corrections for these phenomena have been offered (Drost et al. 1968):

$$q = \frac{v^*}{\alpha}$$

where q is the specific discharge of groundwater in the aquifer and α is a factor that corrects for convergence of flow in the borehole. The latter factor can only be calculated with a detailed knowledge of the casing screen, sandpack characteristics, and hydraulic properties of the aquifer. However, it is thought to be generally insensitive to formation hydraulic properties as long as the screen and sandpack are substantially more permeable than the formation. When αcannot be calculated directly, formation flow estimates are made using convergence factors of 2.5 to 4 (Momii et al. 1993; Wilson et al. 2001). In the present work, these corrections have not been made and only "in borehole" flow rates (v^*) are presented.

Scanning colloidal borescope flow meter

The colloidal borescope was developed in the early 1990s at the Oak Ridge National Laboratory (Kearl et al. 1992; Kearl 1997). The instrument described in the Oak Ridge system is very similar to an earlier device that was the subject of a patent (Foster and Fryda 1990). The principal differences being the type of illumination (laser vs. lamp) and imaging device ("Optiram" vs. CCD camera for the Foster and Fyda, and Kearl versions, respectively). The tool consists of a downward-viewing camera with a microscope objective, a source of illumination directed towards the camera creating a "bright-field" effect, a magnetometer to detect tool orientation, supporting cables, and a viewer/recorder package at the well head. Video recordings are made once the tool has been lowered to the target depth and colloidal scale particles, in the size range of 2-20μ, are detected as

dark objects. If nearly laminar flow is detected (particles stay within the quite thin plane of focus for much or all of their traverse across the viewing field) many particles can contribute to a single reading. Computer software is then used to detect the particles, match them between subsequent frames, and calculate their velocity and direction (Kearl and Roemer 1998). The magnetometer output is recorded at each depth to correct azimuth estimates, as twisting of the tool is unavoidable when using flexible cables to suspend the instrument.

- The LLNL scanning colloidal borescope adds an additional feature to the basic design of the Kearl and Foster and Fyda instruments: the plane of focus is continuously adjustable over a distance of almost 1/2 meter, so that once the tool has been placed at a target depth, a range of image "planes" can be visualized without movement of the tool. This is thought to offer more flexibility in locating optimum particle fields for logging without creating turbulence as the tool is repositioned.
- Because the SCBFM directly visualizes particle transport across the borehole, velocities are estimated using only simple calibrations of the camera objective. However, the tool is subject to the same biases as the HPL and other borehole-deployed devices, in that the presence of the sandpack and screens unavoidably alter flow lines near the well. Kearl (1997) has stated that borescope measurements in the field should be reduced by a factor of from one to four to calculate fluid velocities in adjacent aquifers, and that the observed velocities represent an upper limit to true aquifer flow rates.

Analysis of aquifer response, groundwater flow, and plume evolution

Summary

These measurements expanded on a previous analysis of the hydrogeology, ISPFS results, aquifer response, and changes in the TCE groundwater plume at OU 1 (Oldenburg et al. 2002). This incorporated new information including treatment system totalizer data, recent water level and chemistry data, and data collected from new wells to discern trends in contaminant migration and groundwater flow that may be useful for ongoing remediation efforts.

Data and data transfer

The company MacTec (Oakland, CA) provided well, water level, and chemistry data in electronic form. New well coordinates for all the wells, including wells installed after those analyzed in Oldenburg et al. (2002), were provided based upon a new state plane. Additional water levels from the period from the second quarter of 2000 through the last quarter of 2003, inclusive, were provided. Groundwater chemistry data were provided that extended the period of coverage from the beginning of 1986 to the end of 2003. The earliest chemistry records analyzed in Oldenburg et al. (2002) were from the second quarter of 1992 and the most recent were from 2000.

Well coordinates used in Oldenburg et al. (2002) were apparently surveyed relative to two different state planes depending upon when the well was installed. Wells surveyed to the earlier state plane were resurveyed relative to the newer state plane and new coordinates provided. Comparison of the old and new well coordinates revealed that the coordinates for extraction wells EW-OU1-17-A and –18-A apparently had not been updated to the new state plane. Comparison of the other early OU 1 wells revealed a relatively consistent difference in the coordinate values. This difference (+22.80 easting, -8.52 northing) was applied to the extraction well coordinates in order to place them in the proper position relative to the other wells. The former well PZ-OU1-31-A was changed to MW-OU1-31-A to conform to MacTec's naming convention.

Water level and chemistry data were imported into GIS\Key™ using utilities provided with the program. These utilities perform a variety of integrity checks. Any errors resulting from these checks must be resolved prior to import. We analyzed the data and made figures using GIS\Scout™ and AutoCAD™.

Totalizer data (cumulative volume of water produced) for the extraction wells from the second quarter of 1999 through the end of 2003 were provided by Ahtna Governmental Services Corporation (AGSC). These data were stored in Excel™, from which graphs depicting average flow from each well through time were developed.

Precipitation

Precipitation data from the Fritzsche AAF meteorological station are only available for the years 1969 to 1978. The least squares fit of the annual precipitation at this station versus the Monterey station is shown on Figure 7. This shows that the precipitation at OU 1 (adjacent to the Fritzsche AAF station) is generally 86% of the Monterey precipitation minus one inch (0.025 m). Rather than apply this correction to the Monterey data, the Monterey totals are assumed to apply to OU 1 throughout this report.

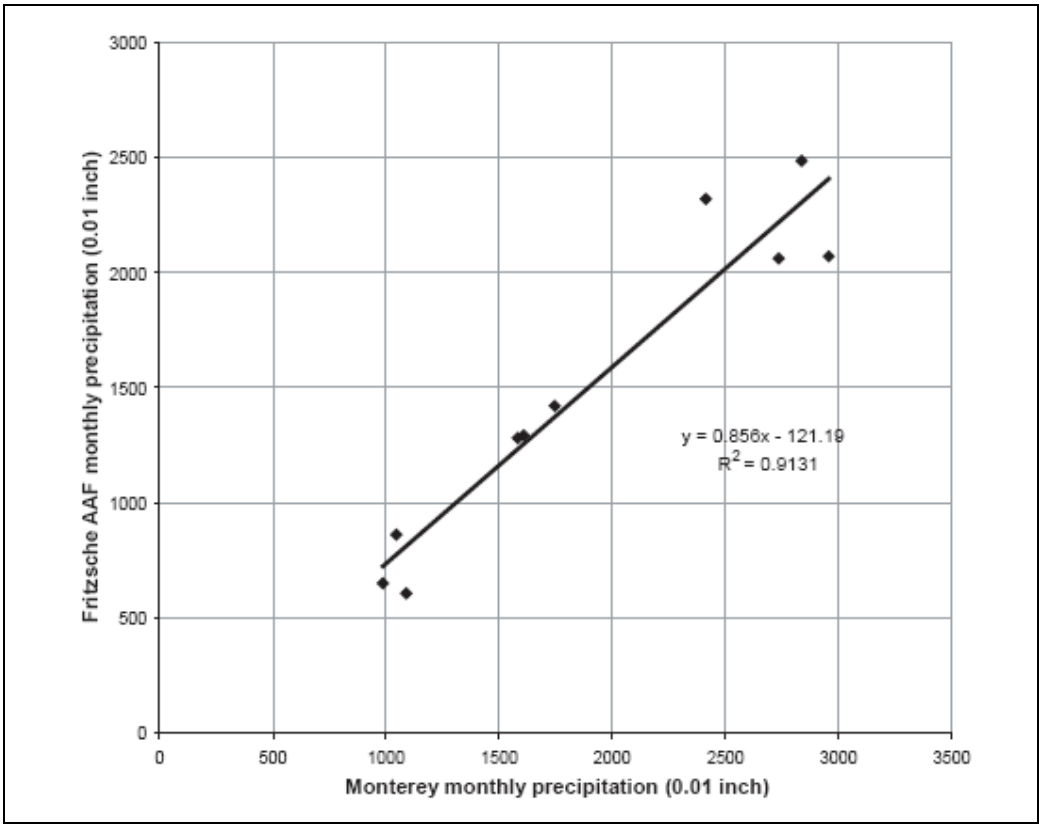

Figure 7. Comparison of precipitation totals at Monterey and Frizsche AAF meteorological stations.

Monthly precipitation totals for the period January 2001 to August 2003 were downloaded from the National Oceanic and Atmospheric Administration data server for the Monterey meteorological station. An updated hydrologic year precipitation total chart for the Monterey station is shown in Figure 8. The hydrologic year is July 1st to June 30th.

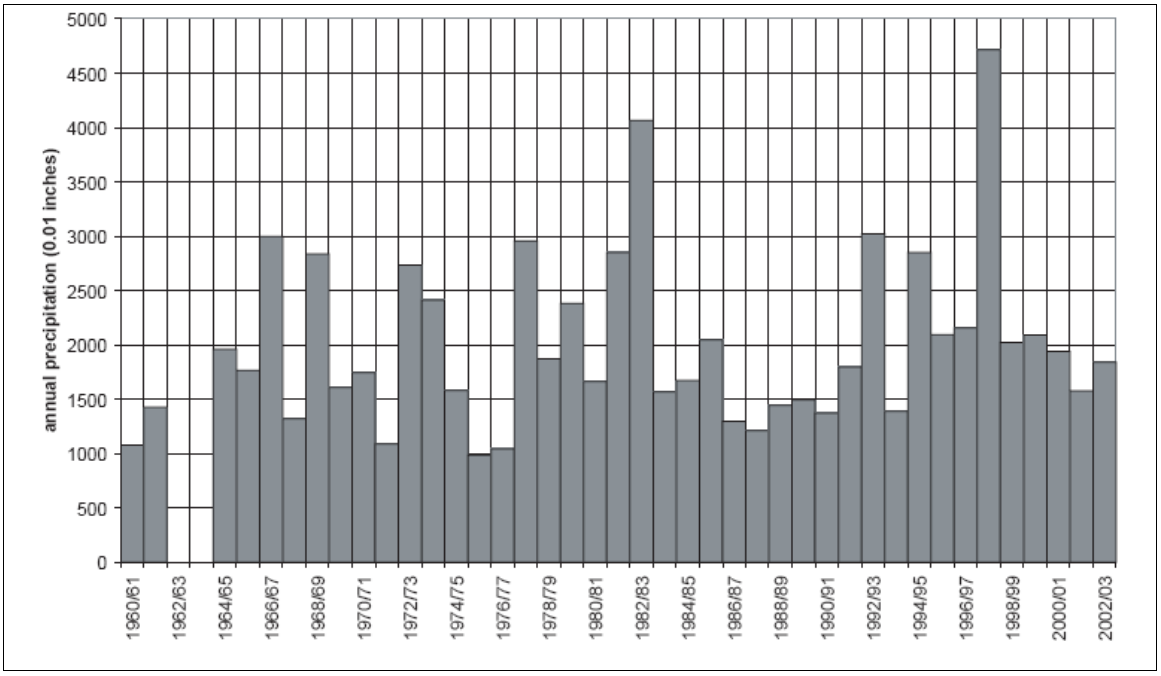

Figure 8. Jordan et al. Hydrologic year (July 1st to June 30th) precipitation totals at Monterey meteorological station.

Hydrostratigraphic model

Elements of the hydrostratigraphic model presented in Oldenburg et al. (2002) are occasionally referenced in this report. Briefly, this hydrostratigraphic model consists of four sand layers and three clay layers. The clay layers collectively comprise the FO-SVA. The sand and clay layers are numbered independently from the deepest to the shallowest. The clay layers range up to 12 ft (3.6 m) thick and average approximately 5 ft (1.5 m) thick. Sands 1, 2, 3, and 4 average 15, 6, 8, and 92 ft (4.6, 1.8, 2.4, and 28 m) thick, respectively.

The deepest layer in the model is Clay 1. Clays 1 and 2 and intervening Sand 1 are continuous throughout the area. Clays 3 and 4 are discontinuous and consist of two patches each within OU 1. The northwestern patch of Clay 4 is sometimes referred to as the "Airfield Clay." Sands 2 and 3 are discontinuous and pinch out between the adjacent clay layers in places. Sand 4 is continuous throughout OU 1.

Simulation of in-situ permeable flow sensors for measuring groundwater velocity

Summary

Numerical simulations of three-dimensional non-isothermal flow around a Hydrotechnics® ISPFS were made to investigate temperature profiles along the instrument that might give rise to spurious indications of downward flow. The flow sensor operates by constant heating of a nearly one-meter-long, 5 cm diameter cylindrical probe, which contains 30 thermistors in direct contact with the formation. The temperature evolution at each thermistor can be inverted to obtain an estimate of the groundwater flow velocity vector (i.e., horizontal and vertical components, and azimuth). Data were monitored from three Hydrotechnics® in-situ permeable flow sensors installed in a shallow aquifer comprised of unconsolidated dune sand bounded below by a clay aquitard at the former Fort Ord Army Base. While the magnitudes of the vertical velocities were expected to be much less than the horizontal velocities at this site because of the underlying clay layer, standard data analysis of the flow sensor data suggested a strong and unexpected component of downward flow. In order to investigate these large downward flow velocities, we conducted numerical simulations to study the effect of different combinations of thermal conductivity and permeability on the temperature profile around the sensor. These simulations show that a decrease in the thermal conductivity of the formation near the bottom of the sensor can perturb the temperature profiles along the instrument in such a manner that the temperature shift could be interpreted by the standard data analysis as downward flow, even though the flow is actually horizontal.

Horizontal and vertical flow velocities

Horizontal and vertical components of groundwater flow estimated at Fort Ord from the Hydrotechnics flow sensor data are summarized in Table 1 for the three working flow sensors at Fort Ord, designated as OU1-36, OU1-37, and OU1-39. Although nearly continuous data from the flow sensors have been collected since January 2001, the results presented in the table are from mid-2003 and are representative of the relative magnitudes of the horizontal and vertical velocities estimated by the flow sensors over the time period that data have been recorded. In OU1-36, the horizontal flow velocity estimated from the flow sensor was nearly an order of magnitude less than the vertical velocity, while the horizontal velocities in OU1-

37 and OU1-39 were nearly the same as the vertical ones. The vertical velocities are expected to be much less than the horizontal velocities because of the underlying low permeability clay layer.

Table 1 also presents the horizontal Darcy velocities calculated for mid-2003 using the average hydraulic conductivity of 1.8×10^{-5} m/s estimated from pump tests (Oldenburg et al. 2002) and the hydraulic gradient obtained from water level measurements. The Darcy velocities are remarkably similar to the horizontal Darcy velocities estimated from the flow sensors, differing by only up to a factor of two. This provides confidence that the flow sensors are giving reasonable estimates for the horizontal velocities.

Table 1. Summary of horizontal and vertical flow velocities at Fort Ord.

	OU1-36	OU1-37	OU1-39
Well screen (m)	15.5 - 24.5	18.8 - 26.4	21.1 - 28.6
Flow sensor (m)	24.5 - 26.1	26.4 - 27.8	28.6 - 30.2
Distance from sensor base to clay (m)	1.3	0	0.45
Vertical velocity - flow sensor, mid-2003 (m/s)	-1.12×10^{-6}	-4.21×10^{-7}	-3.51×10^{-7}
Horizontal velocity - flow sensor, mid-2003 (m/s)	1.0×10^{-7}	3.3×10^{-7}	4.6×10^{-7}
Hydraulic Gradient (2nd quarter 2003)	0.0058	0.0090	0.027
Horizontal Darcy velocity[a] (m/s)	1.0×10^{-7}	1.6×10^{-7}	4.9×10^{-7}

[a]Calculated with hydraulic gradient and hydraulic conductivity of 1.8×10^{-5} m/s from pump tests.

Vertical profiles of groundwater temperature in observation wells can also provide information on horizontal and vertical groundwater flow (e.g., Lu and Ge 1996; Reiter 2001). Downward groundwater flow typically produces a concave upward temperature profile (Figure 9a) because of the cooler shallower water advecting downward, while upward flow causes the temperature profile to be convex upward since warmer water from below is advected up (Figure 9b). Horizontal flow that brings cool water also produces a temperature profile that is concave upward (Figure 9a), while warm horizontal flow causes a convex upward temperature profile (Figure 9b). Although it is usually difficult to distinguish between predominantly horizontal and vertical flow from these profiles, a temperature profile that decreases at shallow depths and then increases at greater depths indicates the importance of cool horizontal flow (Figure 9c). Downward flow only

cannot lower the temperatures below the coolest temperatures observed at the top of the flow zone (e.g., Mansure and Reiter 1979). In addition, density driven vertical flow tends not to occur if temperatures decrease with depth.

Ambient groundwater temperature profiles recorded in March 2004 over a 2.4 - 3.0 m section of the OU1-36 and OU1-39 monitoring wells at Fort Ord are shown in Figure 9. Although only a shallow portion of the temperature profile was recorded (the profiles were recorded to the well bottom), the temperatures in this interval decrease with depth which is similar to the upper portion of the profile shown in Figure 3c. Reiter (2001) estimated a horizontal flow component that was two orders of magnitude larger than the vertical component for a profile similar to Figure 3c. While this type of temperature profile does not completely rule out the possibility of vertical flow, it does suggest that a strong horizontal flow component exists in the formation.

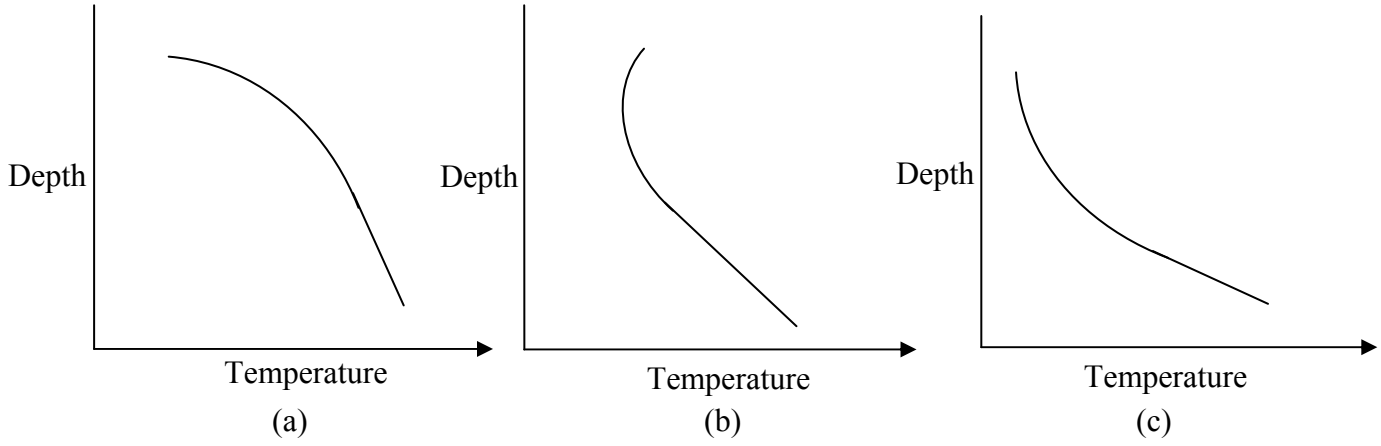

Figure 9. Schematic of groundwater temperature profiles with depth.

Ambient groundwater temperature profiles recorded in March 2004 over a 2.4–3.0 m section of the OU1-36 and OU1-39 monitoring wells at Fort Ord are shown in Figure 10. Although only a shallow portion of the temperature profile was recorded (the profiles were recorded to the well bottom), the temperatures in this interval decrease with depth, which is similar to the upper portion of the profile shown in Figure 9c. Reiter (2001) estimated a horizontal flow component that was two orders of magnitude larger than the vertical component for a profile similar to Figure 9c. While this type of temperature profile does not completely rule out the possibility of vertical flow, it does suggest that a strong horizontal flow component exists in the formation.

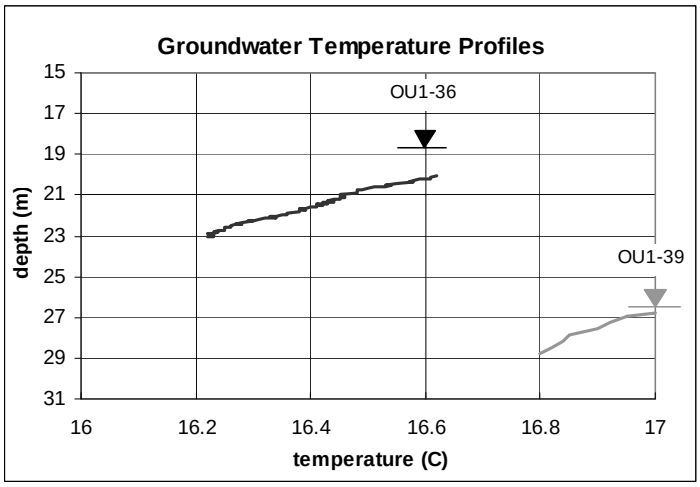

Figure 10. Measured groundwater temperature profiles in observation wells OU1-36 and OU1-39 at Fort Ord.

Grid generation and model development

Three-dimensional simulations were conducted using TOUGH2 (Pruess et al. 1999) to investigate the possible reasons for the high downward flow velocities estimated by the Hydrotechnics® flow sensors. Conformal mapping was used to generate a three-dimensional grid for simulating flow and heat transport near a Hydrotechnics® flow sensor. Because conformal maps are angle preserving, the grid that is generated follows the orthogonality requirement of the integral finite difference method used in TOUGH2. The simulation domain generated using conformal mapping is also computationally efficient because the grid is highly refined near the region of interest (i.e., the flow sensor) and then decreases in refinement with increasing distance. For this study, a grid was mapped into a semi-infinite plane outside a half circle with a radius, r, of 0.025 m that represented half of the sensor using the mapping $w \rightarrow 1/z$, where w and z are complex numbers. Figure 11 shows the plan view of the grid domain created by the mapping of the regularly spaced Cartesian array from inside the half circle into the semi-infinite domain. The semi-infinite domain is then truncated into the bounded triangular shape shown, with a maximum distance of 0.6 m from the center. The inside of the half circle represents the location of the flow sensor where heat is generated and no flow is allowed to take place. The region outside of the half circle is the formation where flow occurs. A total of 17 layers were used in the simulations, as discussed below.

Since we are only interested in examining flow and heat transport in the immediate vicinity of the flow sensors, a saturated groundwater flow model was used since the flow sensors are located below the water table. Eight modeling scenarios were conducted, and a summary of the parameters used in the different scenarios is provided in Table 2. The following parameters were varied in the simulations to examine the effect they had on the temperature profile along the heated flow sensor:

- thermal conductivities
- permeabilities
- thickness of sand layer between the sensor bottom and clay layer.

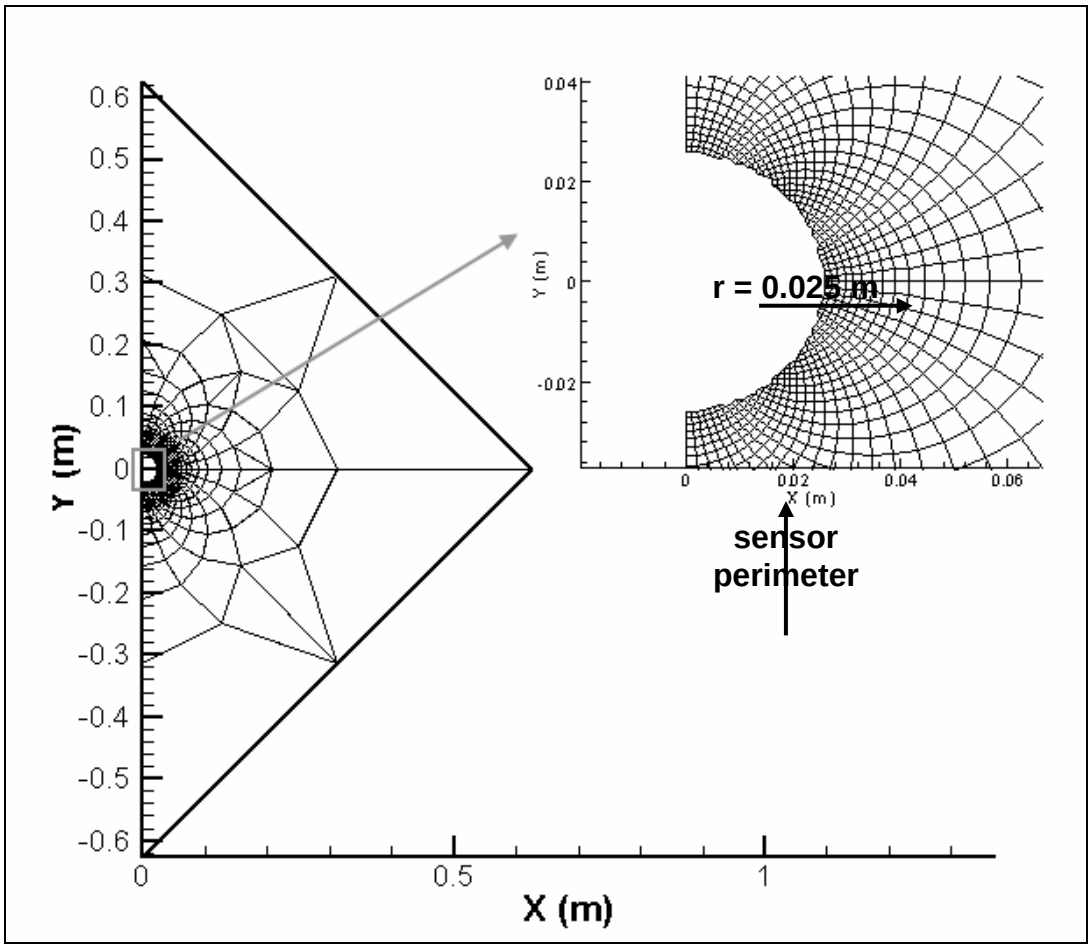

Figure 11. Plan view of the numerical grid generated using conformal mapping of flow and heat transport near a Hydrotechnics® flow sensor.

Table 2. Summary of parameters used in the three-dimensional simulations of flow and heat transport around a Hydrotechnics® flow sensor.

Simulation Scenario	Flow Direction/ Flow Velocity (m/s)	Thermal Conductivity (W/m°C) $K_{t,1}$	$K_{t,2}$	Sand layer thickness between sensor and clay layer (m)	Permeabilities (m^2)
1	Horizontal 2.5×10^{-7}	2.1 layers 1-17	--	N/A	2×10^{-12}, layers 1-17
2	Horizontal 2.5×10^{-7}	2.1 layers 1-13	1.0; 1.8 layers 14-17	0	2×10^{-12}, layers 1-17
3	Horizontal 2.5×10^{-7}	2.1 layers 1-17	--	N/A	2×10^{-12}, layers 1-13 2×10^{-18}, layers 14-17
4	Vertical 5×10^{-7}	2.1 layers 1-17	--	N/A	2×10^{-12}, layers 1-17
5	Horizontal 2.5×10^{-7}	2.1 layers 1-14 layers 1-15 layers 1-16	1.0 layers 15-17 layer 16-17 layer 17	0.072 0.144 0.288	2×10^{-12}, layers 1-17
6	Horizontal 2.5×10^{-7}	2.1 layers 1-17	--	N/A	2×10^{-12}, layers 1-11 1×10^{-12}, layers 12-17
7	Horizontal 2.5×10^{-7}	2.1 layers 1-17	--	N/A	2×10^{-12}, layers 1-11 4×10^{-12}, layers 12-17
8	Horizontal 2.5×10^{-7}	2.1 layers 1-11; 14-17	2.0 layers 12-13	N/A	2×10^{-12}, layers 1-17

A 17 layer model was used for all the modeling scenarios. The top and bottom layers (layers 1 and 17, respectively) had thicknesses of 0.288 m, layers 2 and 16 had thicknesses of 0.144 m, and the remaining eleven layers had thicknesses of 0.072 m (Figure 12). The heated portion of the flow sensor was represented by nine layers in the center (layers 5-13). Horizontal flow was imposed across the domain in all the scenarios except for Scenario 4 where vertical flow was imposed. The density and the porosity of the sand and clay were the same in all the simulations, 2650 kg/m^3 and 0.3, respectively. The saturated thermal conductivities used in the simulations were 2.0 and/or 2.1 W/m°C for the sand and 1.0 or 1.8 W/m°C for the clay. These values are within the range of thermal conductivity values measured for these soil types (van Wijk and de Vries 1966; de Marsily 1986).

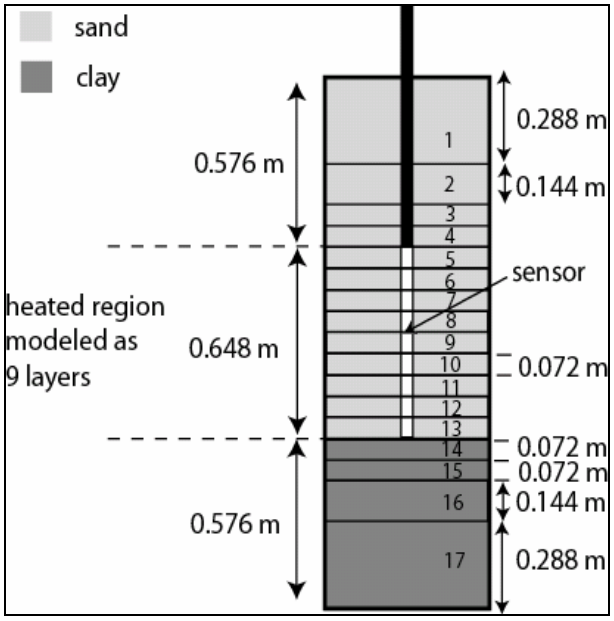

Figure 12. Seventeen-layer model used in the simulations.

The thermal conductivity and permeability in all 17 layers were uniform in Scenarios 1 and 4. In Scenario 2, layers 14-17 had a lower thermal conductivity compared to the layers above it to represent the clay aquitard. In Scenario 3, the permeability in layers 14-17 was lowered to 2×10^{-18} m² while the permeability in the remaining layers remained at 2×10^{-12} m². A sand layer separated the sensor bottom and the top of the clay aquitard in Scenario 5. A thermal conductivity of 2.1 W/m°C was assigned to the appropriate combination of layers 14, 15, and 16 to create a sand layer with a thickness of 0.072 m (layer 14), 0.144 m (layers 14-15), or 0.288 m (layers 14-16). A thermal conductivity of 1.0 W/m°C was assigned to the clay aquitard below this sand layer. The permeability in layers 12-17 was decreased and increased in Scenarios 6 and 7, respectively, by a factor of 2 relative to the permeability assigned to layers 1-11. In Scenario 8, the thermal conductivity of layers 12 and 13 was set at a slightly lower value than the remaining layers.

Time-invariant pressure boundary conditions were specified along the upstream and downstream boundaries to create horizontal flow across the domain, and on the top and bottom layers of the domain to create vertical flow (Scenario 4 only). The horizontal flow velocity in the simulations was around 2.5×10^{-7} m/s, while the vertical flow velocity in Scenario 4 was approximately 5×10^{-7} m/s. These velocities were around the same magnitude as the velocities estimated by the flow sensors at Fort Ord (Table 1).

Isothermal flow simulations were initially run until steady flow conditions were established. After reaching steady-state, a total of 35 watts of heat was then applied to the boundary nodes located along the half circles in the nine layers representing the heated portion of the sensor. The rate at which heat was applied to each boundary node was proportional to the interface areas of the boundary grid blocks. The heater power used at Fort Ord was approximately 70 watts; therefore, 35 watts was used in our simulations since only half of the sensor was modeled.

Inorganic contaminant sampling and analyses

Sampling

Trace metal clean techniques, as delineated in Creasey and Flegal (1999), were used for all sample preparation and sampling techniques, to the extent possible using existing wells and pumping systems. Groundwater was also directly sampled from a well OU1-36 with a bailer using an acid-cleaned bailer to determine whether comparable levels of trace element concentrations would be obtained with the two techniques. This was done to test the disparity in results in groundwater analyses in samples collected with the two different methodologies, as described in Creasey and Flegal (1999).

Filtered water samples for the analysis of Cr(VI), dissolved organic carbon (DOC), and nutrients were filtered (Osmonics™ polypropylene, 0.45 μm calyx filter cartridge), while unfiltered samples were collected for the analysis of total chromium. The total chromium and Cr(VI) samples were collected in acid-clean low density polyethylene (LDPE) bottles. They were rinsed (5x) with the groundwater before being filled, then were encased in two LDPE bags and were stored on ice. The DOC samples were collected in 5 mL glass vials; and the nutrient samples were collected in 30 mL LPDE bottles, which were cleaned with 1% (reagent grade) HCl. Immediately after sampling, DOC and nutrients samples were refrigerated until analysis.

Chromium analyses: The Cr(VI) samples were analyzed within 48 hours of collection. They were first put through a liquid membrane extraction in order to separate Cr(VI) from Cr(III) substrates (Djane 1999; Ndung'u 1999). Samples were then analyzed with the graphite fluorescent atomic absorption spectrometer (GFAAS) system.

Total dissolved (< 0.45 μm) chromium samples were filtered in the lab within a few hours of collection. These samples were returned in either new 500 mL TMC LDPE or its original LDPE bottle, which were rinsed 5 times in between stages with high purity (18 Ω cm) water [Millipore Milli-Q water™ (MQ)]. Five hundred mL aliquots were acidified with 2 mL of 6M high purity HCl, and were then stored until analysis. Total dissolved chromium concentrations, as well as those for manganese and iron were determined with a Finnegan Element high resolution, magnetic sector inductively coupled plasma-mass spectrometer (HR-ICP-MS) using indium as an internal standard for each sample. Along with the groundwater samples, certified standard reference material for trace elements in natural water (SRM 1640) of the National Institute of Standards and Technology (NIST) were analyzed concurrently. Calculated maximum detection limits (MDLs) were 0.01 μg/L for total chromium, 0.02 μg/L for manganese, and 0.1 μg/L for iron. The average recoveries for each element in the SRM was >96 %.

Other trace element analyses: Analyses of cadmium (Cd), cobalt (Co), copper (Cu), nickel (Ni), lead (Pb), and zinc (Zn) were made with a Finnegan ELEMENT high resolution inductively coupled plasma mass spectrometer (HR-ICP-MS). Following UV-oxidation, the solutions were prepared with deionized water (18 MΩ cm^{-1}) from a Milli-Q® analytical reagent grade water purification system (Millipore, Bedford, MA). HNO_3 (Optima grade, Fisher Scientific, Pittsburgh, PA) was diluted with Milli-Q® to make up 1.5 M HNO_3 eluent, and then spiked with 10 μg/L each of ^{103}Rh and ^{69}Ga to be used as an internal standard. Acetic acid/ammonia buffer solution was prepared by slow addition of 15 mL of aqueous ammonia (20–22%, Optima grade, Fisher Scientific) to 13 mL of glacial acetic acid (trace metal grade, Fisher Scientific), diluted to 500 mL in an acid cleaned polyethylene bottle. The pH was adjusted to pH 5.0 with ammonia or acetic acid. A pH 5.0 wash solution was prepared by a ten-fold dilution of the above buffer and adjusted to pH 5.0 with HNO_3. The pH 9.0 buffer was similarly prepared by adding 18 mL of ammonia solution to 13 mL of glacial acetic acid and making up to 500 mL. For external calibration determination, multi-element working standard solutions were prepared by dilution of 1000 μg/L stock solutions in 1.5 M HNO_3. Working standard solutions were acidified with hydrochloric acid to the same pH as the samples. Other analyses of iron (Fe) and manganese (Mn) concentrations were then made with direct injections into an inductively coupled plasma optical emission spectrometer (ICP-OES).

Quality assurance/quality control of trace element analyses

In addition to the use of trace metal clean protocols in sample collection, processing, and analyses, concurrent analyses of reference materials and blanks were made to establish the Quality Assurance/Quality Control (QA/QC) of the measurements. National Research Council of Canada (NRCC) certified reference materials for trace elements in water SLEW-1, SLEW-2 and SLRS-1 were used to assess the accuracy of the analyses. Measured and certified values of trace element concentrations of those reference materials are listed in Table 3. Minimum detection levels (MDL) of the analyses, based on 3-standard deviations of the blanks are listed in Table 4.

Comparisons of the QA/QC with previous measurements of trace metal concentrations were limited. No values for reference materials concurrently analyzed in previous trace element measurements were reported. In addition, previously reported MDLs were markedly higher (e.g., orders of magnitude) than the new MDLs. For example, the MDL for cobalt (0.0018 µg/L) for the study was 100-fold less than the previous reported value (1.0 µg/L), as was the MDL for copper (0.267 µg/L: 1.8 µg/L); and the MDL for lead (0.0022 µg/L) was 1000-fold lower than previously reported values (e.g., 1.6 µg/L), as was the MDL for zinc (16.5 µg/L: 0.0442 µg/L). That difference in sensitivity also limited comparisons of most of the new measurements with previous measurements, because most previous trace element measurements were below the MDL and, therefore, reported as non-detected (ND).

Table 3. Measured and certified values of trace element concentrations of NRCC reference materials (SLEW-1, SLEW-2, SLEW-3, and SLRS-1) processed and analyzed concurrently with trace element measurements in groundwater samples collected at OU 1.

Analyte	SLEW-2 measured value	SLEW-2 certified value	SLEW-2 recovery (%)	SLRS-1 value (%)	SLRS-1 certified value	SLRS-1 recovery (%)	SLEW-3 measured value	SLEW-3 certified value	SLEW-3 recovery (%)
Cd (µg/L)	0.0182	0.0190	96	0.0193	0.0150	129			
	0.0170	0.0190	90						
	0.0176	0.0190	93						
	0.0168	0.0190	88						
	0.0162	0.0190	85						
	0.0179	0.0190	94						
	0.0153	0.0190	81						
Fe (mg/L)				0.0351	0.0315	111			
				0.0348	0.0315	111			

Analyte	SLEW-2 measured value	SLEW-2 certified value	SLEW-2 recovery (%)	SLRS-1 value (%)	SLRS-1 certified value	SLRS-1 recovery (%)	SLEW-3 measured value	SLEW-3 certified value	SLEW-3 recovery (%)
Mn (mg/L)	0.0160	0.0171	94	0.0019	0.0018	105			
	0.0157	0.0171	92	0.0018	0.0018	103			
Co (µg/L)	0.0743	0.0550	135	0.0359	0.0430	84	0.0423	0.0420	101
	0.0768	0.0550	140				0.0459	0.0420	109
	0.0773	0.0550	140				0.0426	0.0420	101
	0.0743	0.0550	135				0.0416	0.0420	99
	0.0772	0.0550	140				0.0436	0.0420	104
	0.0780	0.0550	142				0.0443	0.0420	106
	0.0766	0.0550	139						
Ni (µg/L)	0.7359	0.7090	104	1.1143	1.0700	104	1.1379	1.2300	93
	0.7178	0.7090	101				1.2388	1.2300	101
	0.6834	0.7090	96				1.2198	1.2300	99
	0.7337	0.7090	103				1.2688	1.2300	103
	0.6756	0.7090	95				1.2754	1.2300	104
	0.7048	0.7090	99				1.1778	1.2300	96
	0.6822	0.7090	96						
	0.7215	0.7090	102						
Cu (µg/L)	1.8103	1.6200	112	3.9738	3.5800	111	1.6374	1.5500	106
	1.7285	1.6200	107				1.5730	1.5500	101
	1.6297	1.6200	101				1.6990	1.5500	110
	1.7207	1.6200	106				1.6885	1.5500	109
	1.7146	1.6200	106				1.6846	1.5500	109
	1.7097	1.6200	106				1.7213	1.5500	111
	1.7135	1.6200	106						
	1.7516	1.6200	108						
Zn (µg/L)	1.3395	1.1000	122	1.3449	1.3400	100			
	1.2056	1.1000	110						
	1.1127	1.1000	101						
	1.1792	1.1000	107						
	1.2048	1.1000	110						
	1.1289	1.1000	103						
	1.1789	1.1000	107						
	1.2592	1.1000	114						
Pb (µg/L)	0.0219	0.0270	81	0.1515	0.1060	143	0.0092	0.0090	102
	0.0204	0.0270	76						
	0.0229	0.0270	85						
	0.0251	0.0270	93						
	0.0230	0.0270	85						
	0.0234	0.0270	86						
	0.0233	0.0270	86						

Table 4. Method blanks and detection limits for trace element analyses of groundwater at OU 1.

FORT ORD 2003 METHOD BLANKS AND METHOD DETECTION LIMIT								
ID	Cd (µg/L)	Fe (mg/L)	Mn (mg/L	Co (µg/L)	Ni (µg/L)	Cu (µg/L)	Zn (µg/L)	Pb (µg/L)
QB-1	0.0012	0.0010	0.0000	0.0015	0.0015	0.0535	ND	0.0044
QB-2	0.0010	0.0008	0.0001	0.0017	0.0160	0.0521	ND	0.0039
QB-3	0.0019	0.0003	0.0002	0.0025	0.0233	0.0541	ND	0.0034
QB-4	0.0021	0.0018	0.0002	0.0026	0.0066	0.0317	ND	0.0050
QB-5	0.0012	0.0009	0.0001	0.0019	0.0128	0.0426	ND	0.0052
QB-6	0.0013	0.0011	0.0002	0.0009	0.0176	0.0413	ND	0.0051
QB-7				0.0053	0.0904	0.0347	ND	0.0036
QB-8				0.0001	ND	0.0638	ND	0.0009
QB-9				ND	ND	0.0694	ND	0.0017
QB-10				0.0005	0.0118	0.0702	ND	0.0020
QB AVG	0.0014	0.0010	0.0001	0.0019	0.0130	0.0459	ND	0.0045
QB STDV	0.0004	0.0005	0.0001	0.0006	0.0079	0.0089	0.0147	0.0007
MDL	0.0013	0.0015	0.0002	0.0019	0.0236	0.0267	0.0442	0.0022

ND = non-detected

On-line sampling system

An on-line sampling system for trace element collections and processing was installed on the groundwater monitoring wells and located at various sites to monitor VOC contamination in the OU 1 aquifer (Figure 2). After a preliminary examination of the monitoring wells, it was determined that the sampling equipment (pipes, pumps, and tubing) used on-site was sufficiently trace metal clean to be suitable for collecting samples for relatively low level trace metal concentration measurements. As a result, existing sampling equipment was modified to enable additional collections of samples for complementary trace element analyses.

The automated sampling setup involves pumping groundwater from the wells through cation exchange mini-columns (part #MC-1CNM, Global-FIA, Fox Island, WA) packed with Toyopearl AF-Chelate-650M iminodiacetate resin (Tosohaas, Montgomeryville, PA). Use of this resin allows the

extracted metals in the column to be easily preserved and eliminates the lengthy logistics and laborious preservation techniques associated with the collection of water using sample bottles (Creasey and Flegal, 1999; Ndung'u *et al*, 2003). The resin columns are subsequently returned to the laboratory, where the trace metals are eluted with dilute, quartz-distilled HNO_3 (Optima® grade, Fisher Scientific, Pittsburgh, PA) and analyzed for elemental concentrations with a magnetic sector inductively coupled plasma mass spectrometer (Finnigan ELEMENT, Thermo Electron Corporation, Bremmen, Germany) using a Glass Expansion Conikal nebulizer and a Scott-type double pass spray chamber cooled to 10° C (Ndung'u *et al.*, 2003).

All the monitoring wells are connected to an eight channel peristaltic pump (Rainin Instruments, Oakland, CA) via small gauge (1/16 in.) PVC or Teflon tubing. The pump is connected to an electrically activated 10-port multi-position valve (Valco Instruments, Houston, TX), which directs the flow from a single well to a second multi-position valve which redirects the flow to a specific cation exchange column. A separate line designated for waste is attached to the second multi-position valve (Figure 3). Between each discrete sample, the sample line is flushed with groundwater from the next well to be sampled and that water is redirected into a waste container. The duration of flushing is dependent upon the speed of the pump, but is long enough to completely replace the water currently in the line with groundwater from the next well to be sampled. This systematic flushing ensures that the columns are always exposed to uncontaminated water from the correct well. The peristaltic pump and valve switching are controlled by a simple computer program written in Pascal (Turbo Pascal v. 5.5 and 6.0, Borland, Scotts Valley, CA).

Weather sampling system

A Real-time Environmental Information Network and Analysis System (REINAS) meteorological station (Rosen et al. 1998) was installed at the Fort Ord Natural Reserve. The station allows real-time weather conditions at the site to be remotely monitored over the Internet. The weather station is connected to the UCSC (LAN) networks and Internet T1 connection via a 33-mile line-of-sight wireless link. Using two 900 MHz, 128 Kbaud transceivers, the REINAS meteorological station is connected by a point-to-point link to a relay computer in the Santa Cruz Mountains. From there, the relay computer is attached to the Internet with a wired DSL line, allow-

ing computers at the Fort Ord site access to the network. The REINAS software package uses a multi-stream capable publisher that allows multiple programs access to the current weather data from the meteorological equipment. For the system at Fort Ord, the main instrument on the REINAS Weather Station is the rain gauge.

Automated sampling system

In order to remotely trigger the pump to begin sampling, two computer programs are needed. The first program, RCHECK, analyzes the real-time meteorological conditions while the second program, AUTO, controls the pump and sample collection automation. By using the REINAS software libraries, RCHECK acts as a REINAS client program, giving it access to the current weather data produced by the meteorological station. The RCHECK program then monitors a user defined instrument on the weather station (i.e., rain gauge) and waits for the value of this instrument to reach a user defined trigger level. Once the desired trigger value is reached, the RCHECK program sends a signal through a serial line to the pump directing the pump program to start. RCHECK then logs the date and time the signal was sent, along with whether or not the pump control program sent back an acknowledgement. A script is then run which e-mails a message to a list of people informing them of the sample collection.

The control of the sampling set-up (i.e., switching of the peristaltic pump and multi-position valves) is by a computer via digital TTL signals using a digital I/O card (DCI SmartLab 8255 I/O card, Decision Computers, Taiwan). The program that controls the I/O card was written in Pascal (Turbo Pascal v. 5.5 and 6.0, Borland, Scotts Valley, CA). The program was a slight modification of the one used by Malcus et al. (1996) for automated trace element enrichment in the lab which required user input through a menu system to load a specific program and/or perform operations.

That code was modified to eliminate the menu system and, instead, use predetermined settings to initialize the program for its sampling operations. The program was further modified to initiate when it received a signal over the serial port from the REINAS client program, RCHECK. The modified pump automation program polls the serial line waiting for a signal, and then it performs the sample preload operation when a signal is received. After the pump program has completed, it returns to polling the serial line for another signal to start pumping again. Thus the combined

use of the three programs (REINAS, RCHECK and AUTO) allows full automation of entire sampling process during a user defined rainfall period.

3 Results and Discussion

Groundwater flow monitoring technologies

ISPFS

Three of the ISPFSs installed in 1999 have produced reasonable data since that time, and data extracted from these devices, associated with MW-OU1-36-A, MW-OU1-37-A, and MW-OU1-39-A, are discussed in this report. Detailed analyses of the entire records for these sensors, and how their data correlate with aquifer characteristics at the site, are presented in a companion report (Jordan et al. 2005). Preliminary evaluation of ISPFS data from the site indicated suspiciously large vertical components to groundwater flow; in some cases downward vectors were calculated to be as large or larger than the horizontal vectors calculated with the Hydrotechnics® data processing software, HTFlow95. Since this result was highly counterintuitive, given installation in a homogeneous sand aquifer with very low water-table gradients, a detailed simulation analysis of ISPFS thermal behavior was executed (Su et al. 2005; in press). The reader is referred to this work for greater detail. Owing to possible complications described in the simulation study, vertical components of flow are not presented here.

Logging with the HPL and SCBFM systems took place between March 17 and March 25, 2004. Both horizontal flow velocity and azimuth were very stable, as had been the case for these sensors. During this interval, pumping was continuous on extraction well EW-OU1-17-A. Azimuth values were corrected for magnetic declination based on compass readings taken during installation of the ISPFS devices. Velocities and azimuths for the data are shown in Table 5. Means and standard deviations of direction were calculated utilizing Yamartino's method (Yamartino 1984).

Table 5. Comparison of ISPFS azimuth and horizontal flow velocities at OU 1, March 14 to March 22, 2004.

Source	MW-OU1-36-A	MW-OU1-37-A	MW-OU1-39-A
Azimuth	312±1.4°	311±0.3°	298±1.33°
Horizontal velocity	1.52 ft/day	0.107 ft/day	0.154 ft/day

Further discussion of the response of the ISPFS sensors to changes in extraction well pumping rates can be found in Jordan et al. (2005).

Hydrophysical logging

Logging of fluid electrical conductivity (FEC) and temperature was conducted by RAS, Integrated Subsurface Evaluation, Inc., in monitoring well MW-OU1-39-A on March 23, 2004, and well MW-OU1-36-A on March 24 and March 25, 2004. Although an attempt to introduce the HPL tool into MW-OU1-37-A was made on March 24, a bend in the casing approximately 20 feet below the ground surface prevented entry.

Details of the lithology and construction of the combined ISPFS/monitoring wells installed in 1999 can be found in Oldenburg (2002). Monitoring well MW-OU1-36-A is a 2-inch diameter, pvc cased well with a screen from 51 to 81 ftbgs. Groundwater was reached at 63.42 feet below ground surface prior to an initial "ambient" HPL scan to establish background conductivity and temperature conditions on March 24, 2004. Emplacement of deionized water took place the following morning, in the same manner described in Wilson et al. (2001). The HPL tool was calibrated with salt solutions prior to insertion in the well and placed just below the water surface. Then 20 μS/cm water was pumped into the well with a peristaltic pump through a tube inserted to the bottom of the well. Thirty-seven gallons of low FEC water were injected, while 35.3 were extracted, all the while monitoring the HPL conductivity readings to detect the time at which formation water had been displaced by the low FEC fluid. Subesquent logging of the well was performed at approximately hourly intervals. A total of 8 scans were completed, as shown in Figure 13.

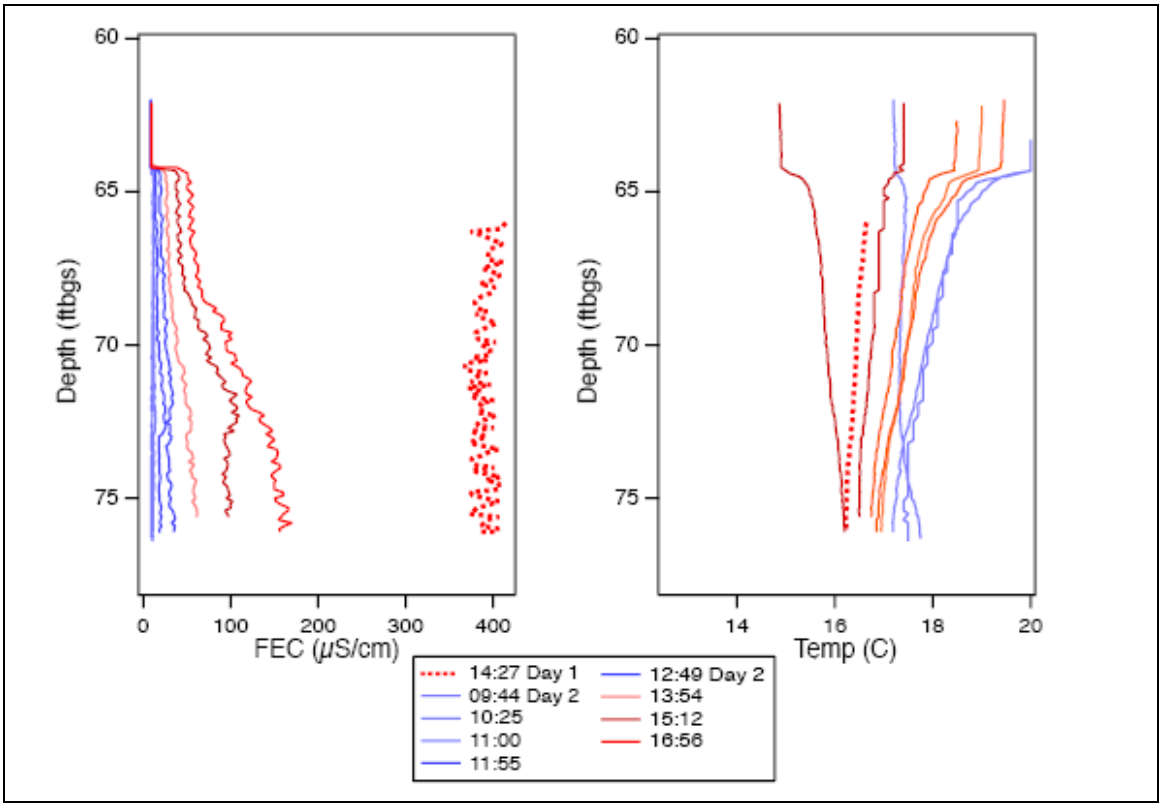

Figure 13. Hydrophysical logging data from MW-OU1-36A, March 25, 2004: depth profile of electrical conductivity (a) and fluid temperature (b) following an initial scan of ambient conditions (dotted lines), replacement of borehole fluid with deionized water, and reinfiltration with formation water.

MW-OU1-39-A is also a 2-inch, pvc cased monitoring well with a screened interval between 69.5 and 94.5 feet. The ambient water level prior to initial scanning was 86.70 feet below the ground surface on March 23, 2004. Setup, tool calibration, ambient scanning, low FED fluid emplacement and logging took place on the same day and the following morning, and was performed as described above. There were 12 post-emplacement scans in all (Figure 14). Both monitoring wells exhibited reasonably uniform rates of FEC displacement over the vertical extent of logging, and the results were calculated by treating the entire borehole as a single “inflow feature.” The interval specific flow rate, borehole velocities and specific discharge values for these wells are shown in Table 6.

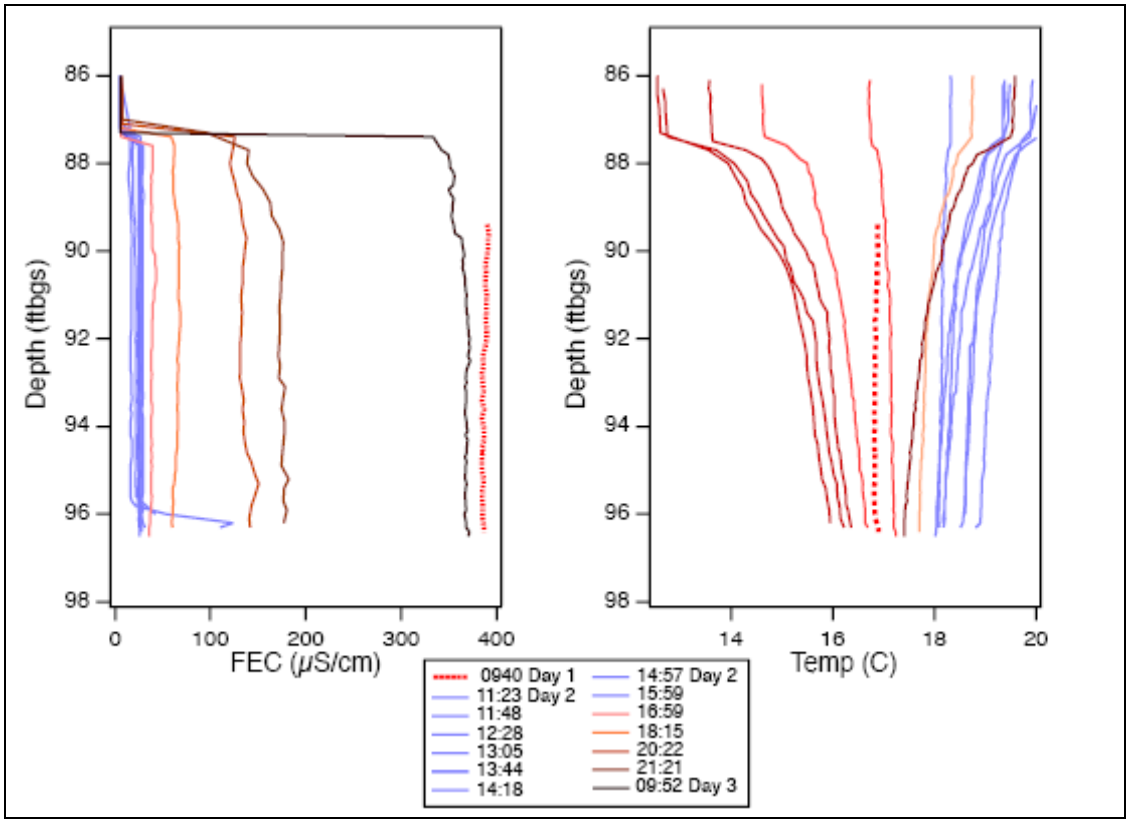

Figure 14. Hydrophysical logging data from MW-OU1-39A, March 23, 2004: depth profile of electrical conductivity (a) and fluid temperature (b) following an initial scan of ambient conditions (dotted lines), replacement of borehole fluid with deionized water, and reinfiltration with formation water.

Table 6. Hydrophysical logging estimates of flow rate, within-borehole velocity and specific discharge at OU 1, March23 to March 25, 2004.

Monitoring Well	Depth Interval (feet below ground surface)	Interval Specific Flow Rate, Velocity, and Specific Discharge for Ambient Conditions.		
		q (gpm)	*v** (ft/day)	Sd (ft/day)
MW-OU1-36-A	64-78	0.001	0.22	0.10
MW-OU1-39-A	87-97	0.001	0.21	0.08

Scanning colloidal borescope flowmeter

The LLNL Scanning Colloidal Borescope Flowmeter was used to log particle velocities in all three OU 1 monitoring wells selected for this study, and the entire vertical extent of water was scanned for each at approximately 2-foot intervals. MW-36-A was scanned on March 17, 2004 at seven depths, from 62.37 ft to 71.37 feet. MW-OU1-37-A was scanned on March 20 and 21, 2004, at fourteen depths, and MW-OU1-39-A was scanned on

March 22, 2004, at five depths. In each case the SCBFM magnetometer reading was checked against a compass prior to insertion into the well, the tool was lowered to the desired depth, which was detected from permanent marks on its supporting cable, and clamped to the pvc casing to allow the groundwater flow to equilibrate. The video signal could be monitored in a trailer at the wellhead. recording generally commenced within 10 minutes of reaching a new position.

Particle transport was observed on the video monitor and recorded on standard VHS tape for later processing. The particle tracking code used was a Beta-test version of DOS-based software developed by John Wilson (at the time with Oak Ridge National Laboratory). In general, numerous particles were visible in recordings from the OU 1 wells and the average values for their velocities and directions were averaged by the tracking software to contribute to each data point used for subsequent plotting and data reduction. The average numbers of particles tracked per point for each depth are given in Tables 7, 8, and 9, along with the calculated average particle velocity and azimuth. Reported azimuth values were corrected for magnetic declination. In order to minimize errors in calculating average azimuth, owing to data clustered around true north, a spreadsheet formulation implementing the Yamartino algorithm (originally developed for calculating average wind direction and standard deviation) was used (Yamartino 1984).

Table 7. SCBFM logging estimates of within borehole groundwater velocity and direction from MW-OU1-36-A, collected on March 17, 2004.

Depth (ftbgs)	Average # of particles tracked[1]	Velocity (ft/day)[1]	Azimuth (°±S.D.)[2]	Remarks
62.37	35	—	—	Variable flow and direction
63.87	46	—	—	Variable flow and direction
65.37	43	5.5	190 ± 56.5	Stable flow
66.87	39	—	—	Variable flow and direction
68.37	60	3.0	4.8 ± 23.0	Stable flow
69.87	60	3.1	83.8 ± 23.6	Stable flow
71.37	36	3.3	310 ± 58.2	Stable flow

[1]Arithmetic means for the number of particles tracked, per point, for entire scan

[2]Calculated as per Yamartino (1984).

Table 8. SCBFM logging estimates of within borehole groundwater velocity and direction from MW-OU1-37-A, collected on March 20 and March 21, 2004.

Depth (ftbgs)	Average # of particles tracked[1]	Velocity (ft/day)[1]	Azimuth (°±S.D.)[2]	Remarks
62.92	35	7.0	144 ± 23.9	Stable flow
64.42	35	—	—	Stable flow, unstable direction
65.92	38	6.5	93.5 ± 32.0	Stable flow
67.42	26	7.5	91.4 ± 11.0	Stable flow
68.92	47	8.0	282 ± 33.2	Stable flow
70.42	30	16.3	208 ± 17.5	Stable flow
71.92	19	11.3	130 ± 22.3	Stable flow
73.42	52	10.4	173 ± 7.4	Stable flow
74.92	44	22.7	139 ± 3.3	Stable flow
76.42	28	11.3	103 ± 10.4	Stable flow
77.92	44	22.7	139 ± 5.2	Stable flow
79.42	27	13.7	148 ± 6.7	Stable flow
80.92	32	9.6	112 ± 5.0	Stable flow
82.42	32	10.2	162 ± 8.8	Stable flow

[1]Arithmetic means for the number of particles tracked, per point, for entire scan

[2]Calculated as per Yamartino (1984).

Table 9. SCBFM logging estimates of within borehole groundwater velocity and direction from MW-OU1-36-A, collected on March 17, 2004.

Depth (ftbgs)	Average # of particles tracked[1]	Velocity (ft/day)	Azimuth (°±S.D.)[2]	Remarks
86.01	45	—	—	Variable flow and direction
87.51	27	5.64	41.9 ± 8.3	Stable flow
88.01	48	18.8	27.6 ± 10.0	Stable flow
89.51	52	11.0	27.4 ± 6.1	Stable flow
91.01	60	8.2	25.2 ± 31.6	Stable flow

[1]Arithmetic means for the number of particles tracked, per point, for entire scan

[2]Calculated as per Yamartino (1984).

Time series plots of groundwater flow rates and azimuth estimates from SCBFM image analyses are illustrated in Figures 15–24. These are from measurements at MW-OU1-36-A, MW-OU1-37-A, and MW-OU1-39-A at depths ranging from 62.37 to 91.01 ft below the surface. Horizontal bars in the figures indicate regions of stable particle flow rate and direction from which the numerical estimates were made. Dates and measurement depths below ground surface are listed on the upper left side of each figure.

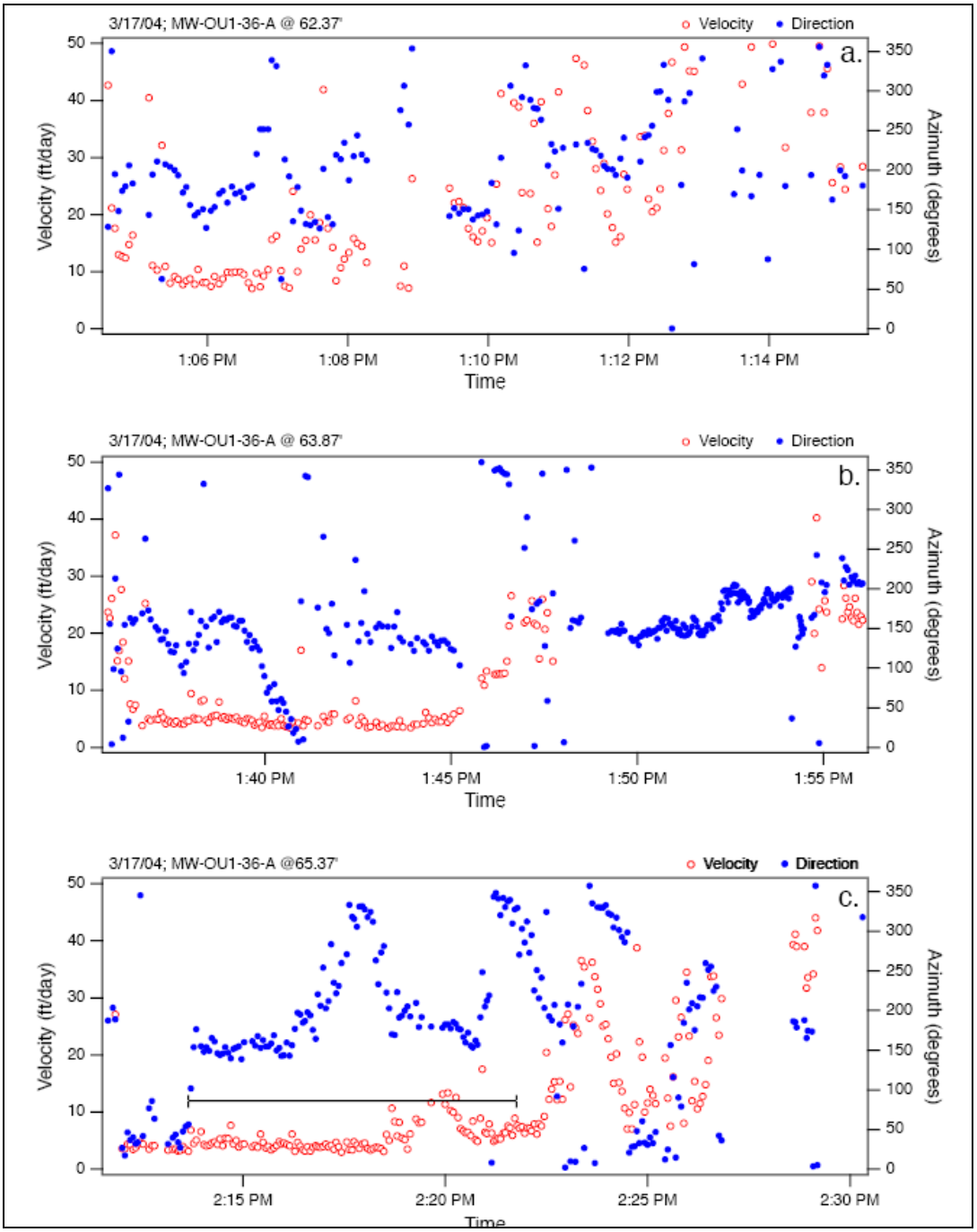

Figure 15. SCBFM flow rates and azimuth estimates for MW-OU1-36-A, depths 1-3.

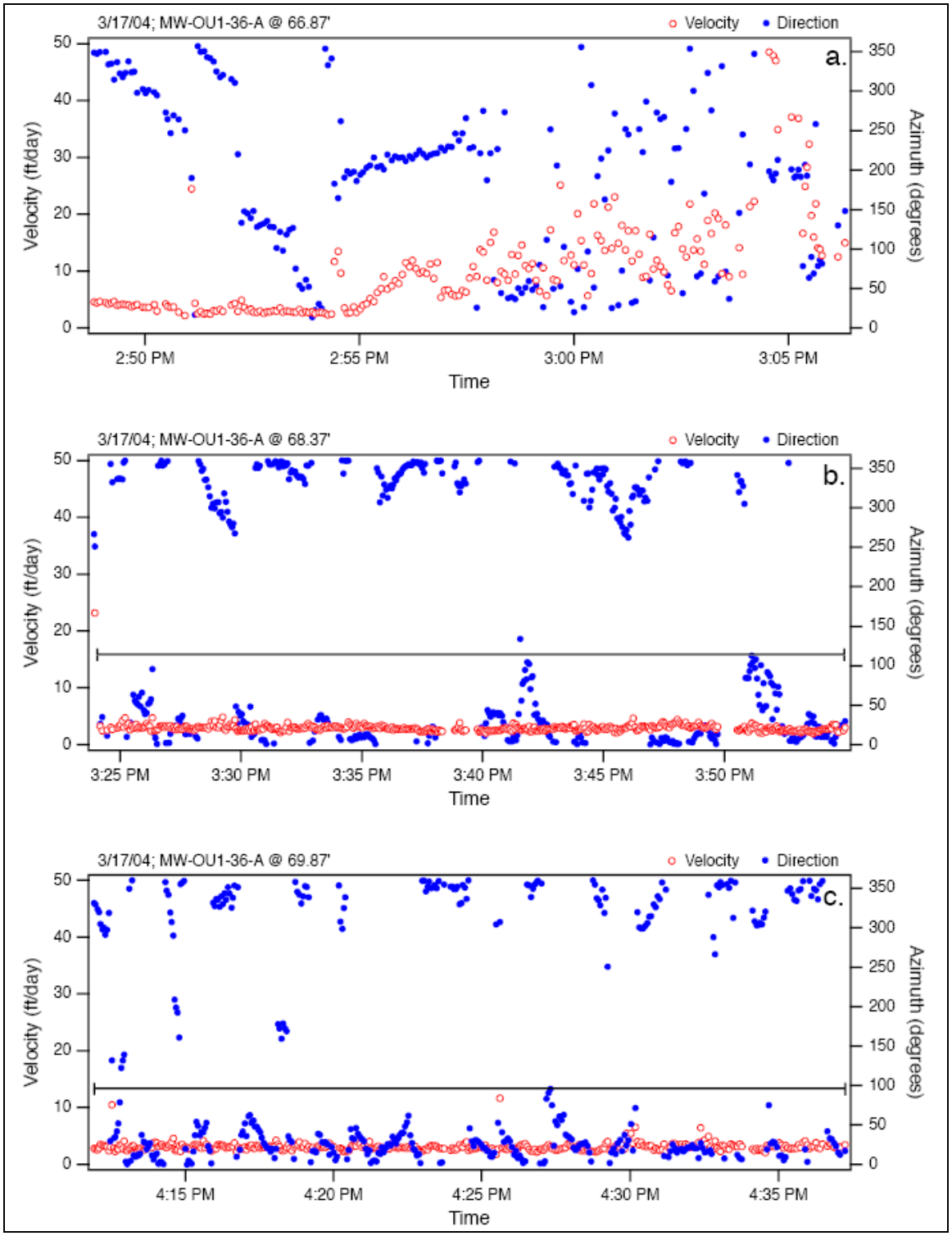

Figure 16. SCBFM flow rates and azimuth estimates for MW-OU1-36-A, depths 4-6.

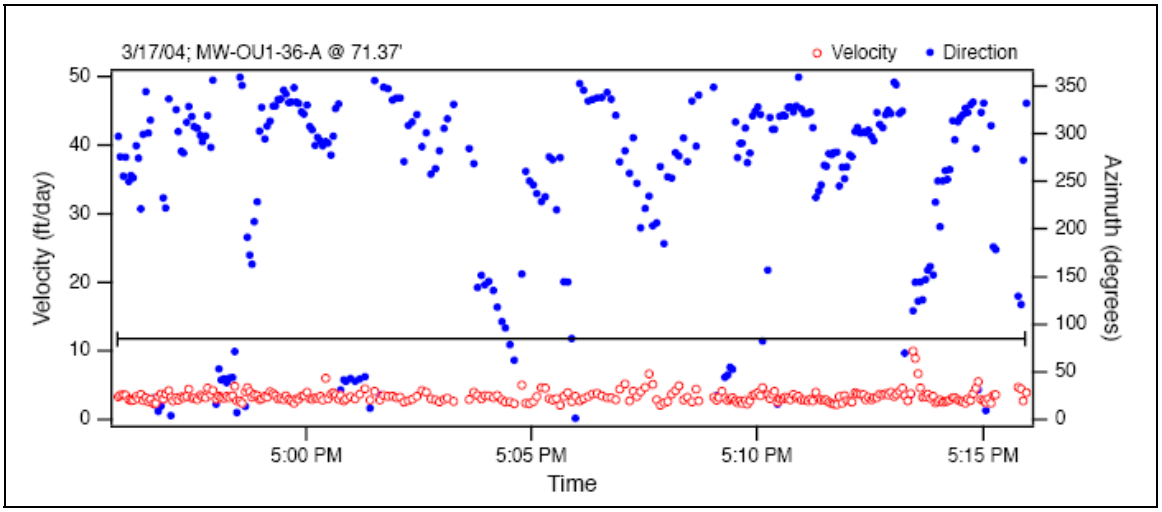

Figure 17. SCBFM flow rates and azimuth estimates for MW-OU1-36-A, depth 7.

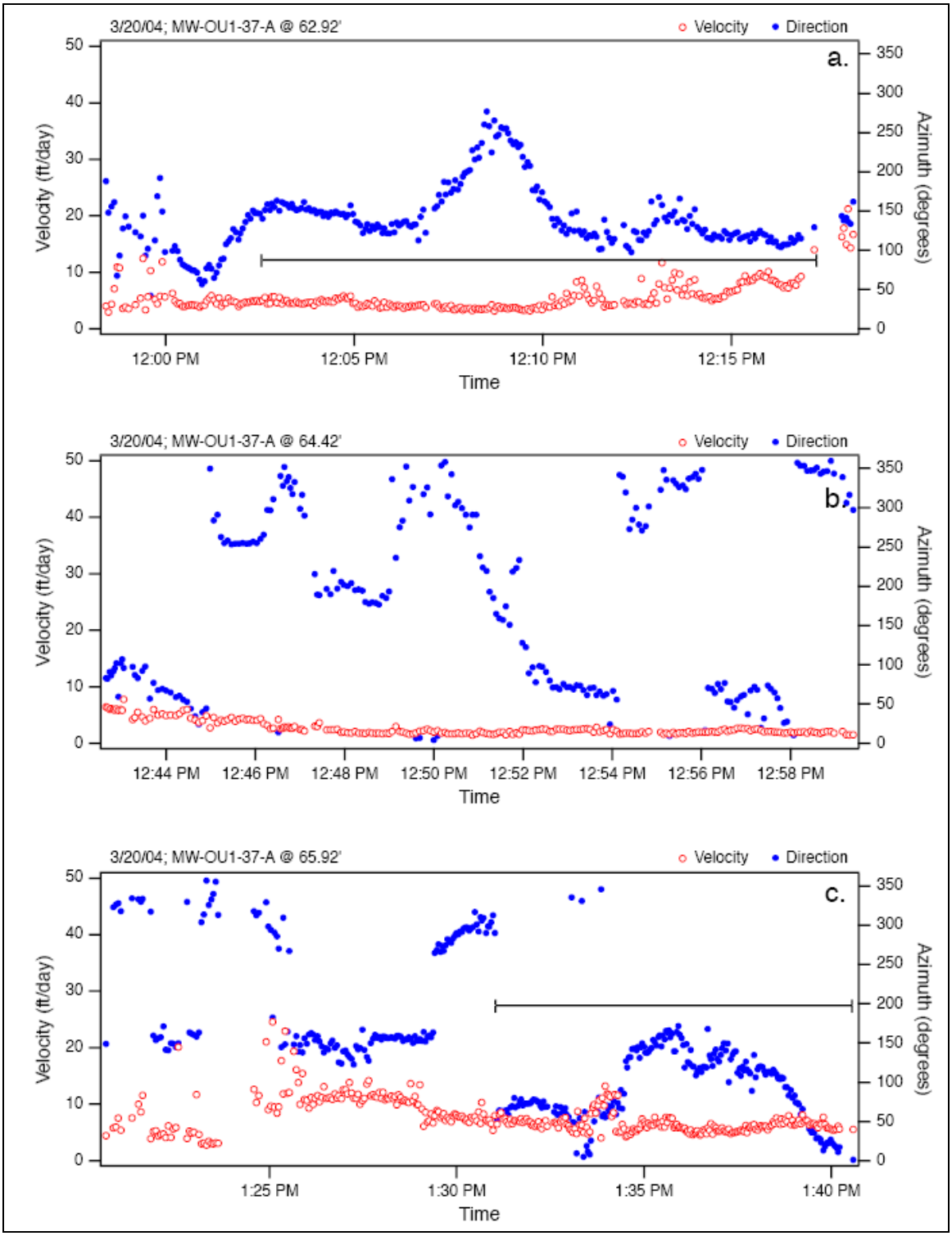

Figure 18. SCBFM flow rates and azimuth estimates for MW-OU1-37-A, depths 1-3.

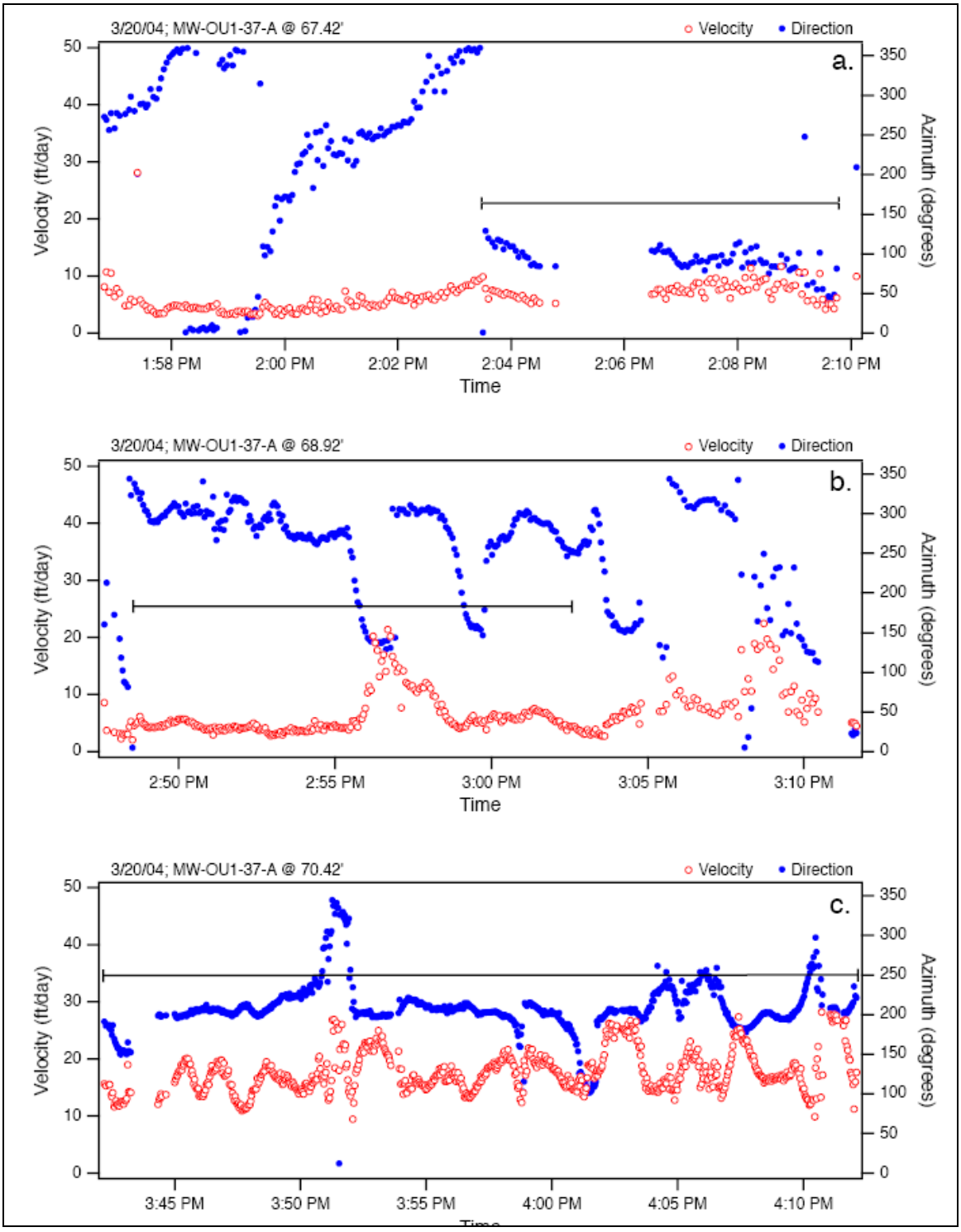

Figure 19. SCBFM flow rates and azimuth estimates for MW-OU1-37-A, depths 4-6.

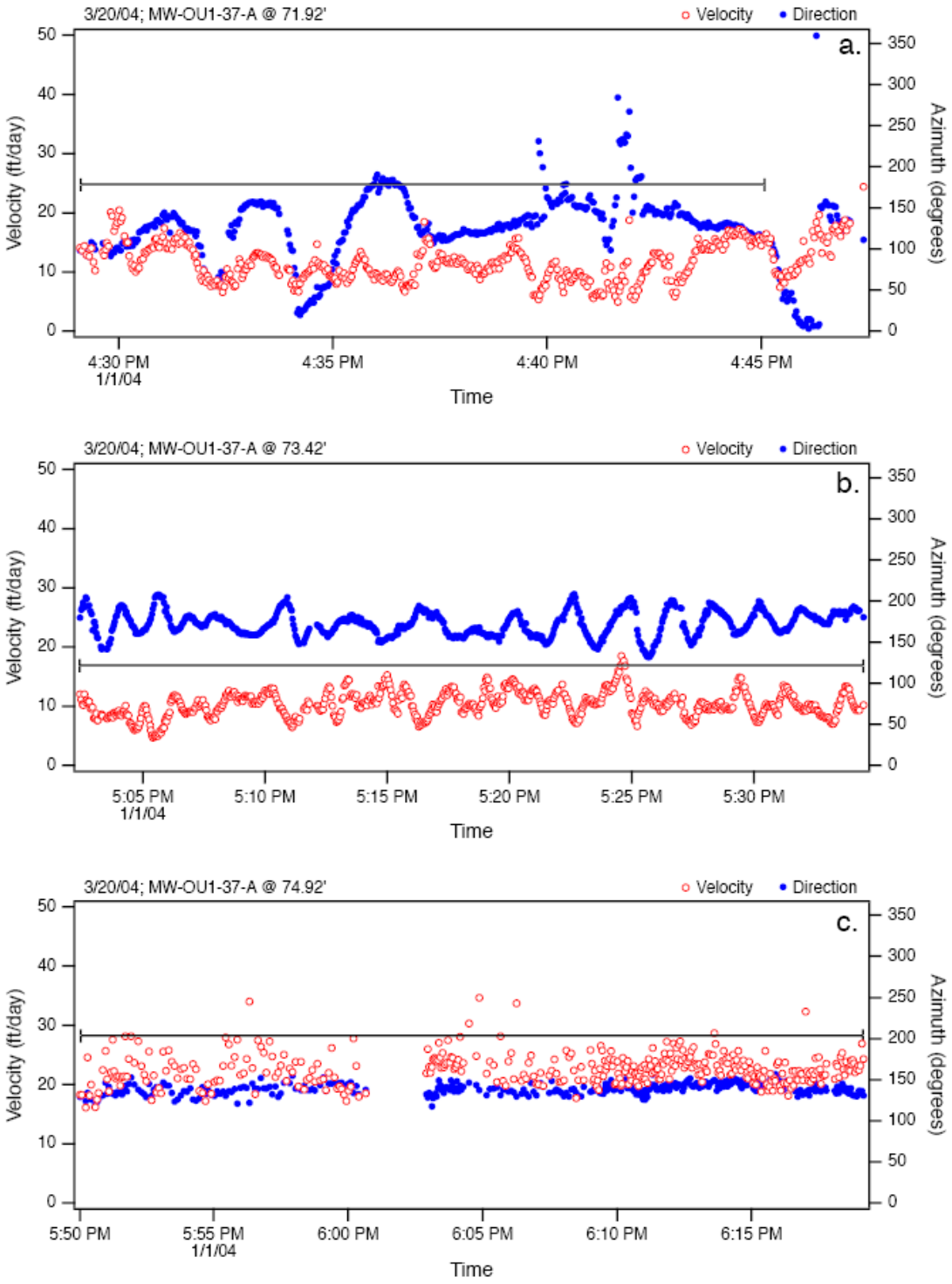

Figure 20. SCBFM flow rates and azimuth estimates for MW-OU1-37-A, depths 7-9.

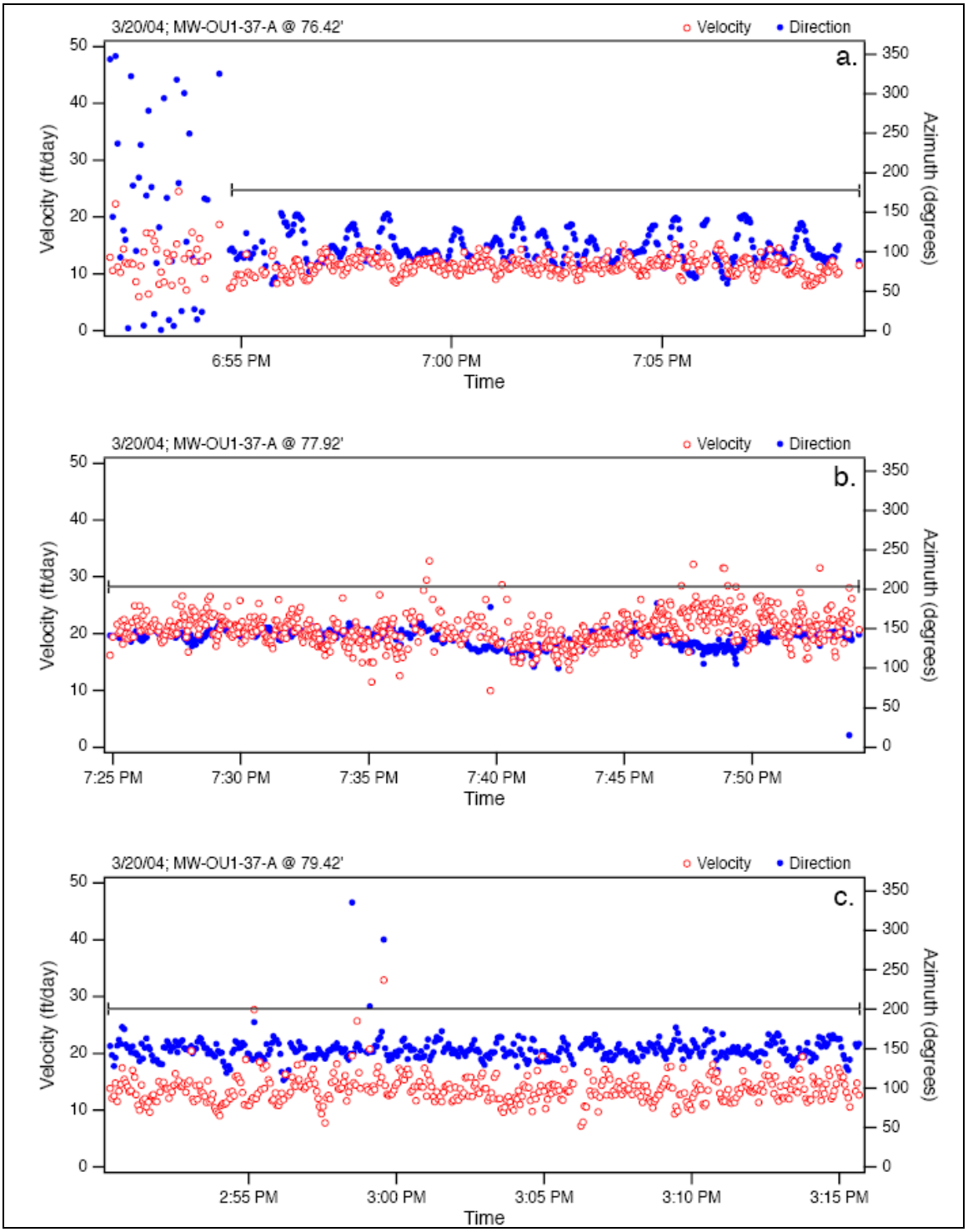

Figure 21. SCBFM flow rates and azimuth estimates for MW-OU1-37-A, depths 10-12.

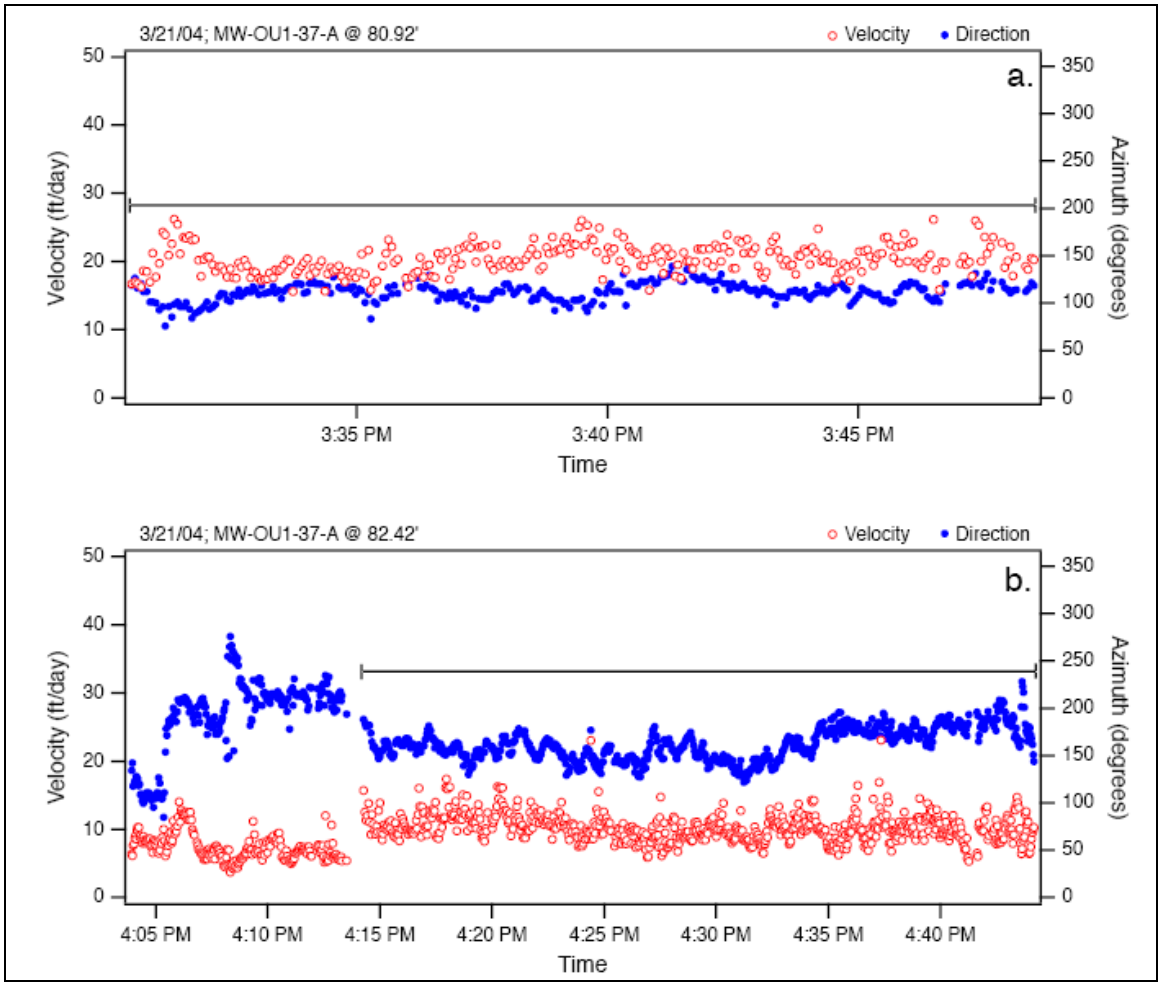

Figure 22. SCBFM flow rates and azimuth estimates for MW-OU1-37-A, depths 13-14.

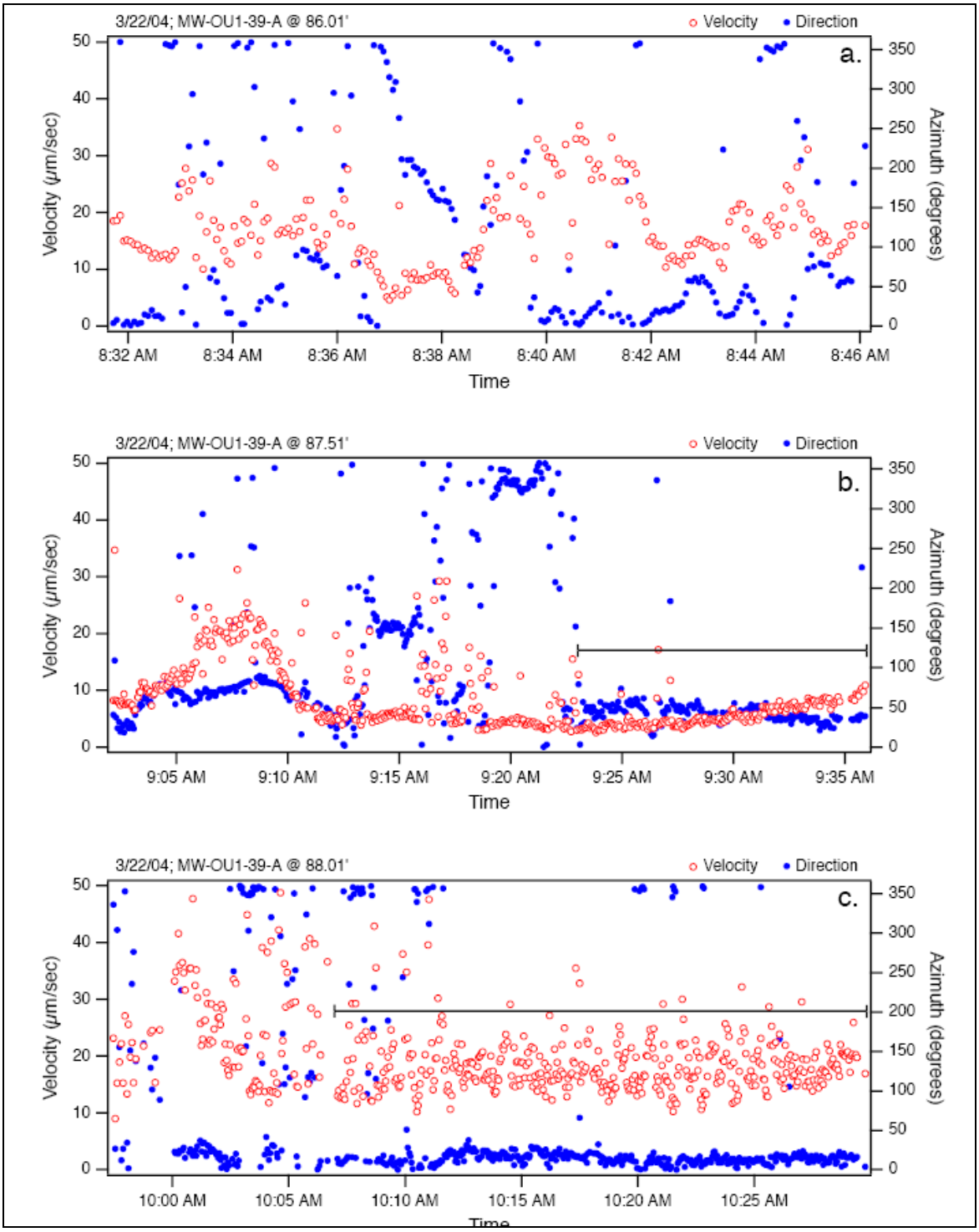

Figure 23. SCBFM flow rates and azimuth estimates for MW-OU1-39-A, depths 1-3.

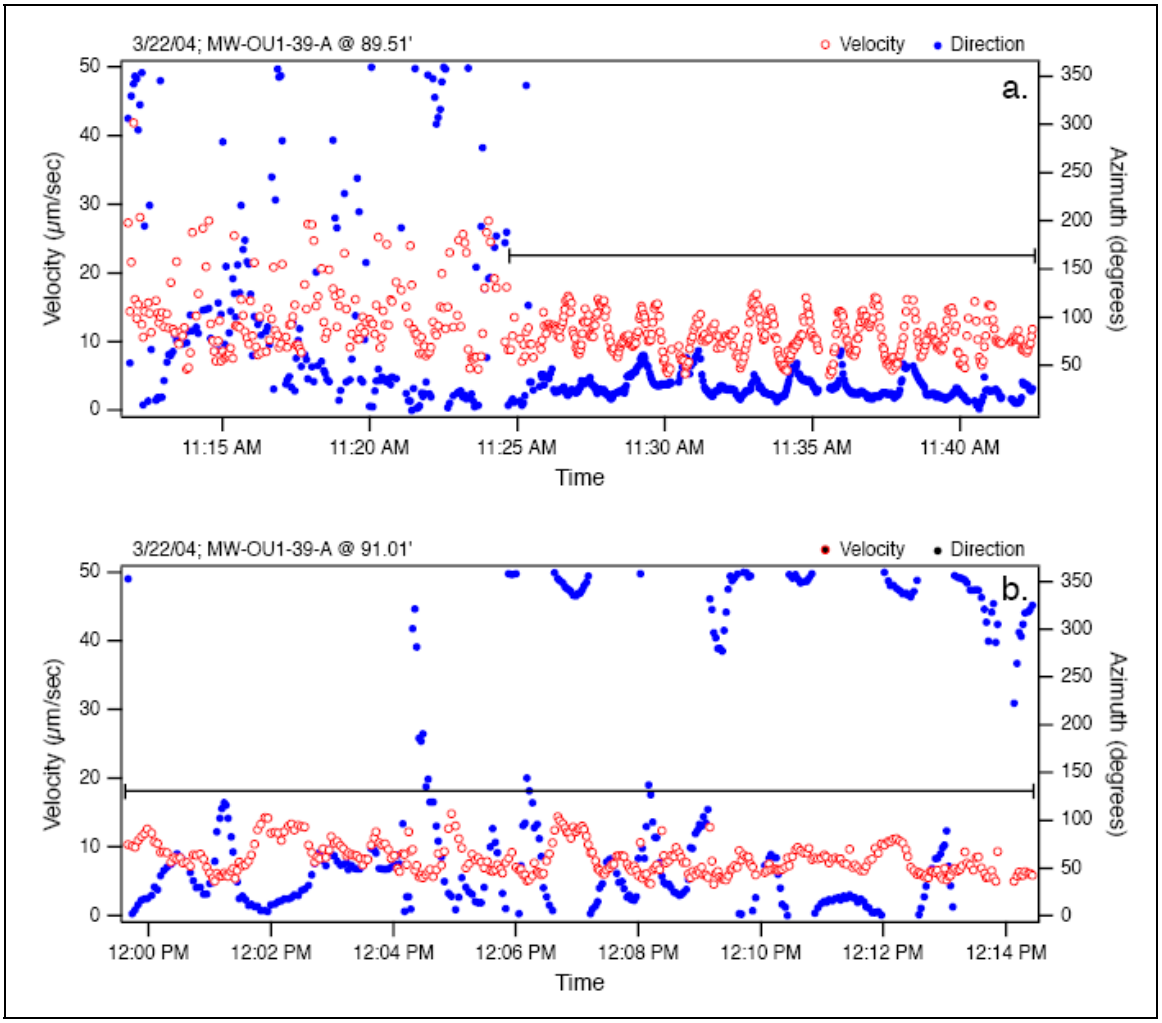

Figure 24. SCBFM flow rates and azimuth estimates for MW-OU1-39-A, depths 4-5.

Analysis of aquifer response, groundwater flow, and plume evolution

Water table

As discussed in Oldenburg et al. (2002), water levels in the A-aquifer rose significantly in response to the precipitation in early (January/February) 1998. As of December 2000 (the latest water levels included in Oldenburg et al. [2002]), the water levels in all of the OU 1 wells and many of the other wells were still increasing or were at their peak in response to the early 1998 precipitation event. The most complete water table map presented in the Oldenburg et al. (2002) report was for the second quarter of 2000. These maps are reproduced as Figures 25 and 26. Figures 27 and 28 show the water table map for the second quarter of 2002. Comparison of the maps reveals that the gradient direction is changing to the southwest and north of the FDA and getting steeper near the edge of the FO-SVA.

Comparison of these maps also reveals that the water table elevation is decreasing in some areas and increasing in others. Finally, the greater well coverage southwest of the FDA in 2002 shows that the gradient upgradient of the edge of Clay 4 is steeper than downgradient, which tends to confirm the hydrostratigraphic model presented in Oldenburg et al. (2002).

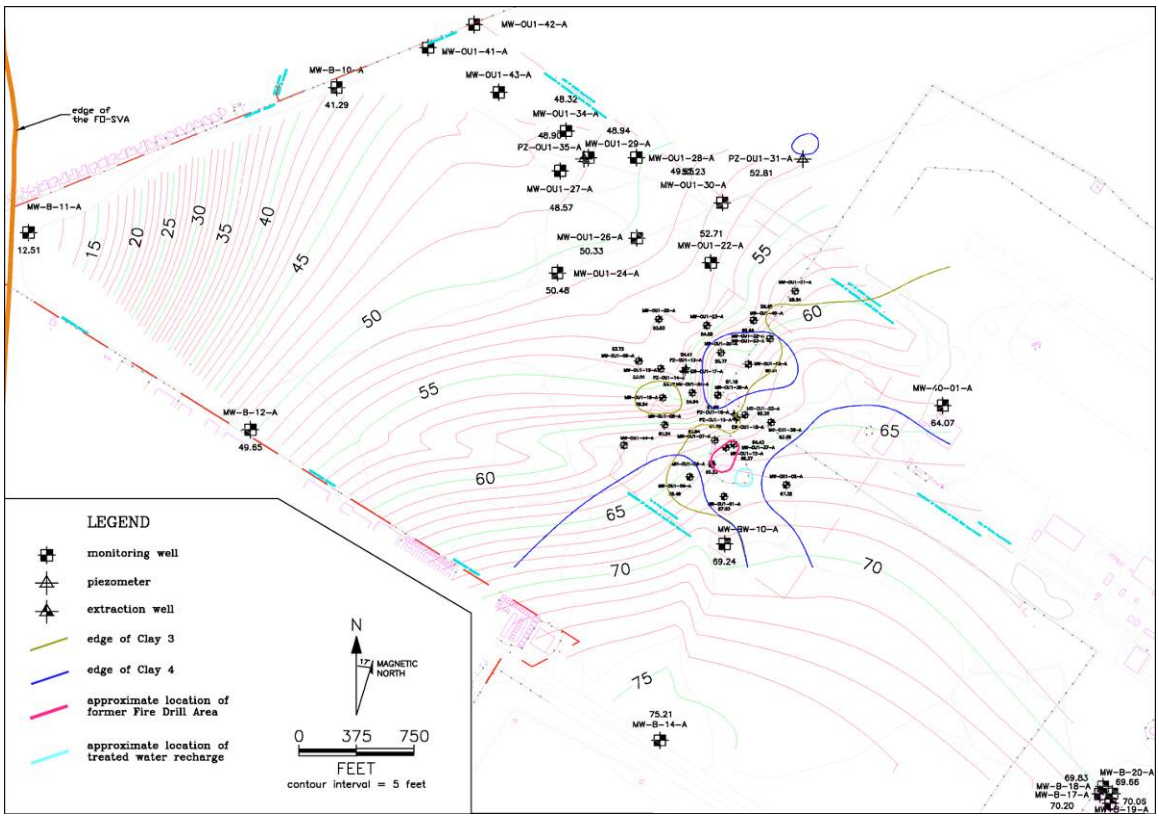

Figure 25. A-aquifer isopotentials for the second quarter, 2000 (modified from Oldenburg et al. 2000).

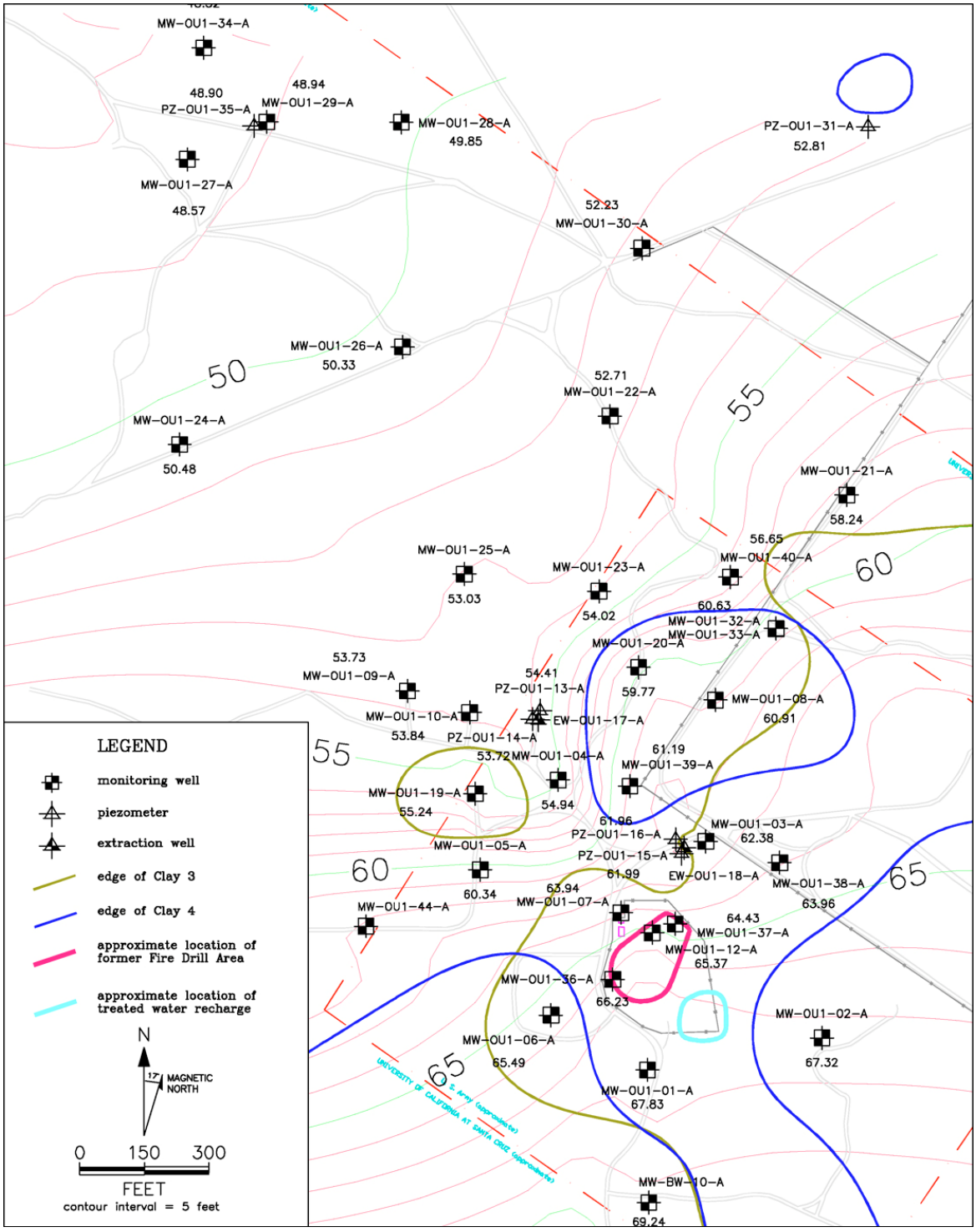

Figure 26. A-aquifer isopotentials for the second quarter, 2000 (modified from Oldenburg et al. 2000).

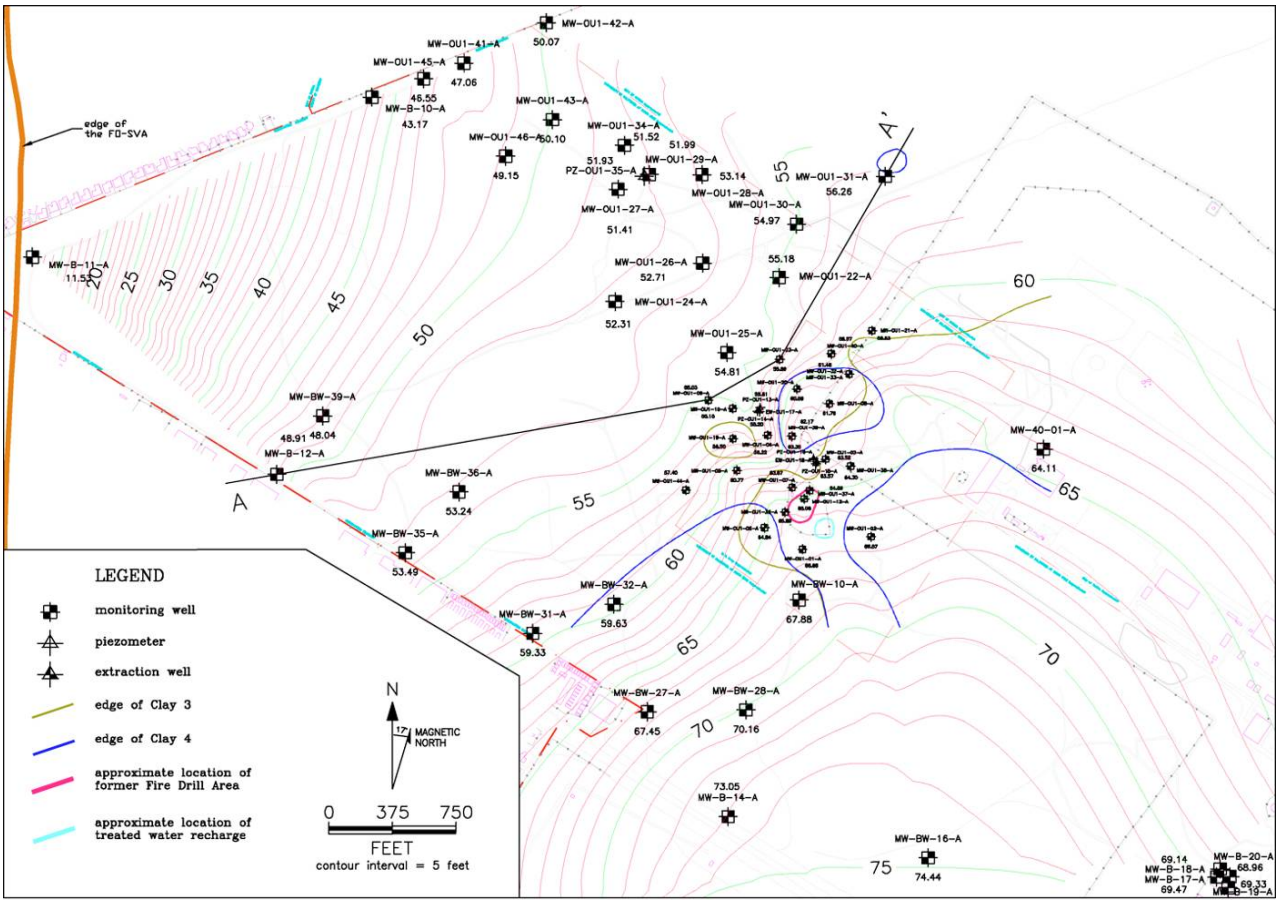

Figure 27. A-aquifer isopotentials for the second quarter, 2002. location of Figure 25 hydrograph transect A-A' shown.

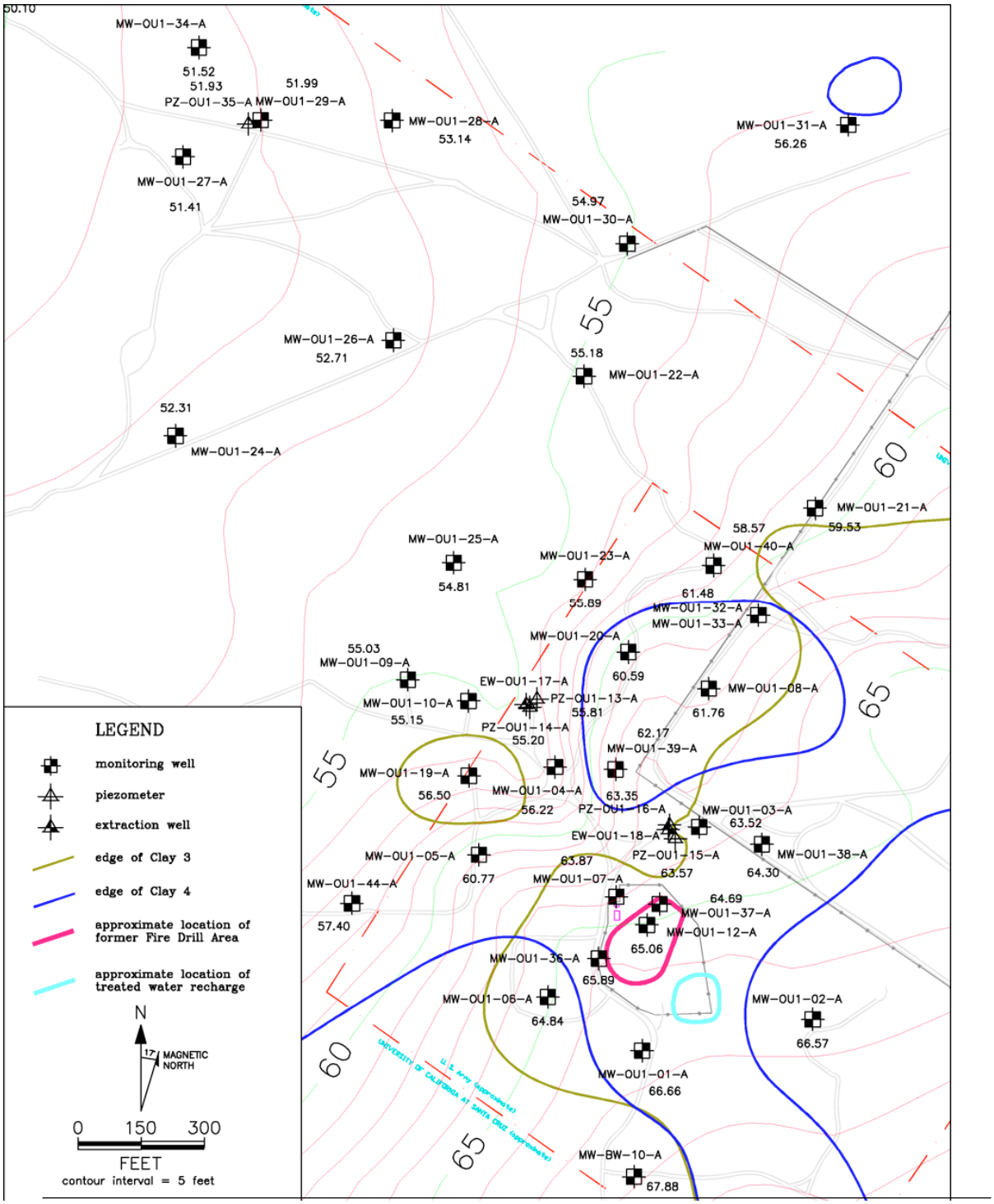

Figure 28. Detail of A-aquifer isopotentials for the second quarter, 2002.

Change in gradient direction: to the north and southwest of the FDA, the gradient was mapped as north northwest-directed in 2000, and northwest-directed in 2002. In the former area, the gradient rotated approximately 20° counterclockwise. Well coverage did not change appreciably

from 2000 to 2002, suggesting the change is real and not due to additional data from new wells. In the latter area, the change is due in part to greater well coverage in 2002. However, some component of this change is probably real. This is demonstrated by the comparison of well hydrographs shown on Figure 29.

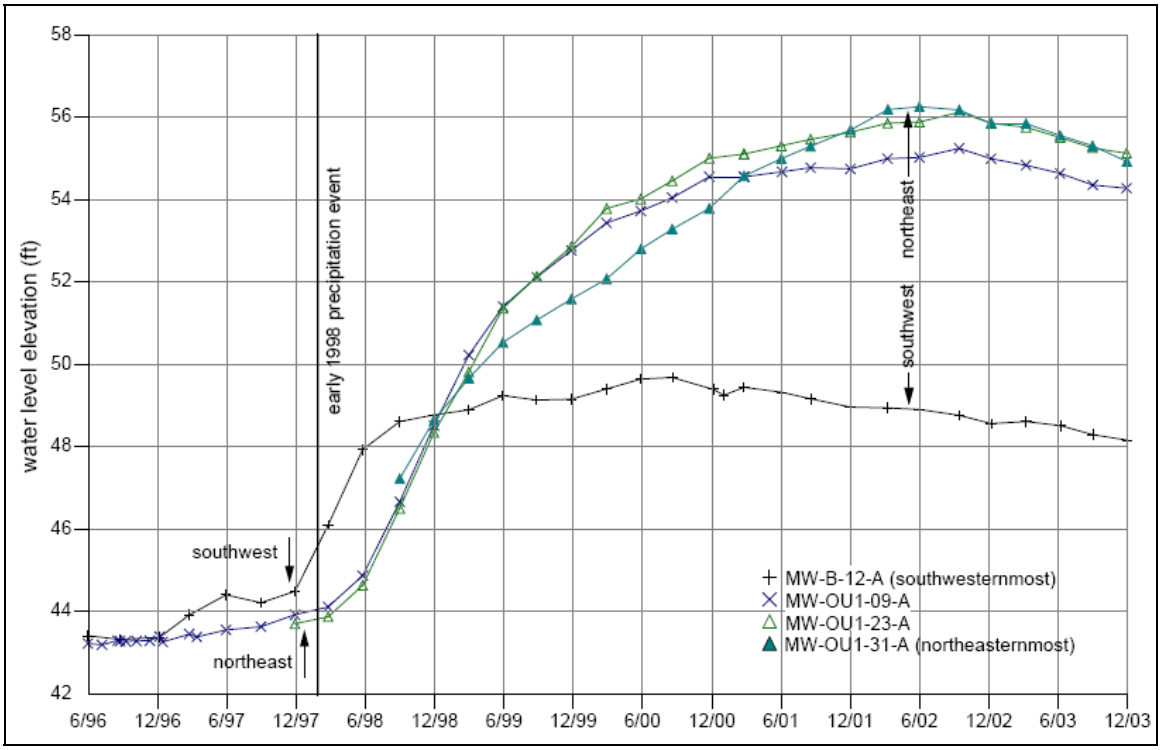

Figure 29. Hydrographs from wells on transect A-A' shown in Figure 27.

The wells in Figure 29 lie on northeast-southwest transect A-A' to the northwest of the FDA, as shown on Figure 27. In general, the water level in each well increases less than in the wells to the northeast and more than in the wells to southwest along the transect. This is demonstrated on a more regional scale by comparing the hydrographs for MW-B-12-A and MW-OU1-31-A, and on a more local scale by comparing the hydrographs for MW-OU1-09-A and –22-A. The effect of this pattern is to rotate the gradient toward the west, which is the location of the edge of the FO-SVA. Therefore, this response appears to be a result of the aquifer's adjustment to transmitting more groundwater after the early 1998 precipitation event.

The well coverage prior to late 1998 is insufficient to resolve the water table north of the FDA during this period. Given the change in gradient direction during the period from 2000 to 2002, however, the actual gradient rotation since 1997 is probably even greater. This supports the conclusion

in Oldenburg et al. (2002) that the gradient from the FDA was directed to the north during much of the time contaminants were being released at OU 1.

Time to peak water level

The variation in the time to peak water levels after the early 1998 precipitation event, as shown on Figures 30 and 31 provides another perspective on the aquifer's adjustment to the early 1998 precipitation event. The distribution of peak times appears to consist of two patterns. One pattern is related to the treated recharge system at OU 1. Water levels in the downgradient area north to northwest of the FDA were apparently depressed prior to 1998 due to evapotranspiration losses from the treated water sprinkler recharge system (Oldenburg et al., 2002). The time to the peak water level throughout this region is relatively long compared to the rest of the aquifer. This is probably due to the longer time required to refill this area with stored water so that the gradient could rotate from alignment along the depression created by the recharge losses to across the depression to optimize the discharge of the increased flow resulting from the early 1998 precipitation event. Figures 32 and 33 confirm this hypothesis by showing that the water level increase in the downgradient area north to northwest of the FDA was greater than throughout the rest of the aquifer on both an absolute basis and as a percentage of the pre-1998 saturated thickness.

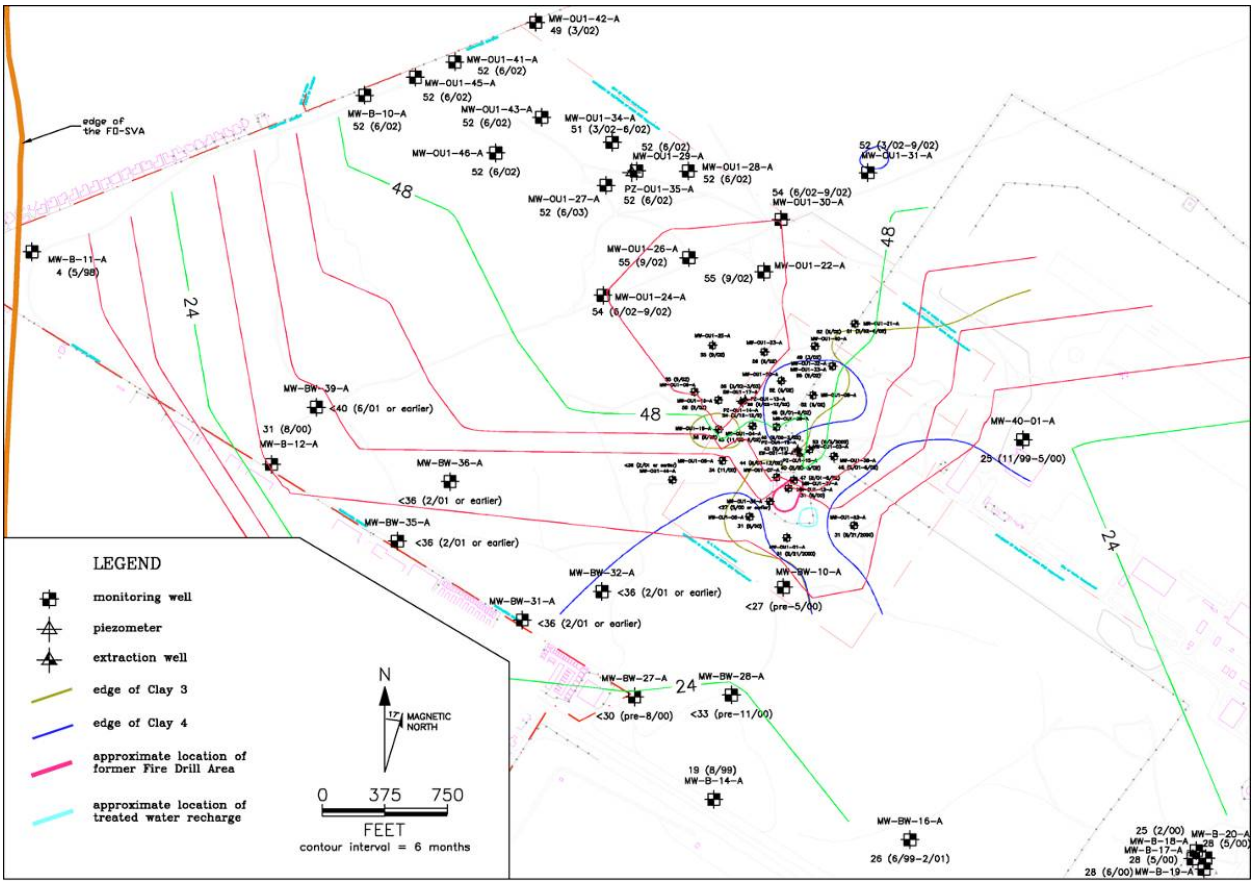

Figure 30. Isochrons (in months) of time to peak water level following the early 1998 precipitation.

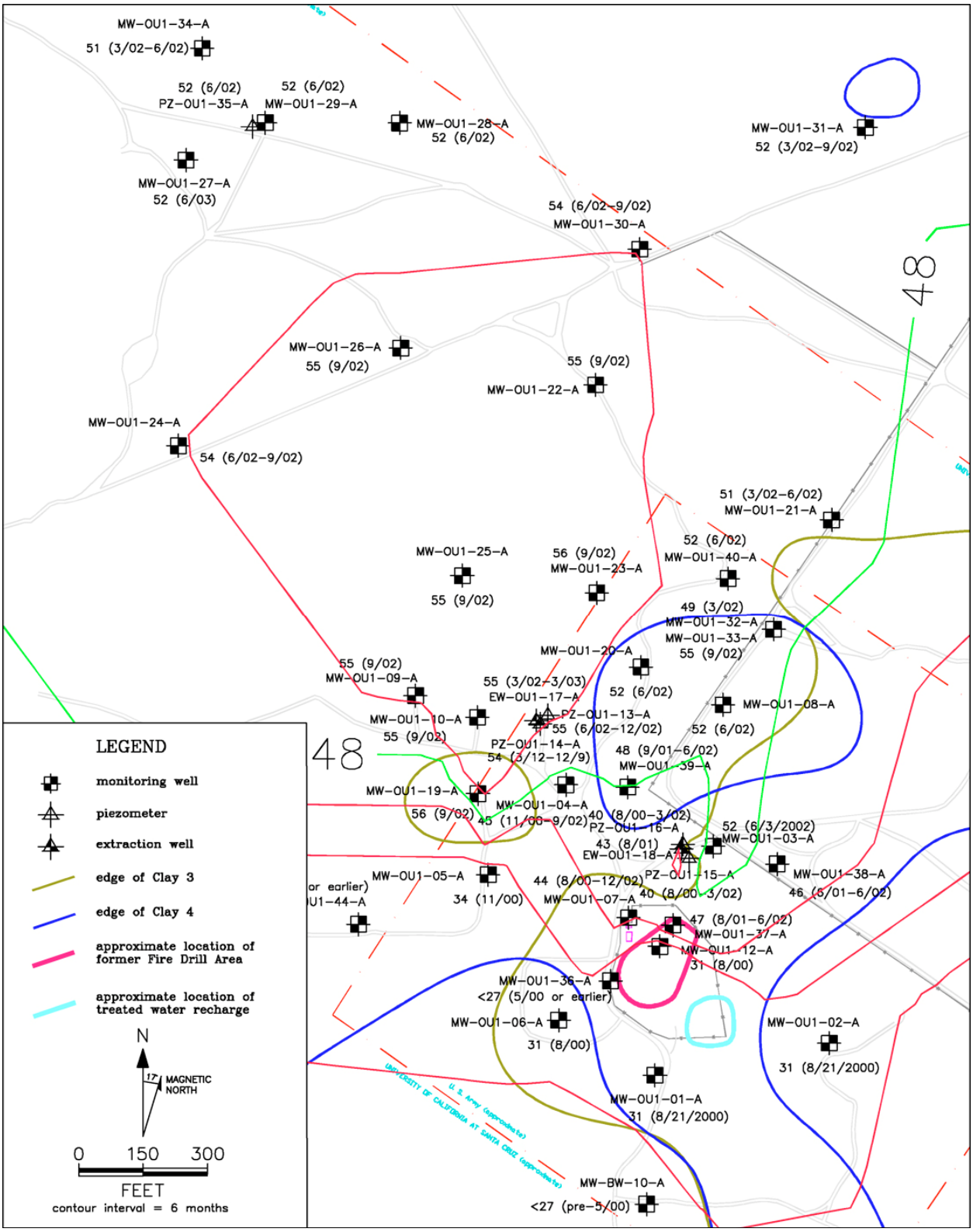

Figure 31. Detail of isochrons (in months) of time to peak water level following the early 1998 precipitation.

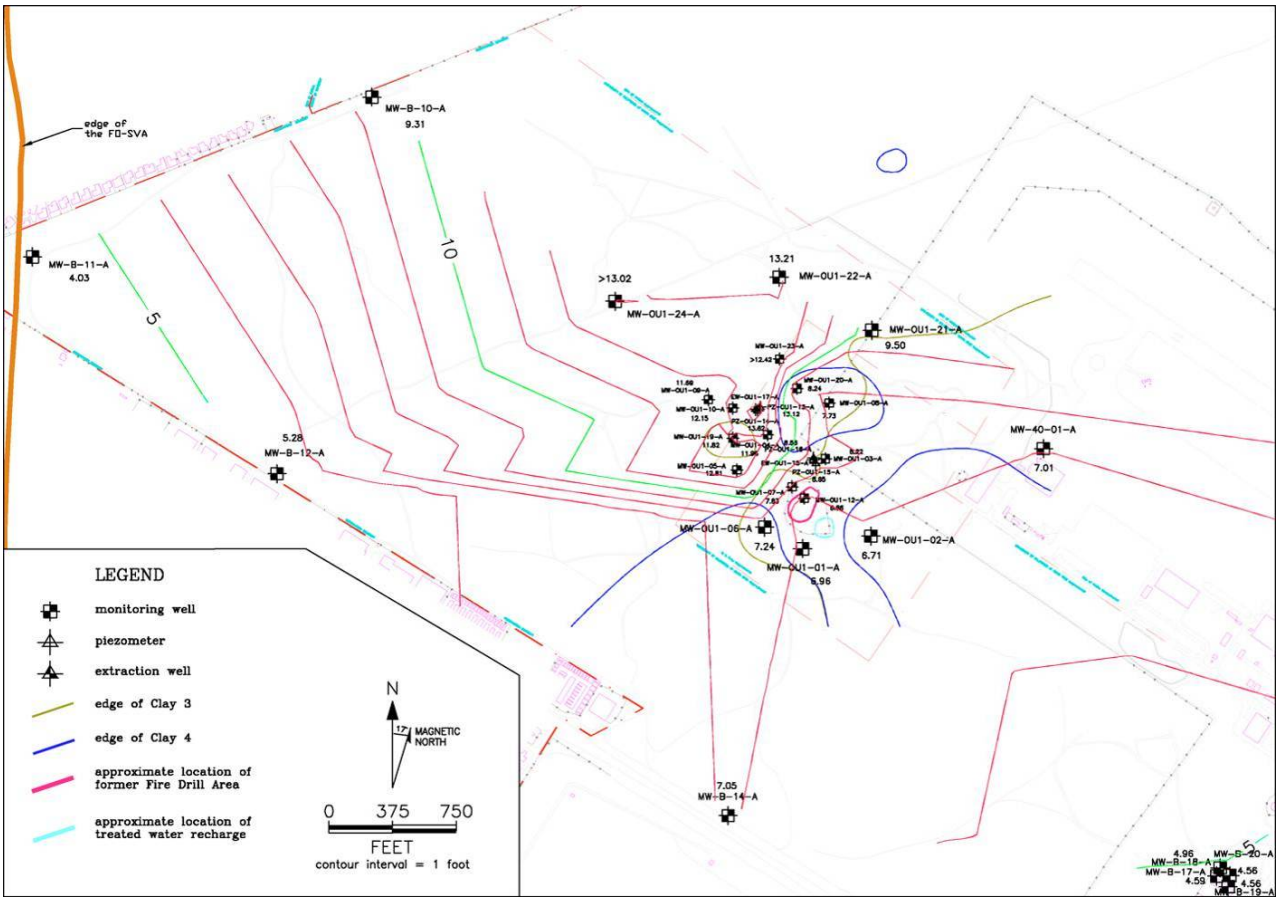

Figure 32. Contours of maximum water level increase following the early 1998 precipitation.

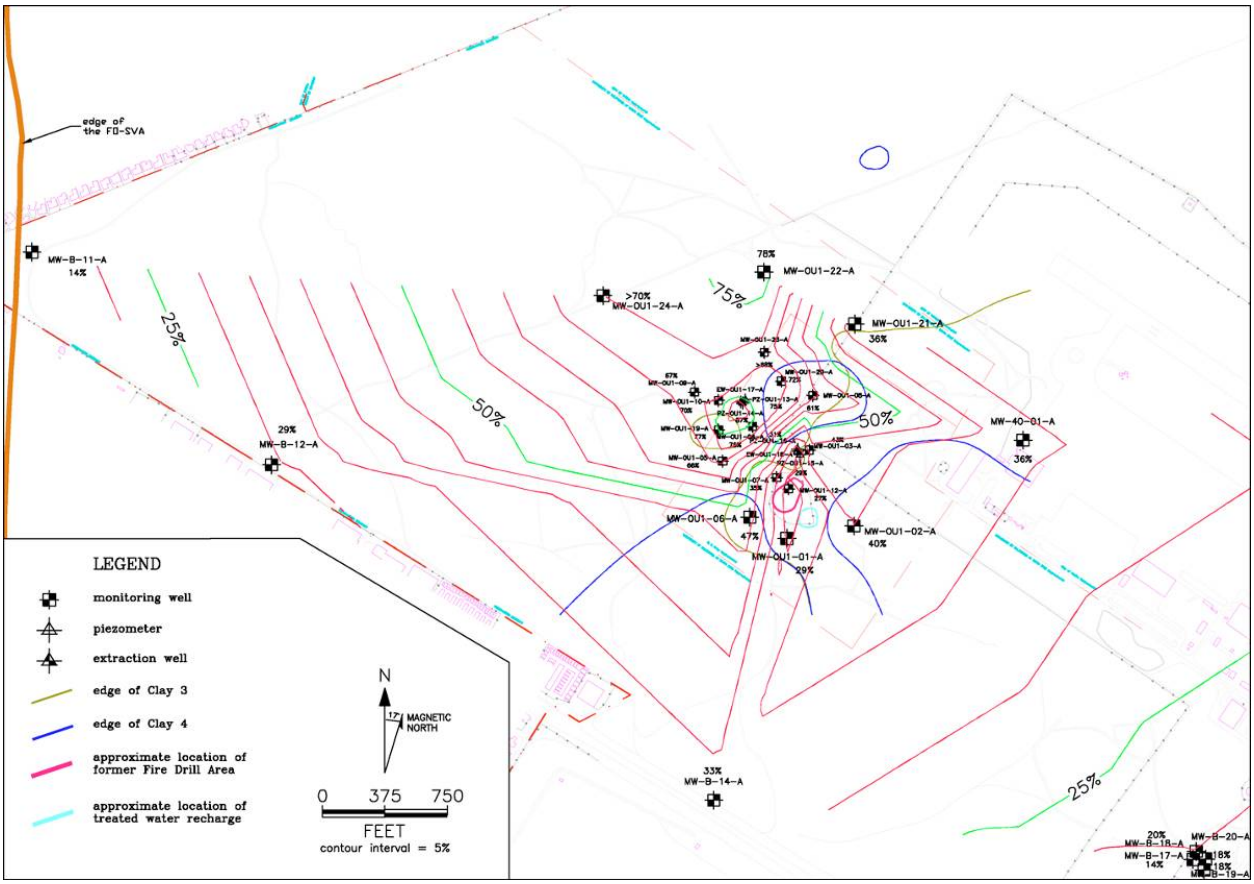

Figure 33. Contours of increase in saturated thickness as a percentage following the early 1998 precipitation.

The other pattern in the peak water level timing is a result of the increased recharge throughout the rest of the aquifer. Figure 34 shows this pattern by comparing hydrographs from wells throughout the aquifer outside of the region impacted by the OU-1 pump, treat, and recharge activities. The water levels near the center and edge peak earlier than in the areas midway between them. This can be understood conceptually by imagining the early 1998 precipitation event as the instantaneous addition of a uniform thickness of groundwater on top of the preexisting A-aquifer water table, which was in equilibrium with the background recharge rate. After the instantaneous groundwater addition, no further inputs above the background recharge rate occur. This conceptual model is justified by the relatively uniform arrival time of the early 1998 precipitation recharge at the water table surface, and by the relatively uniform water level rise of 2–3 ft (0.60–1.8 m) in the six months and 4–6 ft (1.2–1.8 m) in the year following the early 1998 precipitation event (Oldenburg et al., 2002).

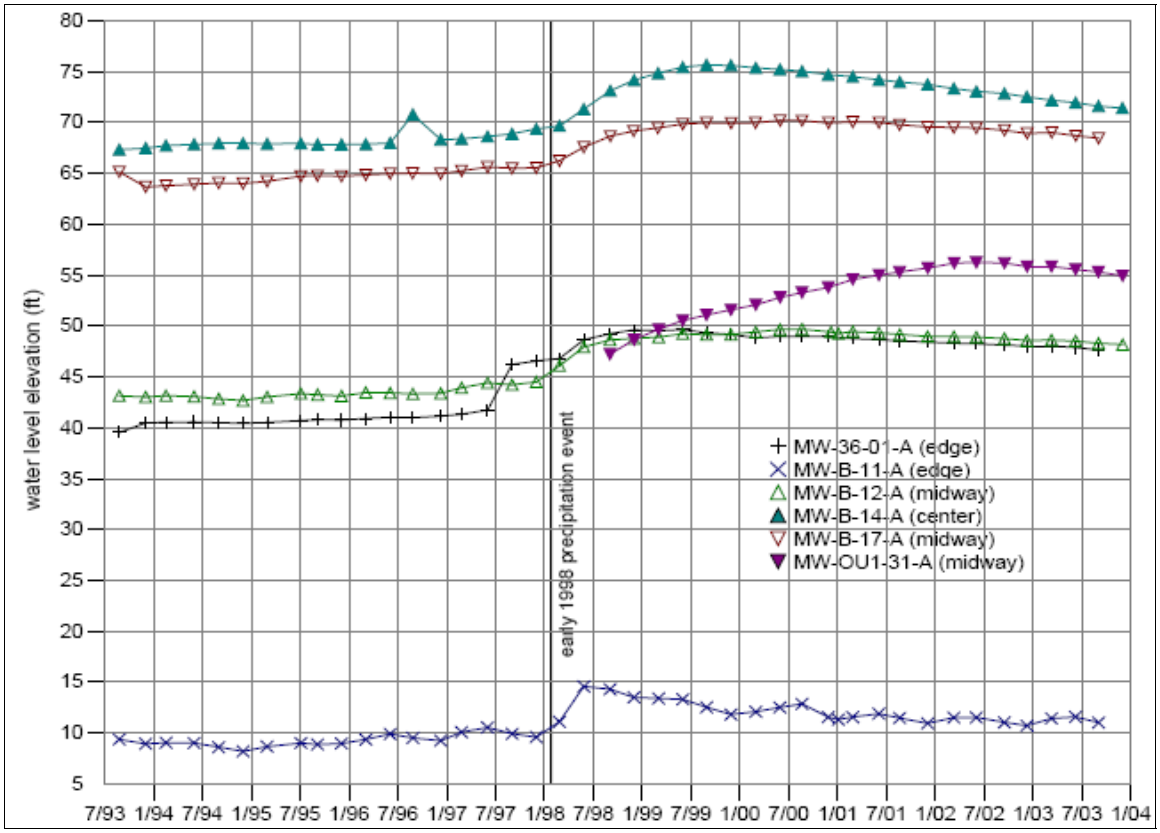

Figure 34. A-aquifer hydographs from the center to the edge of the FO-SVA.

As shown in Figure 35 the water table in the vicinity of OU 1 can be viewed conceptually as a portion of a dome. The gradient remains unchanged on the dome after an instantaneous addition of water as shown on Figure 36. However, the transmissivity increases a constant amount initially throughout the dome, and the gradient at the edge of the dome increases due to the constant discharge elevation (the top of the FO-SVA). At the center of the dome, where there is no long term increase in flow above the background rate, the increase in transmissivity causes the water levels to decline after the instantaneous addition. Away from the center of the dome, the flow rate remains above the background rate for some time after the instantaneous addition due to drainage of the additional water stored in the upgradient areas. Therefore the water level away from the dome center will decline more slowly than the level at the center or may actually increase.

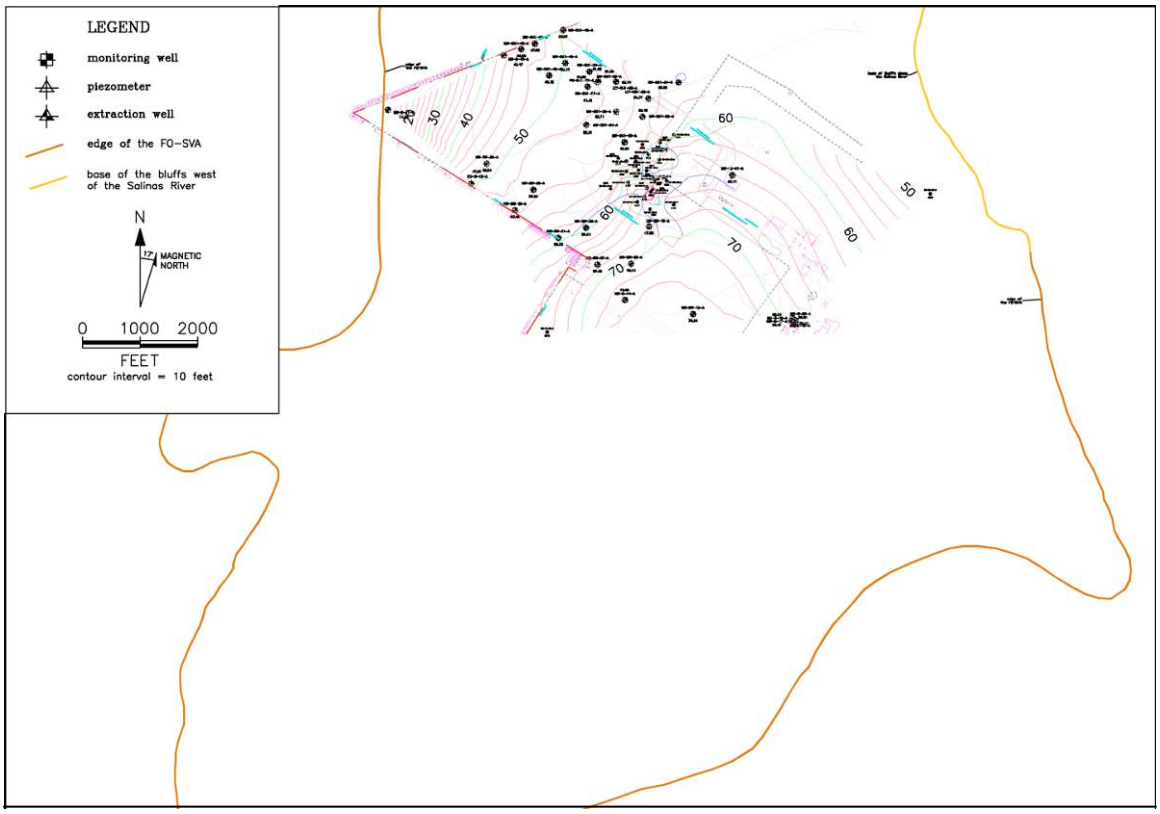

Figure 35. Overview of A-aquifer isopotentials and FO-SVA boundaries in the second quarter, 2002.

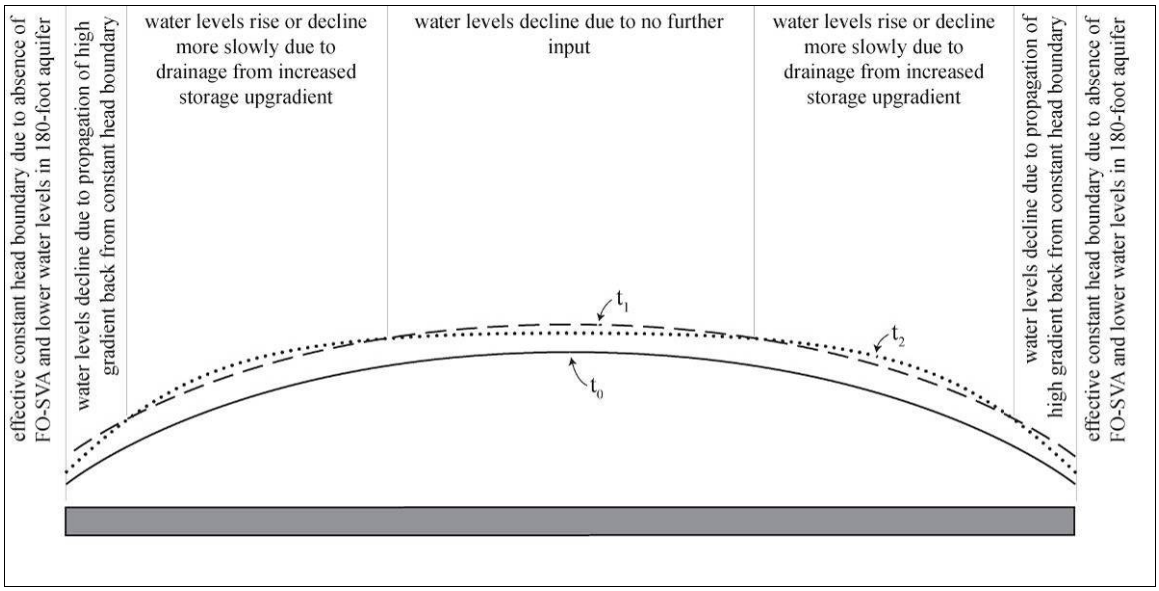

Figure 36. Conceptual model of A-aquifer response to early 1998 precipitation.

At the edge of the dome, the gradient increases after the instantaneous addition due to the constant discharge elevation (in this case the water table

beyond the edge of the FO-SVA). As the transmissivity increase in this region is the same as in the upgradient area, the flow increase is greater at the edge of the dome than within the dome. Therefore the water levels decline more rapidly than in the area upgradient of the edge.

FO-SVA and 180-foot aquifer responses

Response due to A-aquifer weight increase

Oldenburg et al. (2002) (Section 8.6) surmised that the water level increases in MW-OU1-11-SVA and the wells screened in the 180-foot aquifer following the historically high early 1998 precipitation were due in part to precipitation recharge. This conjecture was based upon the increased water levels in these wells less than a year after the precipitation event.

Analyses in the present project suggest that the water level increase in the 180-foot aquifer following the early 1998 precipitation is probably primarily a result of the increased weight of the A-aquifer due to increased water storage. This conjecture assumes that the FO-SVA mechanically transmitted the change in total vertical stress from the A-aquifer to the 180-foot aquifer, but did not hydraulically transmit the change in head from the former to the latter. This interpretation appears plausible for a number of reasons.

First, the water level increases in the deeper, confined aquifers were a fraction of the water-level increases in the A-aquifer as shown on Figure 37 and, to a lesser extent, Figure 38 which compare the responses in the deeper aquifer wells MW-OU1-11-SVA (screened across several sand layers within the FO-SVA) and MW-B-13-180 to those in the nearby A-aquifer wells PZ-OU1-16-A and MW-B-14-A.

Second, Figures 37 and 38 illustrate that the water levels in wells in the deeper aquifers increased through the second quarter of 1998, the only time this has occurred. Water levels decreased in the second quarter in all other years. Water levels in the A-aquifer had just started increasing at the time of the second quarter of 1998. The figures also show that water levels in the deeper aquifer wells decreased in the third quarter of 1998 to approximately the highest dry season levels ever recorded in these wells. At this time only half or less of the water level increases in the A-aquifer had occurred.

Furthermore, the water level increases and peaks in the deeper aquifers occurred predominantly within about six months of the early 1998 precipitation, while the increases and peaks in the A-aquifer occurred within about 18 months. This timing of the deeper aquifer water level change is rapid and consistent with the timing of the increase in weight of the A-aquifer, which would have been essentially simultaneous with the precipitation (which extended into May of 1998). In contrast, the A-aquifer response is delayed, consistent with the time needed for infiltration to migrate through the vadose zone to the water table. If the A-aquifer were transmitting head changes to the 180-foot aquifer hydraulically, water-level increases in the deeper aquifers would have tracked or lagged the A-aquifer changes. Note that a more continuous water level history would help resolve the timing better but we are limited to the quarterly sampling intervals for this analysis.

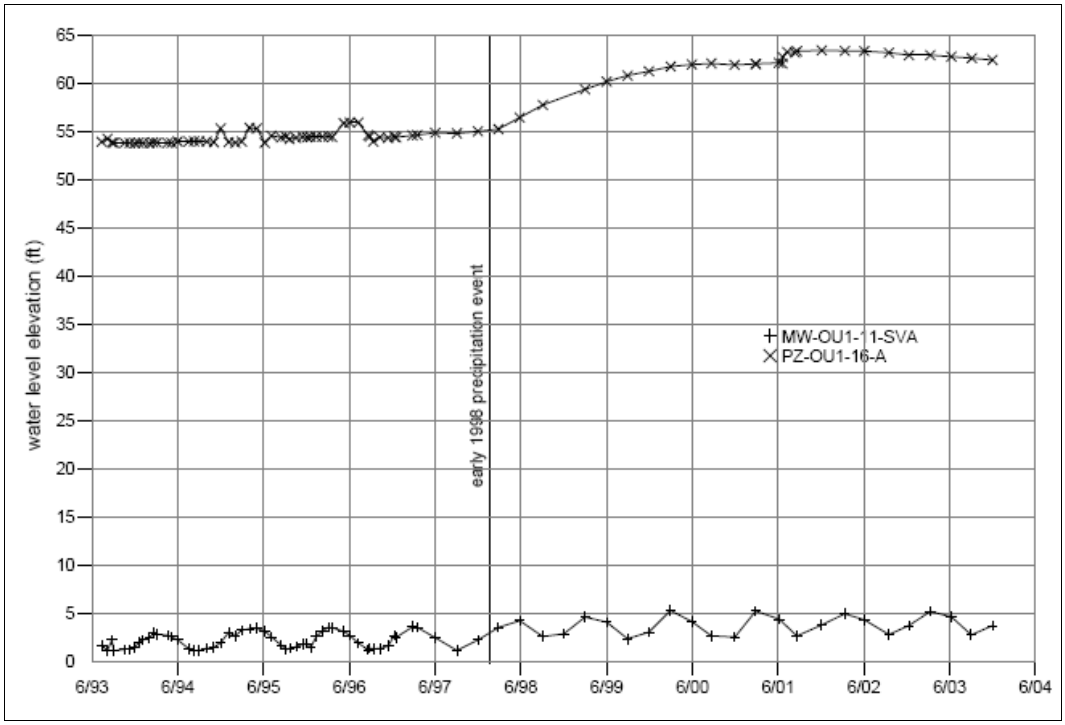

Figure 37. Hydrographs for MW-OU1-11-SVA and PZ-OU1-16-A.

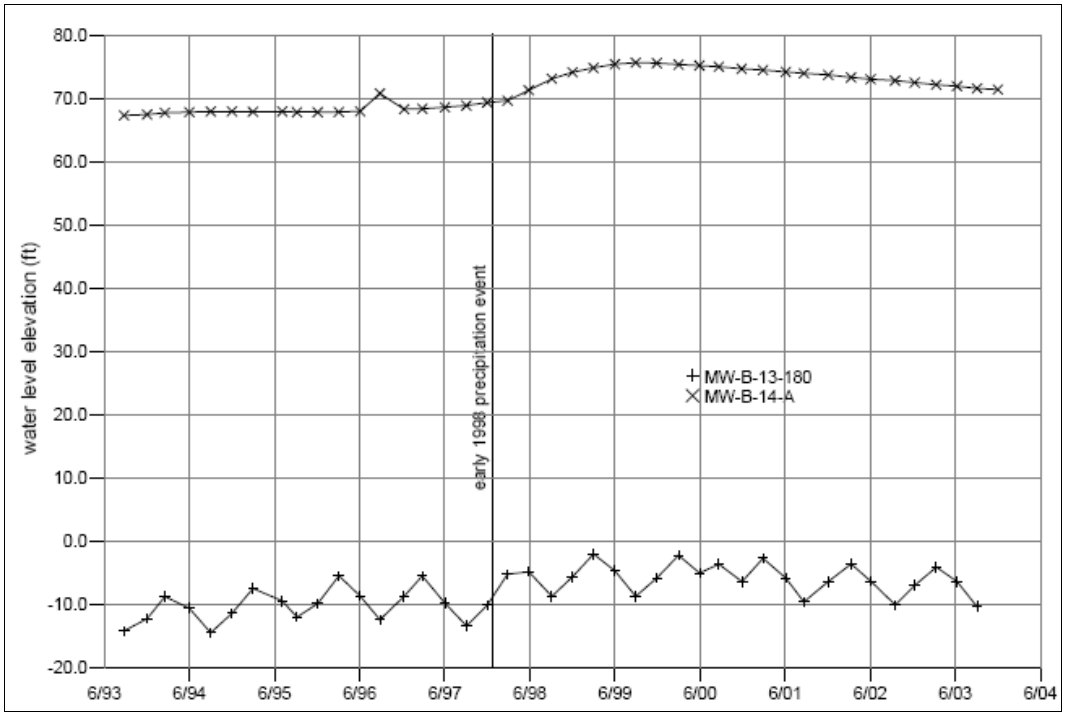

Figure 38. Hydrographs for MW-B-13-180 and MW-B-14-A.

Finally, the hydraulic conductivity of the clay layers in the FO-SVA appears to be much lower than the conductivity of the aquifer materials, as evidenced by the high (three and a half), downward-directed, hydraulic gradient through the FO-SVA coupled with the lack of OU 1 contaminants in the deeper aquifers. This low hydraulic conductivity would cause significant attenuation across the FO-SVA of hydraulic pressure changes occurring at the FO-SVA boundaries.

Specific yield and porosity*:* If the post-1997 water level increases in the FO-SVA and 180-foot aquifers are due to the increased weight of the A-aquifer as argued above, then these water level responses can provide an estimate of the specific yield of the A-aquifer. This calculation is based upon comparing the water level increases in the A-aquifer to those in the deeper aquifers.

The change in total vertical stress ($\Delta\sigma_A$) at the base of the A-aquifer due to the water level rise is

$$\Delta\sigma_A = \rho g \Delta h_A S_y$$

where ρ is the density of water, g is the acceleration of gravity, Δh_A is the change in head in the A-aquifer, and S_y is the specific yield of the A-aquifer. This change in total vertical stress causes a strain in the deeper aquifers. The strain (ε_w) induced in the groundwater, assuming undrained conditions (e.g., no lateral drainage), in these aquifers by the total stress change is

$$\varepsilon_w = -\beta \Delta P$$

where β is the compressibility of water and ΔP is the change in water pressure due to $\Delta\sigma_A$. The strain induced in the sediments (ε_S) constituting the deeper aquifers is

$$\varepsilon_S = -\alpha(\Delta\sigma_A - \Delta P)$$

where α is the compressibility of the sediments. The strain induced in the groundwater and in the sediments are the same under undrained conditions. As the deeper aquifers are confined, the stress response can be approximated by an undrained condition on a short time scale. Setting ε_w equal to ε_S and solving for ΔP yields

$$\Delta P = \frac{\alpha}{\alpha + \beta} \Delta\sigma_A$$

Water is typically more than a thousand times stiffer than sand (Bowles, 1996), of which the A-aquifer consists. Therefore $\alpha \approx 1000\,\beta$ which leads to $\Delta P \approx \Delta\sigma_A$. The change in pressure is given by

$$\Delta P = \rho g \Delta h \approx \Delta\sigma_A$$

where Δh is the change in head in the deeper aquifers. Substituting Eq. 6-1 into 6-5 gives

$$\rho g \Delta h_A S_y \approx \rho g \Delta h$$

Solving for S_y yields

$$S_y \approx \Delta h / \Delta h_A$$

Therefore, the specific yield of the A-aquifer is approximately equal to the water level increase in the deeper aquifers divided by the water level increase in the A-aquifer.

This specific yield calculation rests on two main assumptions. First, the pressure change in the deeper aquifer is due entirely to the weight increase in the A-aquifer rather than other hydrologic changes in the deeper aquifer. Second, all of the weight increase in the A-aquifer can be accounted for by the water level increase in the A-aquifer. The validity of these assumptions is addressed below.

MW-OU1-11-SVA and MW-B-13-180 are the only two sub-A-aquifer wells near A-aquifer wells which have water level measurements before 1998. The water level increase in MW-OU1-11-SVA was 1.5–2 ft (0.45–0.61 m) following the early 1998 precipitation event. This increase was sustained through 2003 (as shown in Figure 37) indicating that the assumption of no pressure dissipation in the deeper aquifer (undrained condition) is approximately met. Additionally, analysis of the water levels in MW-OU1-11-SVA as compared to those in the A-aquifer and 180-foot aquifer at this location indicates that the aquifers screened by this well are not hydraulically connected to the A-aquifer above or the 180-foot aquifer below (Oldenburg et al., 2002).

The closest A-aquifer well to MW-OU1-11-SVA is PZ-OU1-16-A. The maximum water level increase in PZ-OU1-16-A following the early 1998 precipitation was approximately 7.5 ft (2.3 m) (neglecting the increase due to discontinuation of pumping at EW-OU1-18-A). The same increase was measured at nearby A-aquifer well MW-OU1-03-A. The increase in PZ-OU1-16-A was sustained from June 2000 to June 2002, which is sufficiently long after the precipitation event to support the assumption that the vadose zone has predominantly returned to pre-1998 moisture conditions (consistent with the sandy nature of the vadose zone) and therefore the water level change accurately reflects the change in weight of the A-aquifer. The ratio of the water level increases, and therefore the A-aquifer's specific yield, for the PZ-OU1-16-A/ MW-OU1-11-SVA well pair is 20-27%.

The water level increase in MW-B-13-180 after the early 1998 precipitation was 4 ft (1.2 m) as shown in Figure 37. The maximum water level increase in nearby MW-B-14-A following this event was 7 ft (2.1 m). The ratio of these water levels suggests an A-aquifer specific yield of 57%, which is

physically impossible. The maximum increase in MW-B-14-A occurred in August 1999 and was followed by declining water levels. The date of the maximum water level in this well was the fourth earliest of all the A-aquifer wells suggesting that drainage of the vadose zone to background conditions may not have been complete by the time of the water level maximum. Additionally, the water level increase in the 180-foot aquifer may be due in part to recharge of the early 1998 precipitation directly to the 180-foot aquifer beyond the FO-SVA. Therefore the water level increases from MW-B-14-A and MW-B-13-180 likely do not meet the two assumptions necessary for the specific yield calculation.

The specific yield of 20-27% calculated from the MW-OU1-11-SVA and PZ-OU1-16-A water levels is in the center of the generally accepted range of 15-32% for medium-grained sands (Fetter, 1994). The average volumetric moisture content of the OU 1 sand in the region 7.5 ft (2.3 m) above the water table is approximately 10% if we assume it is sand at field capacity (van Genuchten, 1980). Adding this to the specific yield estimate gives a total porosity estimate of 30-37%, which is on the low side of the generally accepted porosity range of 25-50% for well sorted sand (Fetter, 1994). However, it is recognized that despite the plausible result obtained, the analysis is somewhat uncertain due to being based on a single well pair.

1997/1998 precipitation recharge

As discussed above, the change in total vertical stress after the early 1998 precipitation is due to the increase in weight of the A-aquifer resulting from the precipitation recharge. This can be expressed as

$$\Delta\sigma_A = \rho g s$$

where s is the quantity of precipitation recharge. Substituting equation 6-5 into equation 7-1 gives

$$\rho g \Delta h = \rho g s$$

Canceling terms gives

$$\Delta h = s$$

Therefore the water level rise in the confined aquifers is equivalent to the quantity of precipitation recharge. The water level increase in MW-OU1-

11-SVA after the early 1998 precipitation event likely indicates the total depth of water recharged to the aquifer during the 1997/1998 rain year was 1.5–2 ft (0.46–0.61 m). The total precipitation during this rain year was 47.15 in (1.2 m) at the Monterey meteorological station. Dividing 1.5–2 ft (18–24 in, 0.46–0.61 m) by the total precipitation yields a very high recharge fraction of 38-51%.

This high recharge fraction is possible because the early 1998 precipitation was an extreme event. Approximately 25 in (0.63 m) of the 1997/1998 rain year precipitation fell at Monterey during an approximately one month period in January and February of 1998. This rainfall was greater than the average annual total precipitation at Monterey. Such high precipitation rates could be expected to cause higher recharge rates at OU 1 for three reasons. First, the high precipitation rate overwhelms the normal evapotranspiration rate. Second, the high precipitation rate causes higher liquid saturation at the ground surface and in the vadose zone, which increases the effective hydraulic conductivity and therefore creates a higher infiltration rate. Finally, the lack of developed drainages in the hummocky dunes at OU 1 prevents precipitation from flowing laterally away and leads to increased infiltration.

The 1997/1998 recharge fraction of 38-51% is considerably higher than the 27% precipitation recharge fraction derived from an analysis of water level changes during more typical rain years in Oldenburg et al. (2002). As explained above, the 1997/1998 hydrologic year was an extreme event and it makes sense that the recharge fraction would be significantly greater than for a typical rain year.

Groundwater flow velocity

ISPFS instrumentation at OU 1

Hydrotechnics In-Situ Permeable Flow Sensors (ISPFSs) are installed below the well screens in MW-OU1-36-A through -40-A. These instruments contain a heater and an array of 30 temperature sensors (thermistors). The temperature field produced by the heater is distorted by groundwater flow past the instrument. Temperatures measured by the thermistor array in each instrument are recorded once an hour. The software HTFlow95 provided by Hydrotechnics inverts the thermistor data to derive the Darcy groundwater velocity vector (vertical and horizontal velocity magnitudes and horizontal velocity azimuth). The inversion algorithm assumes iso-

tropic hydraulic and thermal conductivity. Details of ISPFS installation and preliminary data analysis can be found in Oldenburg et al. (2002).

Three of the five installed ISPFSs have produced useful data. These are ISPFSs installed in MW-OU1-36-A, -37-A and -39-A. The heater power in the ISPFS in MW-OU1-39-A decreased on June 5, 2001. The analysis of data from this instrument has been improved since Oldenburg et al. (2002) by accounting for the change in heater power. Data from the ISPFSs installed in MW-OU1-38-A and MW-OU1-40-A have been more problematic. The heater in the ISPFS in MW-OU1-40-A failed due to an electrical short in January 2001. While the ISPFS in MW-OU1-38-A appeared to be functional, a detailed examination of the thermistor data revealed an apparently non-uniform flow field around the sensor. When groundwater flow is homogeneous over the surface of the instrument, temperatures along the length of the sensor are highest towards the middle at all sensor azimuths and the temperature around the sensor varies approximately sinusoidally at all distances along the sensor. The thermistor data from MW-OU1-38-A did not conform to either of these patterns but rather to a pattern suggestive of flow twisting around the probe, perhaps due to borehole effects related to the installation. Therefore, consideration of the data in MW-OU1-38-A and MW-OU1–40-A is not included below. The daily average of the hourly results inverted from the MW-OU1-36-A, -37-A and -39-A ISPFS data from January 1, 2001 to November 28, 2003 are discussed below.

Horizontal velocity azimuth

The inverted horizontal flow azimuths from the ISPFSs are shown along with the extraction rates from EW-OU1-17-A and -18-A in Figure 39. Counterclockwise gradient rotations in MW-OU1-37-A and -39-A on a weekly time scale correlate to pumping rate decreases from EW-OU1-18-A. Such rapid rotations are not observed in MW-OU1-36-A, perhaps due to its position in the region dominated by changes in the treated water recharge rate (Oldenburg et al. 2002). Pumping rate decreases at EW-OU1-18-A would tend to cause counterclockwise gradient rotation toward EW-OU1-17-A at this well. Recharge decreases would tend to cause clockwise gradient rotation at this well due to realignment with the regional gradient. Therefore, the azimuth perturbations due to pumping and recharge rate changes would tend to cancel each other. The horizontal flow azimuths have also rotated counterclockwise on a yearly time scale as shown in Figure 39. These rotations are likely due to continuing adjustments to

the cessation of pumping from EW-OU1-18-A in June 2001 and the water level increases due to the early 1998 precipitation. The rotation at MW-OU1-36-A is the greatest and at MW-OU1-37-A is the least.

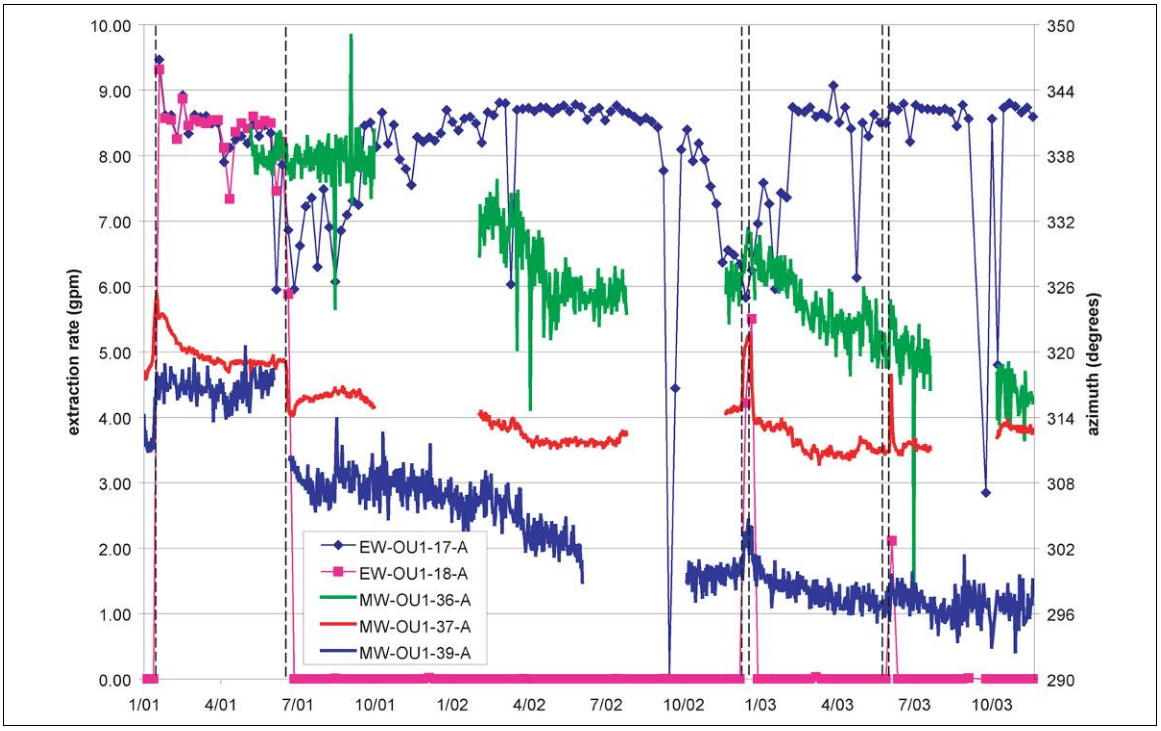

Figure 39. Inverted ISPFS azimuth compared to extraction rates. Dashed lines are EW-OU1-18-A pump switching.

Table 6 compares the azimuths inverted from the ISPFS data to that measured from the water table gradient. The discrepancies between the gradient azimuth and that measured by the flow sensor could be due to sensor installation error, sensor measurement error, borehole effects, actual differences between the gradient direction and the flow field due to anisotropy or heterogeneity, or error in the contoured water table gradient. The comparison in Table 10 indicates that the ISPFS azimuths for MW-OU1-36-A and 37-A are too westerly by 17° to 27° (the MW-OU1-39-A comparison is probably inaccurate due to gradient-azimuth errors caused by insufficient well coverage along the edge of the airfield clay near EW-OU1-17-A). This is in accord with the ISPFS azimuth ranges shown in Figure 39, which appear too westerly given the position of the instrument wells relative to the extraction wells and the treated water recharge area. The consistency of the discrepancy could be due to a northwest/southeast-oriented anisotropy, however the contaminant plume shape (discussed below) does not suggest such an anisotropy. A more likely explanation is an error during installation that resulted in a consistent misalignment (e.g.,

bad measurement of magnetic north, or error in accounting for magnetic declination).

Table 10. Comparison of azimuths during the second quarter, 2003.

Source	MW-OU1-36-A	MW-OU1-37-A	MW-OU1-39-A
ISPFS	316°	311°	298°
Gradient	333°	338°	270°

Horizontal velocity magnitude

The inverted horizontal flow velocities from the ISPFSs are shown along with the extraction rates from EW-OU1-17-A and -18-A in Figure 40. This figure shows a clear correlation between the pumping state at EW-OU1-18-A and the horizontal velocities at the instruments. When extraction from EW-OU1-18-A ceases, the horizontal velocity at MW-OU1-36-A and –37-A decreases and at MW-OU1-39-A, increases. This is readily explained by the location of the former generally upgradient of EW-OU1-18-A, and the position of the latter near the point of stagnation between the two extraction wells. The response at MW-OU1-37-A is greater than at MW-OU1–36-A due to its greater proximity to EW-OU1-18A in a more upgradient direction.

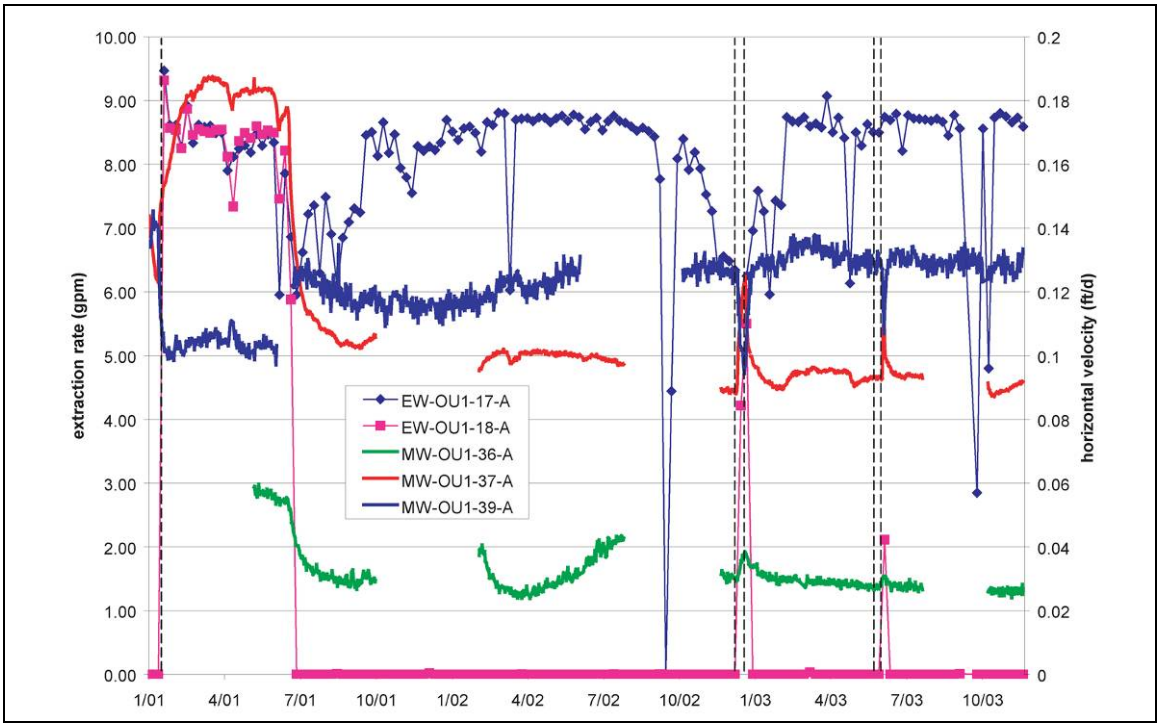

Figure 40. Inverted ISPFS horizontal velocities compared to extraction rates. Dashed lines are EW-OU1-18-A pump switching.

The absolute velocity values are divided by the gradient to estimate the hydraulic conductivity at each instrument. These values are compared against hydraulic conductivities measured via other methods. From these comparisons, it appears that the horizontal velocities measured by the ISPFSs are reasonable.

Vertical velocity magnitude

The inverted vertical flow velocities from the ISPFSs along with the extraction rates from EW-OU1-17-A and -18-A are shown in Figure 41. Comparison of Figures 40 and 41 indicates that the vertical velocities inverted from the ISFPS data are approximately the same as, or much greater than the horizontal velocity at the same instrument, and are directed downward. Furthermore, the inverted vertical velocities are approximately proportional to the horizontal velocities. This result is unexpected and a complete analysis of the data is presented in the companion report (Su et al. 2005), with a summary presented below.

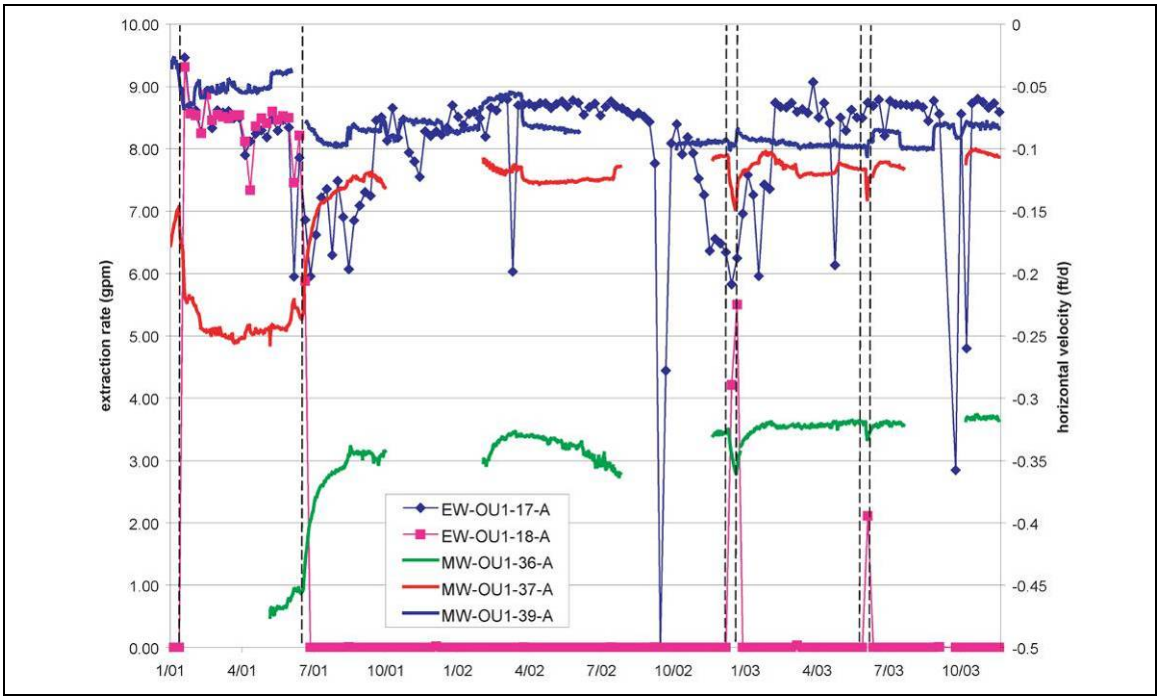

Figure 41. Inverted ISPFS vertical velocities compared to extraction rates. Dashed lines are EW-OU1-18-A pump switching.

The inverted vertical velocities are improbable due to the presence of the FO-SVA aquitard near the base of each instrument. This aquitard would prevent significant vertical flow at this position in the aquifer. Oldenburg et al. (2002) suggested that the temperature at the bottom of the sensor was elevated relative to the top due to the relatively lower thermal conductivity of clay, such as the FO-SVA, near the base of the sensors as compared to sand, such as the A aquifer, which surrounds the sensors.

Non-isothermal flow simulation of various scenarios using TOUGH2 indicates that the thermal heterogeneity introduced by the immediate proximity of the sensor base to the FO-SVA clay could produce a temperature buildup at the bottom of the sensor that HTFlow95 would interpret as due to downward vertical flow (Su et al. 2005). This effect rapidly dissipates as the sensor base is moved away from the clay however. The sensor base in MW-OU1-36-A, -37-A and –39-A is 1.5, 0, and 4 ft (0.45, 0, and 1.2 m), respectively, above the top of the FO-SVA, according to the well installation logs. The TOUGH2 modeling of Su et al. (2005) indicates that at a separation of 1.5–4 ft (0.45–1.2 m) from the clay, the thermal heterogeneity is too far away to create the necessary temperature buildup. This is further confounded by the significantly larger inverted vertical velocity in MW-OU1-36-A compared to those from the other wells, despite the fact

that other wells have both greater and less separation between the bottom of the sensor and the FO-SVA clay.

One possible explanation is that the depth to the top of the FO-SVA is inaccurately represented on the drill logs for the sensor wells. Oldenburg et al. (2002) noted that comparison of the position of the top of the FO-SVA on drill logs and geophysical well logs for the four wells at OU 1 for which the latter data were available indicated discrepancies of up to 3.5 ft (1.1 m) between the two methods. Given this uncertainty, all of the ISFPSs in MW-OU1-36-A, -37-A, and –39-A may be in sufficiently close proximity to the FO-SVA to create the inverted vertical velocities.

Alternatively, the well completion method could have introduced thermal and permeability heterogeneities that would cause false inverted vertical velocities. The borings for the wells were initially piloted 2.5–4 ft (0.76–1.2 m) into the FO-SVA clay with a small auger. The borings were subsequently reamed with a larger auger to a target completion depth at or within 4 ft (1.2 m) of the top of the FO-SVA clay. The ISPFS was installed to the total depth of this larger boring.

Piloting into the FO-SVA would have caused smearing of clay for some distance up the borehole. This smear zone likely existed just below each ISPFS. The smear zone would introduce a thermal heterogeneity as well as a permeability heterogeneity. The TOUGH2 modeling indicated a thermal conductivity decrease of as little as 5% (from 2.1 W m^{-1} C^{-1} to 2.0 W m^{-1} C^{-1}) near the bottom as compared to the thermal conductivity along the rest of the sensor could create a heat buildup sufficient to create the inverted vertical velocities (Su et al. 2005).

In short, we are left to speculate about the in-situ conditions around the installed ISPFSs. However, TOUGH2 modeling demonstrates that thermal and permeability heterogeneities at the base of the ISPFSs are capable of creating apparent vertical velocities (Su et al. 2005). Thus, we conclude that large components of downward vertical velocity in the A-aquifer are unlikely.

Permeable diffusion sampler results

Water sampling methods

Water sampling from 51 of the wells at OU 1 from which chemistry data were available was changed from purge and sample (P&S) to permeable diffusion sampling (PDS) at the end of 2001 as shown in Figure 42. Two wells outside of the area on Figure 42 have PDS results: MW-36-01-A to the east and MW-BW-18-A to the south. The wells without PDS results near the FDA are either piezometers, from which water samples are not collected; extraction wells, from which water samples are collected at the treatment system intakes; or wells connected to the real-time chemistry analysis system, from which samples are collected at the system intakes.

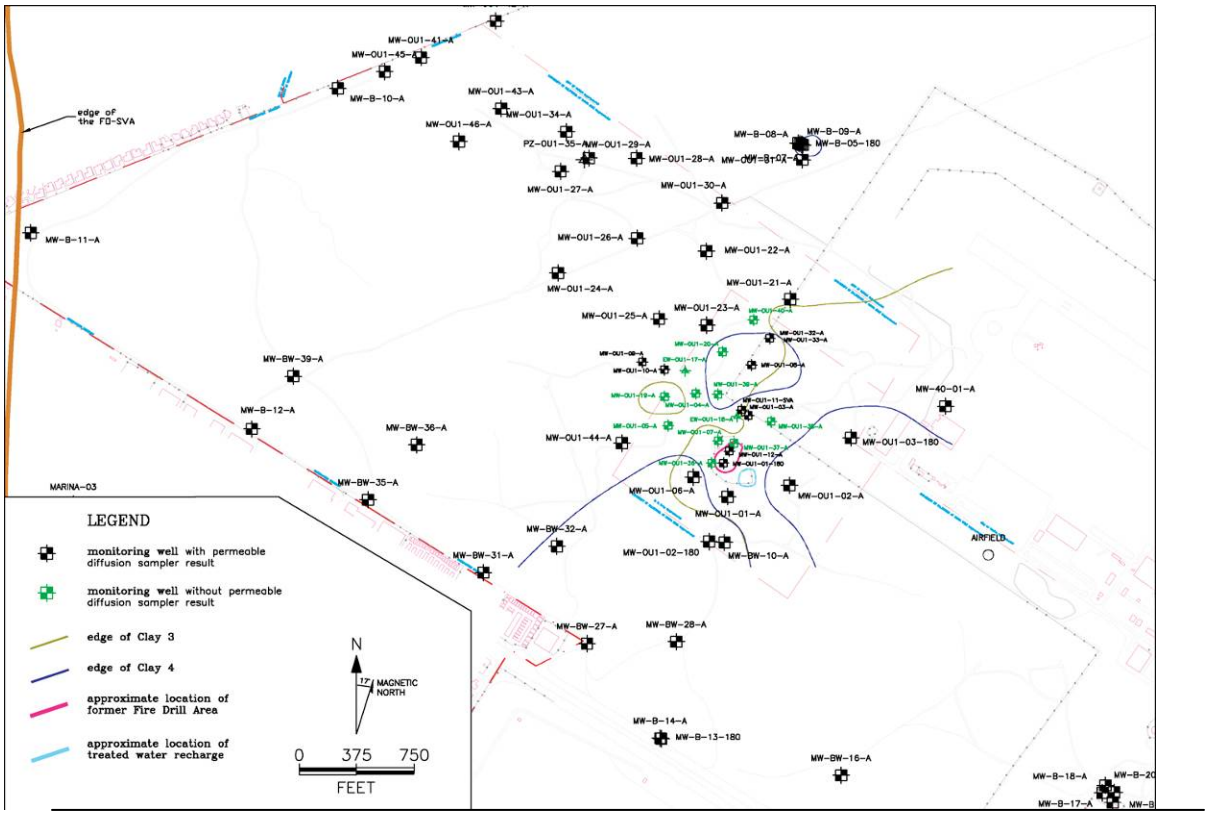

Figure 42. Wells with PDS results.

In P&S, a volume of water equivalent to a number of well-bore volumes is typically purged from a well and then a water sample is collected. The purpose of purging the well is to allow sampling of water representative of the groundwater in the formation rather than in the well. This is because the chemistry of the water in the well may change over time due to interaction with air and other effects. Various water parameters such as temperature,

pH, and conductivity are typically monitored during the purging. Stabilization of these parameters provides a secondary check on whether the purging has been sufficient to bring water to the well representative of groundwater in the formation.

PDS involves placing a polymer bag filled with water (typically deionized) into the water column in the well. The PDS bag is left in place for some time, typically from one sampling event to the next, which is three months at OU 1. The concentration of organic contaminants in the water column in the well and in the water inside the bag equilibrates through diffusion.

Prior to switching the groundwater sampling methodology used at a well, MacTec conducted pilot studies for switching from P&S to PDS. These studies included nearly contemporaneous samples collected via the two different methods. However, these data and the pilot study reports were not available to LBNL. The analyses presented below are based entirely upon the analytical results of record for each well. Analysis of these records ultimately provides a better comparison of the methodologies due to the much greater number of PDS sample results for each well since the switch relative to the PDS results available during the pilot study analysis. A greater number of PDS results affords a more accurate and precise perspective on the concentrations and repeatability of these results and, therefore, a better comparison to the P&S results.

Comparison of purge and sample to PDS results*:* The 51 wells with PDS sampling can be broadly broken into three main groups based on the results from P&S after June 2000 and PDS from late 2001 to early 2003. Contaminants were less than the detection limit in both the P&S or PDS results from 17 of the 51 wells. Trichloroethylene (TCE) and its degradation compound cis-1,2 Dichoroethylene (cis-1,2 DCE) were consistently detected in the P&S and/or PDS results from 19 of the 51 wells. Carbon tetrachloride (CT) and its potential degradation compounds were consistently detected in the P&S and/or PDS results from 15 of the 51 wells. Chloroform, a possible degradation product of CT, and TCE or its potential degradation products were detected in two wells, MW-OU-01-A and –23-A. These two wells are included in both the CT and TCE groups. Two wells had consistently detected contaminants other than those listed above. Freon 113 was detected in MW-40-01-A and MEK and Toluene were detected in MW-B-11-A. Neither of these wells is included in the three main groups.

In general, the contaminant concentrations from samples collected by P&S and PDS were consistent. There was a clear difference between the two result sets for only four of the 19 wells in the TCE group, as summarized in Table 11. For three of the wells, the result sets are different by a factor of two or less, assuming non-detects are near the detection limit, and so are not very significant. The only significant difference is in the result sets from MW-OU1-10-A. The difference in these result sets is an order of magnitude and, due to the position of this well, these differences would alter the interpretation of plume shape. For this reason, the PDS results from this well were discounted for plume contouring.

Table 11. Comparison of chemistry results from purge and sample and PDS.

Well	Contaminant	Concentrations	
		P&S (>6/00)	PDS
MW-OU1-02-180	cis-1,2 DCE	<0.5 µg/L	0.59-1.4 µg/L in greater than half of 184 ft bgs samples; not-detected at other depths
MW-OU1-10-A	TCE	3-7 µg/L	typically <0.5 µg/L; wheredetected, 0.5-0.6 µg/L
MW-OU1-32-A	TCE	0.5-0.7 µg/L	0.6-1.5 µg/L
MW-OU1-33-A	TCE	typically <0.5 µg/L	typically 0.6-0.8 µg/L

µg/L =micrograms/liter

Result sets from some of the other TCE-group wells contained more subtle differences. However, these differences could not be clearly assigned to the different sampling methodologies versus changing contaminant concentrations with time. The difficulty differentiating these two possibilities was in part because the first PDS data available from a well were two and a half months or more after the last P&S data, with two exceptions. Therefore, contaminant concentrations were not available for samples collected simultaneously by the two methodologies.

The focus of this report is on the OU 1 plume, and thus the TCE-group wells. The CT-group well results are compared here simply as an additional comparison of the P&S and PDS methods. Of the 15 wells in this group, there was no significant difference between the P&S and PDS results for seven of the wells, the PDS results were significantly less than the P&S results for five of the wells, and the PDS results were significantly higher than the P&S results for three of the wells. The difference between the result sets was a factor of generally two to six. Therefore, while no well in the CT group had as significant a difference between the result sets as

MW-OU1-10-A in the TCE group, the fraction of wells showing a variance between the two groups was much higher in the CT group (approximately half) than the TCE group (approximately one-fifth).

PDS depth profiling results

At OU 1, the initial sampling event using PDS typically involved sampling from multiple depths in the water column to characterize the concentration profile. Thereafter, sampling was carried out at the depth with the maximum concentrations. In wells where the initial sampling depths were widely spaced, and the contaminant concentrations were not uniform with depth, a subsequent sampling event was often done to resolve the concentration gradients better. In some wells where the concentrations were uniform across a significant portion of the water column, the single sample depth after the initial multi-depth characterization was varied from event to event across the uniform region. In only one well, MW-OU1-27-A, sampling was carried out at more than one depth after the initial depth characterization sampling. These results are shown in Figures 43 and 44. These figures show that although the contaminant concentrations changed through time, the concentrations within the initially identified uniform region generally remained uniform through time. Note that the bottom of the well is above the depth given for some of the PDS results, presumably due to an error in the PDS depths.

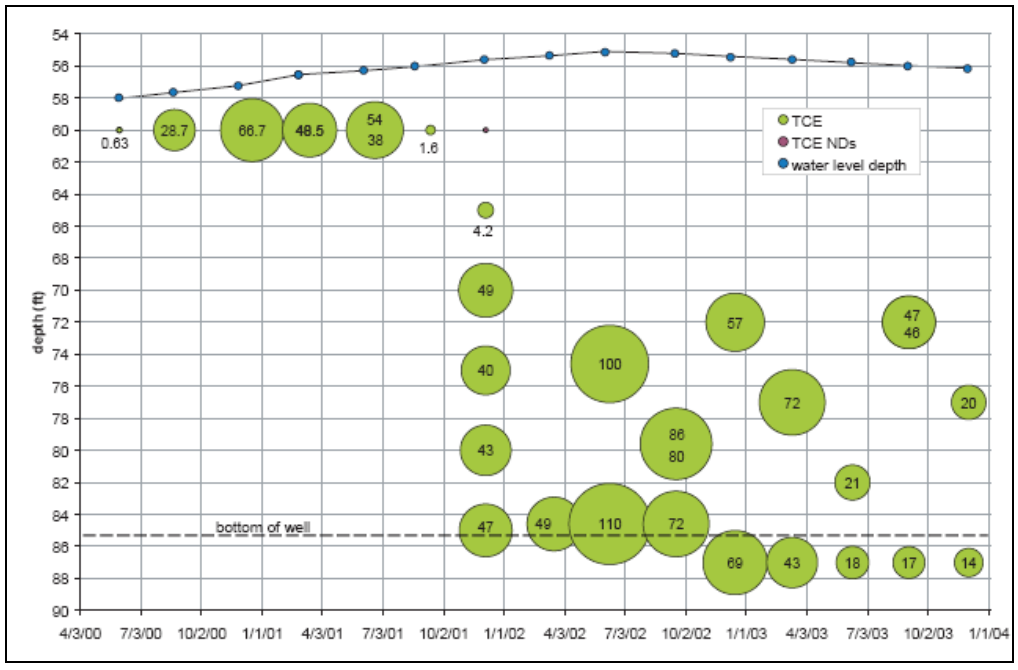

Figure 43. TCE PDS results from MW-OU1-27-A.

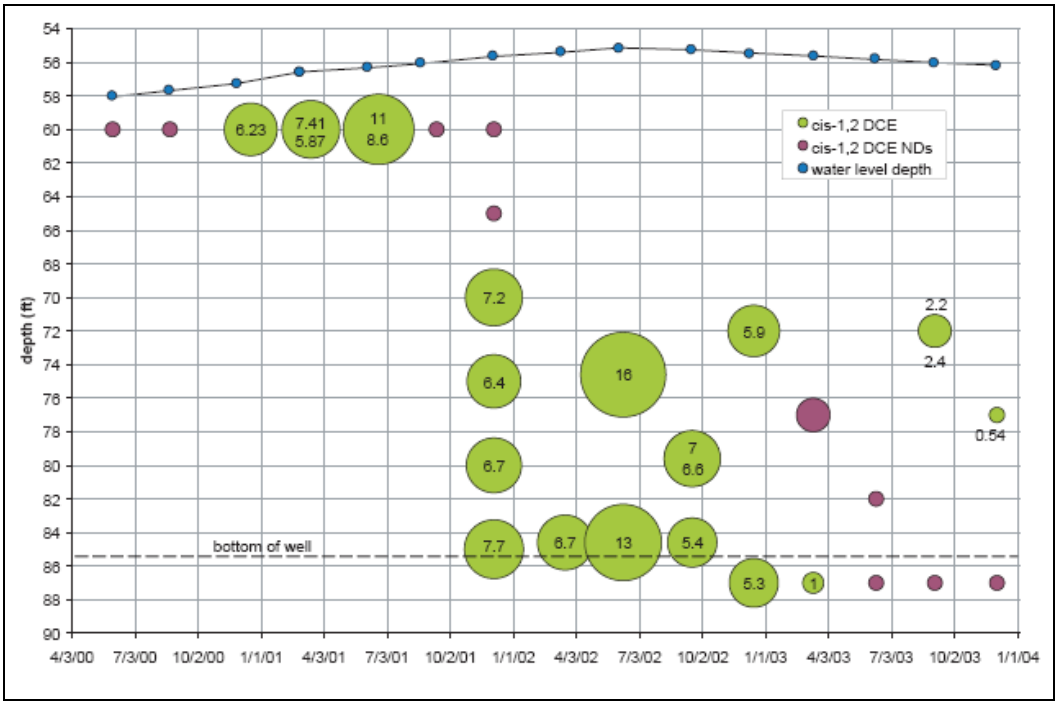

Figure 44. Cis-1,2 DCE PDS results from MW-OU1-27-A.

The contaminant concentrations were relatively constant with depth in 39 of the 51 wells sampled by PDS. Of the 39 wells with constant concentrations with depth, the results from 17 wells were uniformly non-detected. Therefore the actual concentration profile in these wells may not be uniform. The contaminant concentrations from approximately two-thirds of the wells in both the TCE group and the CT group were constant with depth. Contaminant concentrations varied with depth in six of the 19 wells in the TCE group. The initial, multi-depth results from these wells are shown in Table 12. Contaminant concentrations increased with depth in four of the six wells. In three of these wells, no contaminants were detected in the shallowest PDS sample(s). Contaminant concentrations decreased with depth in only one well and were highest toward the middle of the depths sampled in only one well.

As mentioned, the focus of this report is on the TCE-group wells. The CT-group well results are compared here simply as an additional comparison of the P&S and PDS methods. Of the 15 wells in this group, the contaminant concentrations were relatively constant with depth in nine of the wells. In the other six wells, the contaminant concentrations typically increased with depth. In four of these wells, the concentration increased through the upper third of the water column and was relatively constant below.

As indicated, concentrations from slightly less than one third of the wells in the TCE group and slightly more than one third of the wells in the CT group were not constant with depth. Two possible explanations for these variations with depth are: varying horizontal flow velocities and volatilization or other perturbations near the air/water interface. These variations in TCE concentrations with depth listed in Table 12 are generally more consistent with varying horizontal flow velocities with depth than with volatilization at the air/water interface. The concentration variations in the CT wells, as described, are generally more consistent with volatilization or other perturbations near the air/water interface.

Table 12. Non-uniform, contaminant concentration depth profiles.

Well	Consistently detected con- tami-nant(s)	Water column (ft bgs)	PDS depths (ft bgs)	Concentration (ug/L)
MW-OU1-02-180	cis-1,2 DCE	141-195	179 184 189 194	<0.5 0.59 <0.5 <0.5
MW-OU1-23-A	TCE, cis-1,2 DCE	98-128.5	103 108 113 118 123 128	24, 0.56 24, 0.55 25, 0.59 25, 0.58 <0.5 1.6, <0.5
MW-OU1-27-A	TCE, cis-1,2 DCE	56-85.5	60 65 70 75 80 85	<0.5 4.2, <0.5 49, 7.2 40, 6.4 43, 6.7 47, 7.7
MW-OU1-29-A	TCE	59-90	64 88	<0.5 26
MW-OU1-32-A	TCE	83-100	89 94 99	0.76 0.79 1.5
MW-OU1-43-A	TCE	65-96	73 78 83 88 93 98	<0.5 <0.5 0.52 4.2 18 23

A-aquifer hydraulic conductivity

Introduction

The horizontal hydraulic conductivity of the A-aquifer is estimated below from the aquifer scale to the sub-well scale from the plume length, steady-state drawdowns, short term pumping tests, and ISPFS results. The unsaturated vertical hydraulic conductivity at the vadose zone scale is estimated across the site from precipitation and treated water recharge responses. Variation in hydraulic conductivity was investigated using all of these methods as well as the PDS results. The result of this analysis is that the vertical and horizontal conductivities are roughly equivalent, are in the range of 5.0 to 10.0 ft/d ($1.8–3.6 \times 10^{-5}$ m s^{-1}), are relatively uniform and isotropic, and are consistent across scales and across the site as described below.

Plume length and alignment

The gradient from above the recharge mound at the southeast corner of the FDA to the tail of the TCE plume in the second quarter of 2000 was 0.007 (Oldenburg et al. 2002). The total plume length in 2000, thirty-nine years after the start of fire suppression training in the FDA, was 2000 ft (600 m). Assuming an effective porosity of 25% and no retardation, the implied average linear velocity from the start of training through 2000 is 0.14 ft/d (4.9×10^{-7} m s^{-1}). From these values, the calculated hydraulic conductivity across the entire plume is 5.0 ft/d (1.8×10^{-5} m s^{-1}). As the OU 1 aquifer materials probably have low total organic carbon, retardation of TCE is probably low and therefore the actual hydraulic conductivity at the plume scale is probably only slightly greater than this value. Note further that this estimate is based on the tip of the plume and therefore is the maximum hydraulic conductivity for the plume.

Oldenburg et al. (2002) noted that the plume was aligned with the likely pre-1998 gradient, and with the depression in the water table downgradient of the FDA apparently created by evapotranspiration losses during recharge of the treated water. These alignments indicate that the flow direction is coincident with the gradient direction. Therefore it is unlikely there is significant anisotropy in the hydraulic conductivity in the A-aquifer at OU 1.

Early 1998 precipitation event

Water levels shallower than 60 ft (18 m) started to increase 0.5–1.5 months after the early 1998 precipitation event (Oldenburg et al. 2002). Therefore the recharge front advected through this portion of the vadose zone at a rate of 1.3–4 ft/d (4.6–14 x 10^{-6} m s^{-1}). The elapsed time from the precipitation event to the start of the water level increase for water levels deeper than 60 ft (18 m) was proportional to the thickness of the vadose zone below 60 ft (18 m) (Oldenburg et al. 2002). The proportionality between elapsed time to water level increase and thickness of the vadose zone below 60 ft (18 m) indicates the recharge front advected at a rate of 0.7 ft/d (2.5 x 10^{-6} m s^{-1}) (Oldenburg et al. 2002). The decreasing advection rate of the recharge front with depth could be due to higher relative saturation in the upper portion of the vadose zone resulting from precipitation events earlier in the 1997/1998 rain year. Alternatively, the decreasing advection rate of the recharge front with depth could be due to a decrease in the hydraulic conductivity with depth.

Assuming a unit gradient, the advection rates for the recharge front are equivalent to the unsaturated hydraulic conductivity. Therefore, the unsaturated vertical hydraulic conductivities are 0.7–4 ft/d (2.5–14 x 10^{-6} m s^{-1}). The correlation of the recharge front arrival time at the water table to the thickness of the vadose zone at each well also indicates the vertical hydraulic conductivity throughout the vadose zone is relatively uniform with depth.

PDS results

The PDS sample results from most of the A-aquifer wells indicate that contaminant concentrations typically do not vary with depth. Vertical mixing in these wells should generally be minimal due to Darcy flow and the horizontal to near horizontal layering of the hydrostratigraphic units at the site. Therefore, the predominance of constant contaminant concentrations with depth indicates that within the A-aquifer at OU 1 there is typically little variation in the flow velocity with depth in the sandy portion of the A aquifer, suggesting the horizontal permeability is also relatively constant with depth.

Steady-state drawdown

Continuous groundwater extraction from EW-OU1-17-A commenced in early 1988 and continued through 2003. Continuous groundwater extraction from EW-OU1-18-A occurred from early 1988 to June 2001. The water levels in these wells and nearby wells MW-OU1-03-A and PZ –OU1-13-A to -16-A reflect the steady-state response of the aquifer to pumping. The water levels in these wells allow estimation of the hydraulic conductivity in the vicinity of the extraction wells by employing the Thiem equation for steady-state radial flow to a well in an unconfined aquifer (e.g., Bouwer, 1978).

The unconfined aquifer version of the Thiem equation rests on the following assumptions:

1. The aquifer is unconfined.
2. Pumping well and observation wells fully penetrate the aquifer.
3. Pumping rate is constant.
4. Flow has reached steady state.
5. Water-table position is not changing with time.
6. Aquifer is homogeneous and isotropic.
7. Water table is horizontal prior to pumping.
8. Aquifer is underlain by a horizontal aquitard.
9. Pumping well is 100% efficient.

The first assumption is obviously correct and second assumption is correct for the wells under consideration. Available totalizer data indicate the pumping rate for both wells is constant at approximately 8.5 gallons per minute (gpm), thereby in accordance with the third assumption. Figures 45 and 46 show the hydrographs for the wells under consideration. The applicability of the fourth assumption is reflected by the constant pumping rate, the constancy of the water levels in various time periods, and the constant to gradually changing water level differences between the wells. The fifth assumption is valid because measurements presented in Oldenburg et al. (2002) indicate that the time to rebound after the shutdown EW-OU1-18-A was approximately one month, which is much shorter than any similar magnitude natural changes in the water table elevation occurring at these wells with the exception of the period from early 1998 to mid-2000. Therefore, the Thiem equation can be applied to water levels outside of this time period.

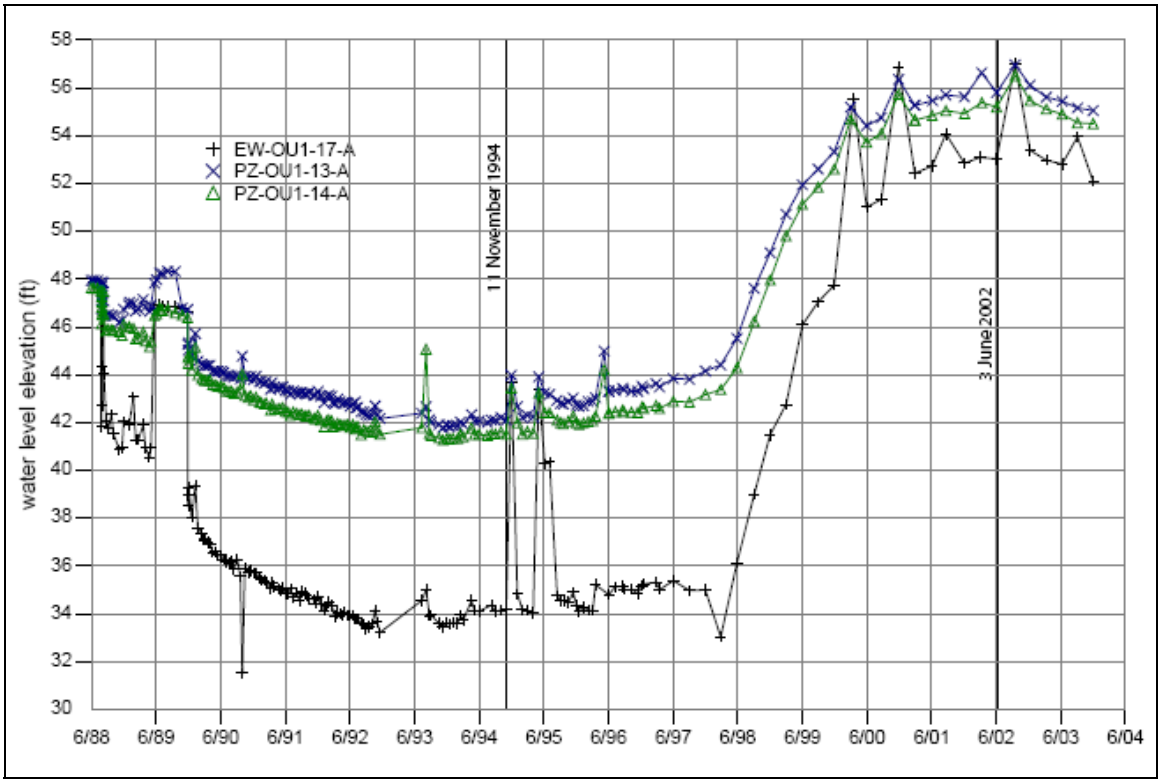

Figure 45. Hydrographs for EW-OU1-17-A, PZ-OU1-14-A.

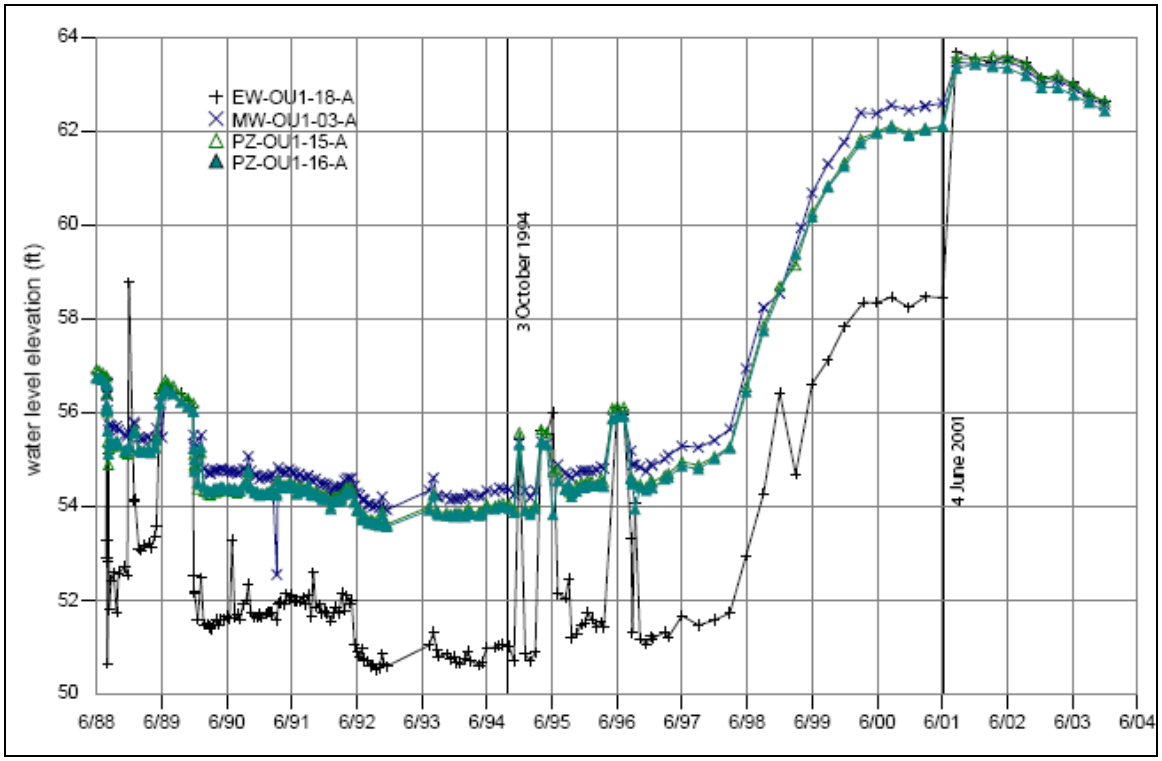

Figure 46. Hydrographs for EW-OU1-18-A, PZ-ou1-15-A and PZ-ou1-16-A.

The applicability of the sixth assumption is suggested by the materials which make up the A-aquifer. The homogeneous, isotropic nature of this material is further confirmed by the alignment of the TCE plume with the water table gradient and the pre-1998 water table depression presumably due to evapotranspiration losses resulting from the method of recharge of the treated water.

Comparison of water levels after shutdown of EW-OU1-18-A indicates that the non-pumping water table elevation in this well is the same as PZ-OU1-15-A, approximately 0.1 ft (0.03 m) above MW-OU1-03-A and approximately 0.2 ft (0.06) above PZ-OU1-16-A. The variances from the assumption for the latter two wells are relatively small compared to the drawdowns of 0.9 and 1.2 ft (0.27 and 0.37 m) at these wells, respectively, prior to the shutdown. Therefore, the seventh assumption is valid for EW-OU1-18-A and the three observation wells.

Comparison of water levels during apparent pumping shutdowns of EW-OU1-17-A, as well as consideration of the position of this well and the two observation wells relative to the surrounding water table and hydrogeologic features, indicates that the non-pumping water table elevation in this well is effectively the same as PZ-OU1-13-A, given the approximately 1.3–2.0 ft (0.40–0.61 m) drawdown at this observation well during pumping. The seventh assumption appears to be met for this well pair also. The non-pumping water table elevation at PZ-OU1-14-A appears to be approximately 0.5 ft (0.15 m) lower than at the other wells, which is in accord with its position farther from the edge of the airfield clay portion of Clay 3 (see Oldenburg et al. (2002) for a hydrostratigraphic description of OU 1). This is a significant fraction of the total typical drawdown at this well of 1.2–2.0 ft (0.37–0.61 m). Due to the smaller drawdowns at the observation wells, this deviation from the seventh assumption will introduce a large error into the hydraulic conductivity estimated from the observation well pair. The 0.5 ft (0.15 m) deviation at PZ-OU1-14-A is small relative to the drawdown of 4–10 ft (1.2–3.0 m) at EW-OU1-17-A, however, so the deviation will cause only slight underestimation of the hydraulic conductivity from this well pair. Therefore, the hydraulic conductivity will not be estimated from the observation well pair, but rather only from pumping well/observation well pairs.

The eighth assumption is valid for EW-OU1-17-A and PZ-OU1-13-A and -14-A as the top of the FO-SVA varies little compared to the observation

well drawdowns as shown in Figure 47. Note that the elevation of the top of the FO-SVA in this figure does not match those in Oldenburg et al. (2002) at all wells. In the former document, the top of the FO-SVA was taken at the base of angled contacts shown on well logs. In this document, the top of the FO-SVA is taken at the midpoint of the angled contacts shown on logs, as is standard in the geotechnical industry.

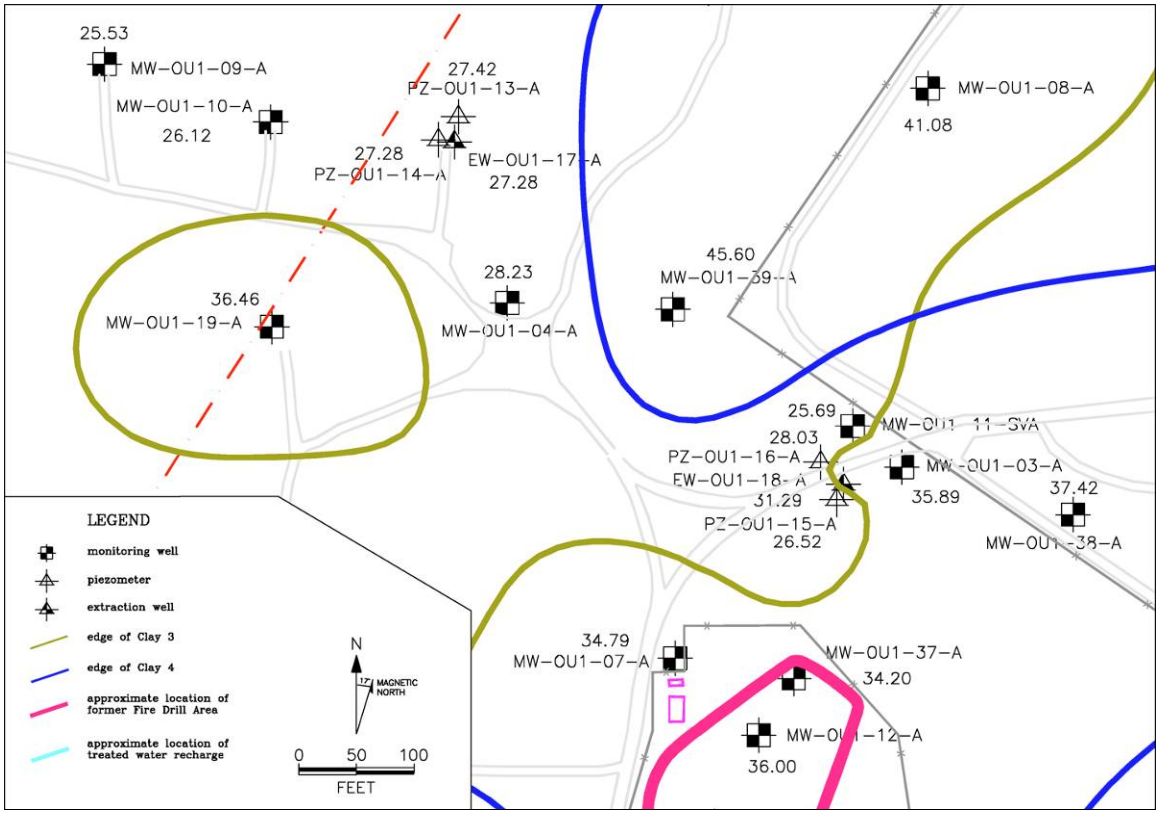

Figure 47. Elevation of the top of the FO-SVA (in feet) in the vicinity of EW-OU1- 17-A and EW-OU1-17-18-A.

The eighth assumption is problematic for EW-OU1-18-A, MW-OU1-03-A, and PZ-OU1-15-A, and -16-A since the top of the FO-SVA varies by 10 ft (3 m) (as shown in Figure 47) which is an order of magnitude more than the drawdown at the observation wells. This error introduces large errors in the hydraulic conductivities estimated using the actual saturated thicknesses from the well pairs using the Thiem equation as shown in Figure 48 and in Table 13. These errors are due to the large errors—even reversals—in the estimation of the gradient. The gradient can be preserved by treating the aquitard elevation as constant. This will in turn introduce errors into the saturated thickness. However, these errors will always be smaller than those where the saturated thickness is preserved and the gradient is altered, and the error introduced will be bounded as described below.

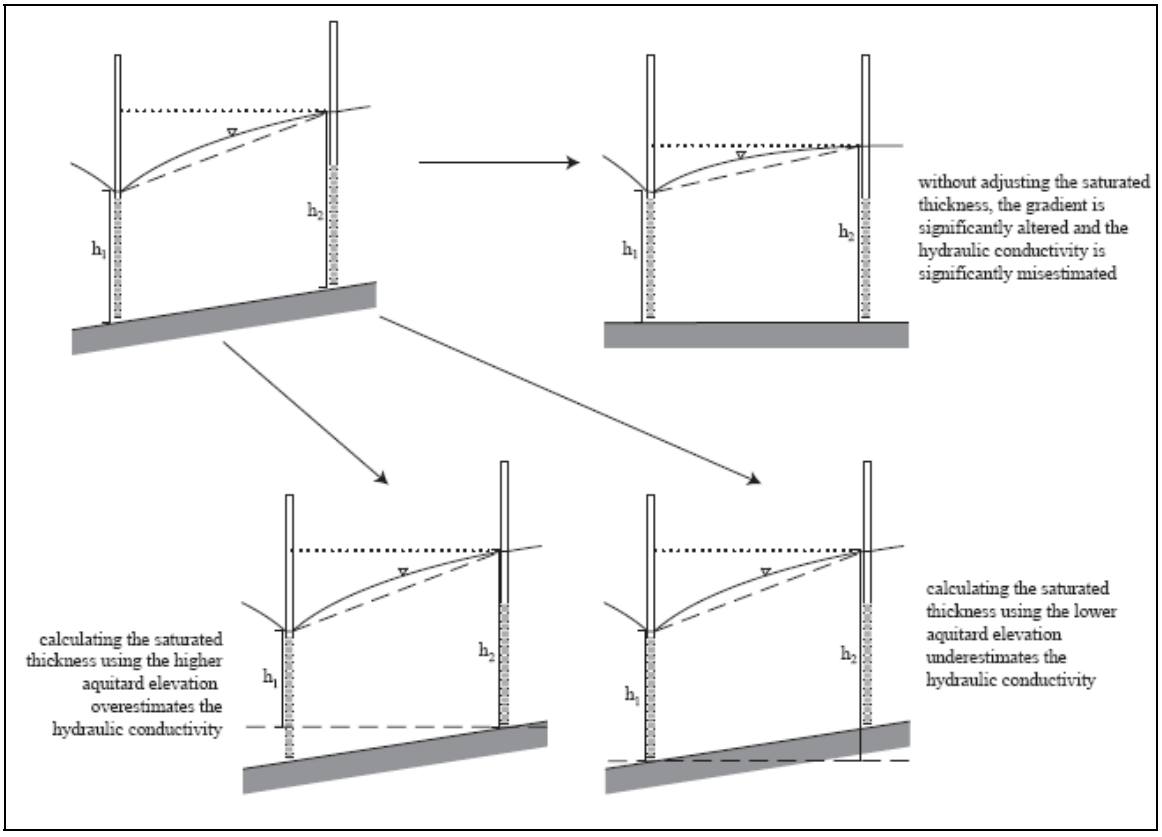

Figure 48. Consequences of variation in the elevation of the aquitard.

Table 13. Erroneous estimates of hydraulic conductivity (ft/d) from EW-OU1-18-A.

3 October 1994 4 June 2001	EW-OU1-18-A	PZ-OU1-15-A	PZ-OU1-16-A	MW-OU1-03-A
EW-OU1-18-A		2.9	4.3	-29.2
PZ-OU1-15-A	2.0		-2.0	-0.5
PZ-OU1-16-A	2.9	-1.7		-0.8
MW-OU1-03-A	-56.3	-0.4	-0.6	

There are two components to the deviation from the eighth assumption. The first component is the variance of the aquitard elevation in the radial direction from the pumping well. The second component is the variation of the aquitard elevation in the tangential direction around the pumping well. This variation will cause tangential gradients gv inconsistent with the radial-flow-only corollary to the sixth, seventh, and eighth assumptions.

The error introduced by setting the FO-SVA elevation constant around EW-OU1-18-A can be bounded by estimating the end-member hydraulic conductivity for each well pair as shown in Figure 48. One estimate of saturated thickness uses the higher aquitard elevation from the well pair,

while the other is based upon the lower aquitard elevation from the well pair. The first method will overestimate the hydraulic conductivity due to the artificial reduction in saturated thickness. The second method will underestimate the hydraulic conductivity due to the artificial increase in saturated thickness. The actual hydraulic conductivity will be between these two estimates.

The tangential variability of the aquitard can be accounted for by only estimating hydraulic conductivity from well pairs along the same azimuth from the pumping well, and by estimating hydraulic conductivity at different azimuths that capture the range of variability in the aquitard. The first strategy eliminates misestimation of hydraulic conductivities due to tangential flow and gradients caused by differing aquitard elevations between observation wells on different azimuths. As none of the OU 1 observation wells are on the same azimuth, this necessitates only analyzing well pairs consisting of the pumping well and an observation well. The second strategy develops a range of estimates that will bracket the actual hydraulic conductivity value. This is because the tangential variability in the aquifer leads to different contributions to the pumping rate from different sectors of the aquifer. The Thiem equation will therefore over- or under-estimate the hydraulic conductivity along a particular azimuth depending upon whether the contribution of that sector of the aquifer is above or below the average. If hydraulic conductivity estimations are made along a number of azimuths, then the variance in the flow contributions will average out between them, as will the hydraulic conductivity estimates. The three EW-OU1-18-A/observation well pairs are along approximately evenly spaced azimuths (as shown in Figure 47), so this approach is valid.

The ninth assumption overestimates the efficiency of any real well. However, the actual efficiency of EW-OU1-17-A and -18-A is probably reasonably high given the lack of fines in the formation and the use of stainless steel, wire-wrapped screens in their construction. Therefore, while there are certainly head losses across the well screen, they are likely a small fraction of the total drawdown. To the extent these losses exist, use of water levels from these wells will underestimate the hydraulic conductivity because use of these water levels overestimates the gradient toward the well. The impact of a less than perfect well efficiency on the hydraulic conductivity estimates is approximated below.

Hydraulic conductivity estimates were developed using water levels from periods of relatively stable pumping (for which data were available from June 2000 through December 2003) and/or water level stability. Estimates were developed for one pre-1998 and one post-1998 water level data set. Table 14 presents the hydraulic conductivity estimates for the EW-OU1-17-A/observation well pairs. Due to the slight variation in the elevation of the top of the FO-SVA between EW-OU1-17-A and PZ-OU1-13-A, and for the sake of consistency, this table presents end-member (calculated based on minimum and maximum elevations of the FO-SVA for each well pair) hydraulic conductivity estimates. Table 15 presents the end-member hydraulic conductivity estimates for the EW-OU1-18-A/observation well pairs.

Table 14. Hydraulic conductivity estimates (ft/d) from EW-OU1-17-A pumping.

EW-OU1-17-A	Pumping well clay elevation		Observation well clay elevation	
	PZ-OU1-14-A	PZ-OU1-13-A	PZ-OU1-14-A	PZ-OU1-13-A
11 November 1994	6.8	7.0	6.8	6.9
~80% efficient	8.4	8.6	8.4	8.3
3 June 2002	9.0	8.4	9.0	7.8
~80% efficient	14.0	12.0	14.0	10.7

Table 15. Hydraulic conductivity estimates (ft/d) from EW-OU1-18-A pumping.

EW-OU1-18-A	Pumping well clay elevation			Observation well clay elevation		
	PZ-OU1-16-A	PZ-0U1-15-A	MW-OU1-03-A	PZ-OU1-16-A	PZ-OU1-15-A	MW-OU1-03-A
3 October 1994	5.0	5.8	5.8	4.3	5.2	6.8
~80% efficient	6.9	7.9	7.6	5.9	7.2	9.0
4 June 2001	8.2	9.9	9.7	6.7	8.5	12.4
~80% efficient	11.3	13.8	12.9	9.3	12.0	16.4

The June 2001 drawdown at EW-OU1-18-A is known directly from measurements following the pump shutdown. The drawdown at the extraction wells for the other dates is calculated by presuming that water level peaks at nearby dates on the hydrographs shown in Figures 45 and 46 are due to short pump shutdowns. This presumption is reasonable as the water level in the extraction wells rises to nearly the same level as in the observation wells on these dates. The extraction well drawdowns were used to develop the hydraulic conductivity estimates assuming a pumping well efficiency of 80%. The hydraulic conductivity estimates assuming 80% well efficiency range from 30% to 60% higher than the estimates, assuming 100% well

efficiency for the single well pair estimates. This is a fairly small error given the natural variability in hydraulic conductivity.

The variation in the end-member hydraulic conductivity estimates for each well pair is less than 25% using the average of the estimates as the basis. The average variation of the end-member hydraulic conductivity estimates is 3% and 17% for the EW-OU1-17-A and EW-OU1-18-A well pairs, respectively. The higher variation in the EW-OU1-18-A well pairs is expected due to the greater variation in the FO-SVA elevation around this well.

The average of all the hydraulic conductivity estimates assuming 100% well efficiency (no head loss across the well screen) is 7.7 ft/d (2.7 x 10^{-5} m s^{-1}) and 7.4 ft/d (2.6 x 10^{-5} m s^{-1}) for EW-OU1-17-A and EW-OU1-18-A, respectively. Assuming 80% well efficiency (20% head loss across the well screen), the average of all the estimates is 10.6 ft/d (3.7 x 10^{-5} m s^{-1}) and 10.8 ft/d (3.8 x 10^{-5} m s^{-1}) for EW-OU1-17-A and EW-OU1-18-A, respectively.

The hydraulic conductivity estimates for every well pair were 30% to 80% greater during the increased water levels after 1998 than before, suggesting the hydraulic conductivity decreases slightly with depth. This relatively small variation is consistent with the typically constant contaminant concentrations with depth from the PDS results. The average of the hydraulic conductivity estimates for the EW-OU1-17-A well pairs, assuming 100% efficiency, are 6.9 ft/d (2.4 x 10^{-5} m s^{-1}) and 8.5 ft/d (3.0 x 10^{-5} m s^{-1}) for 1994 and 2002, respectively. The water levels during the 1994 estimate were 14–19 ft (4.3–5.8 m) lower than during the 2002 estimate, and the water level in EW-OU1-17-A was approximately 6 ft (1.8 m) and 25 ft (7.6 m) above the top of the FO-SVA in 1994 and 2002, respectively. The average of the hydraulic conductivity estimates for the EW-OU1-18-A well pairs, assuming 100% efficiency, are 5.5 ft/d (1.9 x 10^{-5} m s^{-1}) and 9.2 ft/d (3.2 x 10^{-5} m s^{-1}) in 1994 and 2001, respectively. The water levels during the 1994 estimate were 7–8 ft (2.1–2.4 m) lower than during the 2001 estimate, and the water level in EW-OU1-18-A was approximately 20 ft (6.1 m) and 27 ft (8.2 m) above the top of the FO-SVA in 1994 and 2001, respectively. Therefore, the variation in hydraulic conductivity with depth appears to be less at EW-OU1-17-A than at EW-OU1-18-A, particularly considering the much larger water level changes at the former compared to the latter.

The range of well pair averaged estimates assuming 100% efficiency is 6.8–7.0 ft/d (2.4–2.5 x 10^{-5} m s^{-1}) and 7.8– 9.0 ft/d (2.7–3.2 x 10^{-5} m s^{-1}) for the EW-OU1-17-A well pairs in 1994 and 2002, respectively. The range of well pair averaged estimates assuming 100% efficiency is 4.3-6.8 ft/d (1.5–2.4 x 10^{-5} m s^{-1}) and 6.7–12.4 ft/d (2.4–4.3 x 10^{-5} m s^{-1}) for the EW-OU1-18-A well pairs in 1994 and 2001, respectively. The ranges of hydraulic conductivity estimates from EW-OU1-18-A are greater than that from EW-OU1-17-A, probably due to the greater variability in the elevation of the top of the FO-SVA around EW-OU1-18-A.

Treated groundwater recharge response

Water level changes in wells MW-OU1-01-A, -02-A, -06-A and -12-A followed changes in the treated water recharge rate by 20 days to a month (Oldenburg et al. 2002). As the vadose zone is approximately 70 ft (21.3 m) thick in this area, the linear velocity through the partially to nearly saturated vadose zone beneath the recharge area is between 2.3 and 3.5 ft/d (1.2 x 10^{-5} m s^{-1}). Assuming a unit hydraulic gradient and an effective porosity of 25%, the unsaturated vertical hydraulic conductivity in the vadose zone is 0.6–0.9 ft/d (2.1–3.2 x 10^{-6} m s^{-1}).

Short-duration pump tests

Short duration pumping tests were conducted at wells MW-OU-07-A, 08-A, 10-A, and 29-A. The results of these tests were analyzed using the Dupuit-Forcheimer equation to arrive at hydraulic conductivities of 3.1, 3.4, 43, and 7.1 ft/d (1.1, 1.2, 15, and 2.5 x 10^{-5} m s^{-1}) (Oldenburg et al. 2002). Oldenburg et al. (2002) used the harmonic mean of these conductivities (5.1 ft/d (1.8 x 10^{-5} m s^{-1})) for estimating average linear velocities and simple flow modeling used to analyze ISPFS response. The harmonic mean is appropriate for estimating conductivities in one-dimensional flow perpendicular to a series of layers with different conductivities. However, the geometric mean provides a more accurate estimation of average conductivity from point measurements in a two-dimensional domain containing non-layer-dependent conductivity variations (de Marsily, 1986). The geometric mean of the hydraulic conductivities inverted from the short duration pump tests is 7.5 ft/d (2.6 x 10^{-5} m s^{-1}).

ISPFS results

Inversion of the temperature data from the three ISPFS instruments with functioning heaters and conforming temperature data yields a Darcy flow velocity vector in the vicinity of the instrument, as previously described. The apparent vertical Darcy velocities measured by the instruments at OU 1 are likely artifacts of the thermal heterogeneity and borehole skin around the instruments as previously discussed in this report and in Su, et al. (2005). However, the horizontal Darcy velocities appear reasonable. Dividing these velocities by the gradient yields an estimate of the hydraulic conductivity around each sensor. Table 16 lists the inverted velocity and the gradient measured from the June 2003 water table in the vicinity of the ISPFSs along with the estimated hydraulic conductivities.

Table 16. Hydraulic conductivity estimates from ISPFS Vh and gradient.

	MW-OU1-36-A	*MW-OU1-37-A*	MW-OU1-39-A
Vh from ISPFS (ft/day)	0.028	0.093	0.13
Gradient	0.0058	0.0090	0.027
Hydraulic Conductivity (ft/day)	4.8	10.3	4.8

Summary hydraulic conductivity comparison

Table 17 summarizes and compares all of the hydraulic conductivity estimates as well as information regarding heterogeneity and anisotropy. The estimates made by a wide variety of methods are in excellent agreement, falling primarily between 5–10 ft/d (1.8–3.5 x 10^{-5} m s^{-1}). This is a remarkable result given the range of scales over which these estimates are made. Scales range from the length of the entire plume (approximately 3000 ft (900 m)) to the bore-hole scale (ISPFS results). Furthermore, the analyses indicated that the A-aquifer is relatively homogeneous and isotropic with perhaps a slight decline in conductivity with depth. The unsaturated vertical conductivities range from 0.6–4 ft/d (2.1–14 x 10^{-6} m s^{-1}). Given that unsaturated conductivities are less than saturated conductivities for the same material, this range appears reasonable relative to the horizontal, saturated hydraulic conductivities.

Table 17. Comparison of hydraulic conductivity estimates.

Estimate Source Data	K type	K(ft/d)	Notes
Plume length	Horizontal, saturated	5.0	Actual value probably higher due to retardation
Plume alignment	Horizontal, saturated	NA	Alignment suggests no heterogeneity or anisotropy.
Early 1998 recharge – vadose zone above 60 feet deep	Vertical, near saturation?	1.3-4	No significant heterogeneity in vadose zone above 60 feet
Early 1998 recharge – vadose zone below 60 feet deep	Vertical, unsaturated?	0.7	No significant heterogeneity in vadose zone below 60 feet
Treated groundwater recharge	Vertical, near saturation?	0.6-0.9	
PDS results	Horizontal, saturated	NA	horizontal conductivity does not vary greatly with depth
EW-OU1-17-A and -18A drawdown	Horizontal, saturated	7.4-7.7	Assumes 100% pumping well efficiency
EW-OU1-17-A and -18A drawdown	Horizontal, saturated	10.6-10.8	Assumes 80% pumping well efficiency
EW-OU1-17-A and -18A drawdown	Horizontal, saturated	NA	Slight decrease in conductivity with depth, no anisotropy
Short-duration pump tests	Horizontal, saturated	3.1-43	Geometric mean is 7.5
Water-table gradients and ISPFS velocity measurements	Horizontal, saturated	4.8-10.3	

TCE plume evolution

TCE plume history

The TCE plume is shown in late 1993, late 1997, and late 1999 in Oldenburg et al. (2002), which nearly covered the temporal extent of the chemistry data analyzed in that report. The chemistry data analyzed in the present report cover the time period from the beginning of 1986 to the end of 2003. Figure 49 shows the head of the TCE plume in late 1986. Note that the location of the FDA is more accurately depicted as compared to the depiction in Oldenburg et al. (2002), and now includes the flammable materials offloading, storage, and transfer areas as well as the burn pit. The depiction shown is based upon studies by Harding Lawson Associates (1986) and an unreferenced vertical aerial photograph available from the Fort Ord Data Integration System (http://www.fodis.net). This photo was included on the website to show the mosaic pattern of grassland, coast live oak woodland, and central maritime chaparral at Fort Ord. The photo also happened to show the FDA in the period between cessation of fire training activities and the remedial soil excavation.

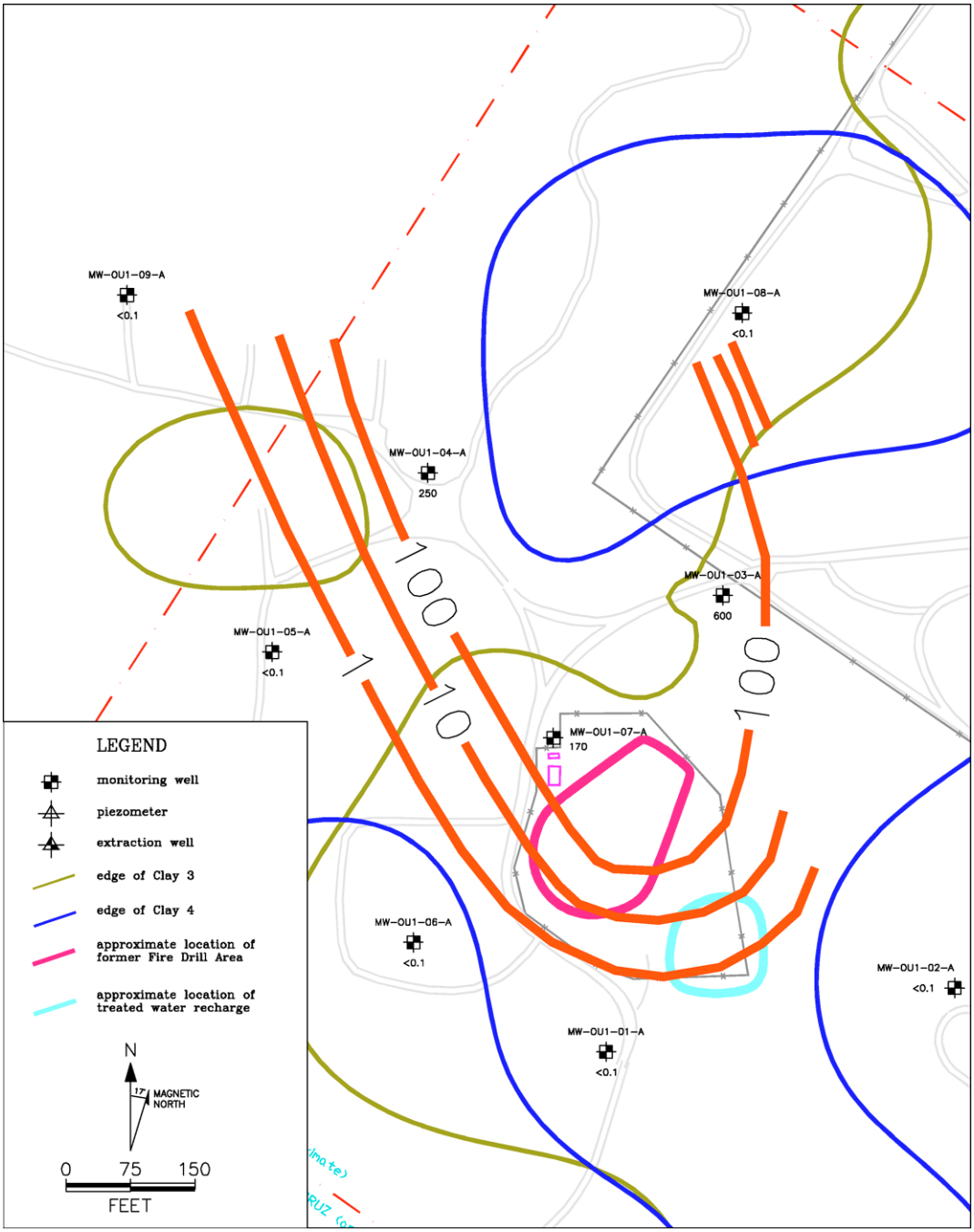

Figure 49. Isoconcentrations of TCE (µg/L) in late 1986.

Plume prior to remediation

The head of the TCE plume shown in Figure 49 was approximately co-located with the FDA. The shape of the plume head suggests a single area of contaminant release with subsequent advection and dispersion with the possible exception of an additional release of contaminants near MW-OU1-03-A, which has the highest TCE concentrations. The axis of the

plume trended approximately 15 degrees west of north which matched the estimate of the pre-extraction gradient direction in Oldenburg et al. (2002). Up to late 1986, TCE was not detected in the transgradient wells MW-OU1-05-A, -06-A, -08-A and -09-A, nor in upgradient wells MW-OU1-01-A and 02-A.

Plume after soil remediation

The TCE plume head in late 1987 is shown in Figure 50. This apparently post-dates soil remediation activities at the FDA. TCE concentrations at MW-OU1-03-A, -04-A and -07-A diminished relative to 1986. The concentrations at the MW-OU1-03-A were the highest and did not decrease as significantly as the concentrations in the other two wells, further suggesting an additional, past contaminant release near this well. TCE was detected at upgradient well MW-OU1-01-A for the first time during this period. The timing of this detection suggests that the soil remediation activities between late 1986 and late 1987 may have moved TCE to the south of the FDA, either by reversing the groundwater flow or by introducing TCE into or mobilizing TCE through the vadose zone in this area. TCE was still not detected at the transgradient wells.

Plume after commencement of pump, treat and recharge

In mid-1988, extraction of contaminated groundwater from EW-OU1-17-A and -18-A commenced. The extraction rate from each well was approximately 8 gallons per minute (gpm) (0.5 L s^{-1}). The water was treated by an on-site granular activated-charcoal system and then spread on the ground surface by sprinkler in the general area shown in Figure 51. Based on Figure 50, the recharge area appears to overlie a portion of the TCE plume. The recharge area is approximately 10 degrees east of south from EW-OU1-18-A, which is almost directly upgradient of this extraction well. Oldenburg et al. (2002) estimated that the recharge rate was 70% of the total extraction rate, which is 40% greater than the extraction rate from a single well. Given these relative rates and the spatial relationship between EW-OU1-18-A and the recharge area, it is likely that some of the flow from the recharge area bypassed EW-OU1-18-A to the east.

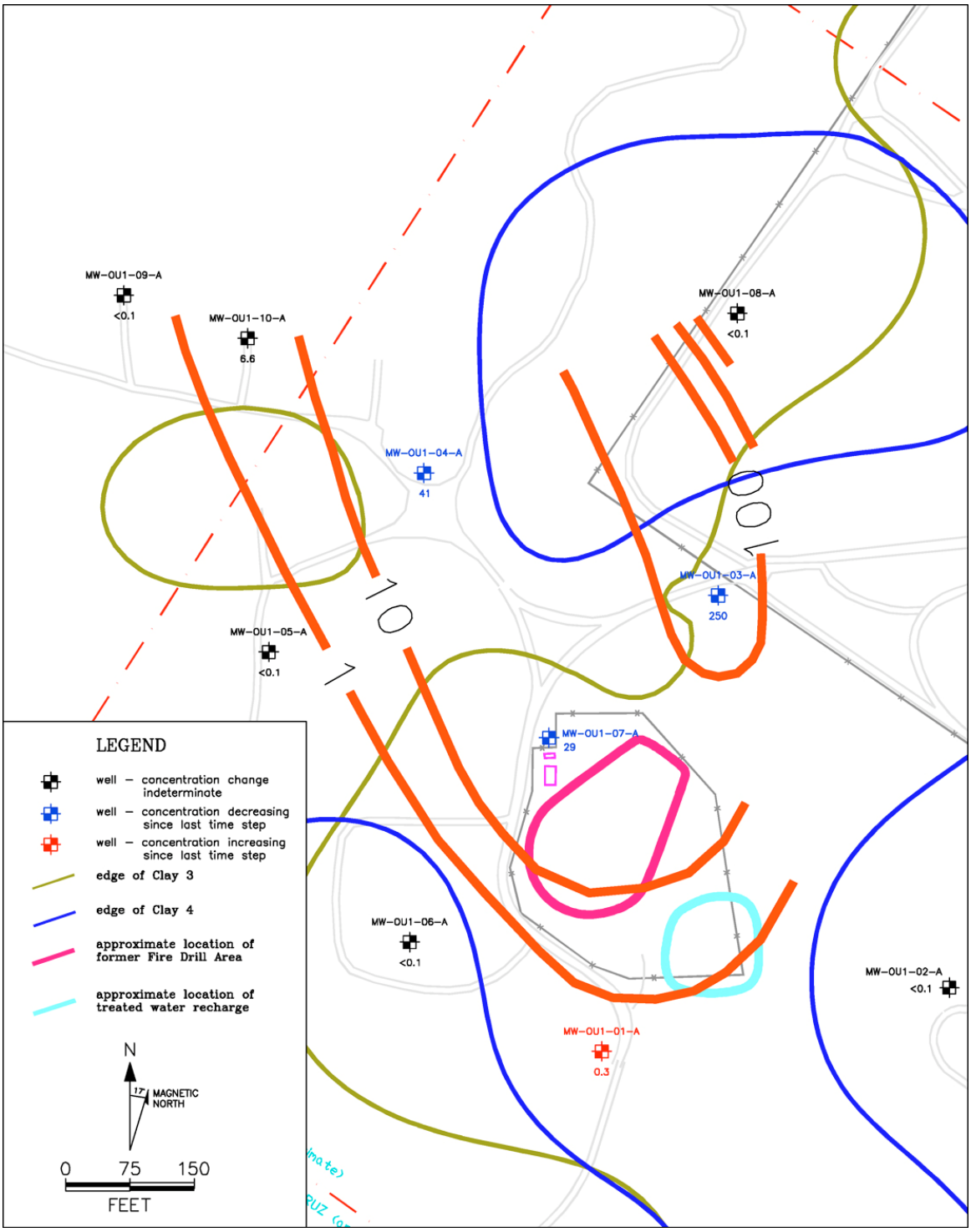

Figure 50. Isoconcentrations of TCE(µg/L) in late 1987.

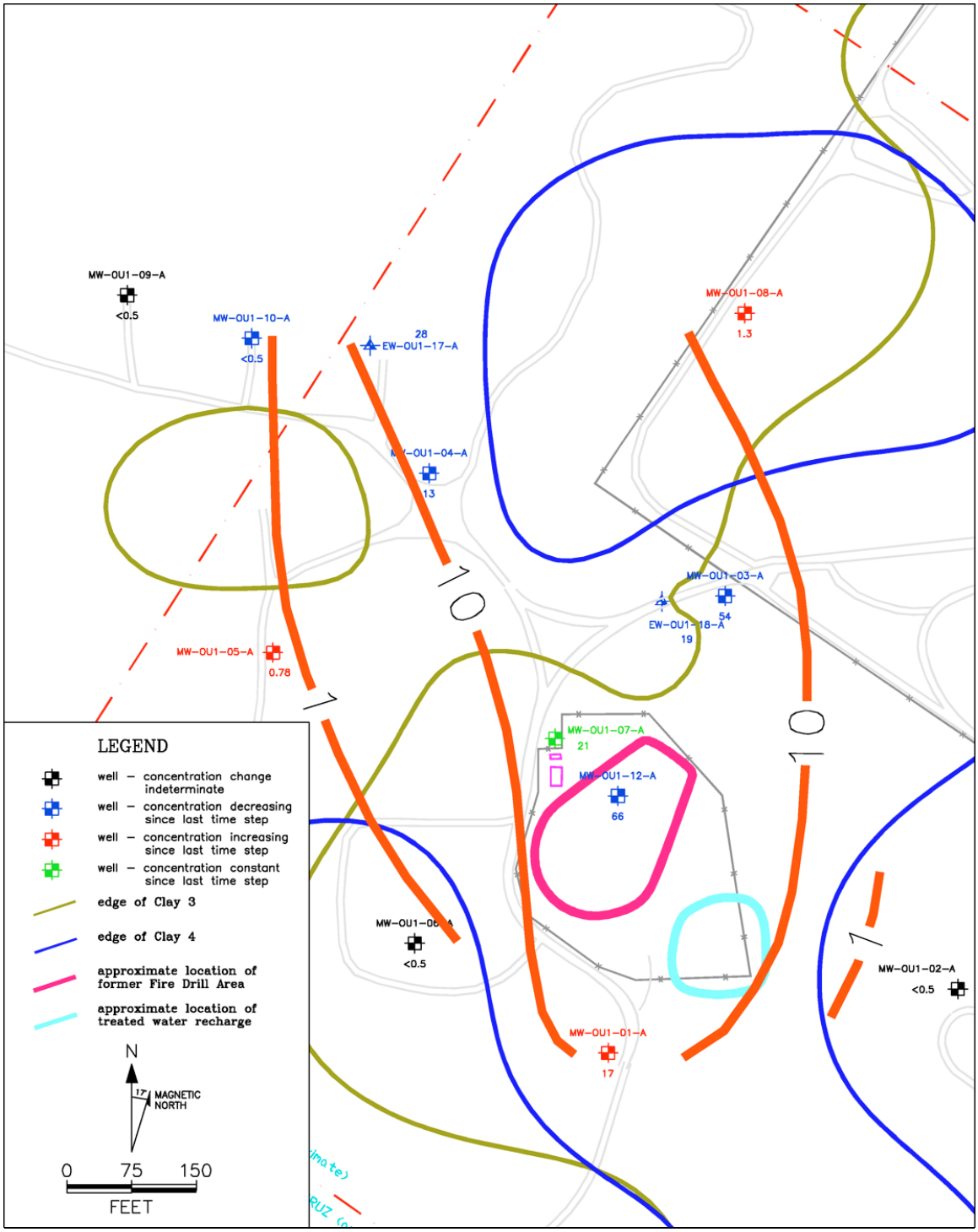

Figure 51. Isoconcentrations of TCE (µg/L) in late 1990.

Figure 51 also shows the TCE plume head in late 1990. Concentrations continued to generally decrease within the plume core. The concentration at MW-OU1-03-A was still the highest. The TCE concentration in trans-gradient well MW-OU1-10-A declined, presumably due to flow of TCE-free

groundwater from beyond the plume boundary to EW-OU1-17-A (throughout the rest of this section, transgradient will be used to refer to wells that were cross-gradient from the TCE plume location in 1986).

In late 1990, the TCE concentration in upgradient well MW-OU1-01-A increased approximately two orders of magnitude relative to the concentration prior to commencement of treated water recharge. Oldenburg et al. (2002) demonstrated that the water levels in this well had the greatest response to this recharge. The TCE concentration increase was likely due to some effect of the treated water recharge. This could be due to placement of the recharge area over a portion of the plume with subsequent reversal of groundwater flow. This reversal would cause TCE-contaminated groundwater to advect southward toward MW-OU1-01-A. However, flow reversal would likely have brought groundwater contaminated with 1,2 Dichloroethylene (1,2 DCE) to the well also. 1,2 DCE is a degradation product of TCE which is present throughout the head of the TCE plume prior to remedial activities in late 1986. 1,2 DCE was not detected in MW-OU-01-A. Therefore, a more likely mechanism for the TCE increase at MW-OU1-01-A is mobilization of residual TCE in the vadose zone by the high rate of treated water recharge (which is several times the peak natural recharge rate (Oldenburg et al. 2002)).

Figure 51 shows TCE was also detected at transgradient wells MW-OU1-05-A and -08-A where TCE had generally not been detected prior to treated water recharge. This is likely a result of the transgradient plume dimension increasing due to divergent flow of contaminated groundwater beneath the treated water recharge area. Specifically, a slight change in the trajectory of contaminated groundwater along west of the FDA and in the vicinity of MW-OU1-03-A would cause the observed increases.

Plume six years after commencing pump, treat, and recharge

The concentration of TCE in the plume core continued to decrease through early 1994 as shown in Figure 52. The TCE concentration in transgradient well MW-OU1-05-A continued to increase. The TCE concentration in transgradient well MW-OU1-06-A increased above non-detected for the first time, probably due to advection of the contaminated water in the vicinity of MW-OU1-01-A in 1990. Meanwhile, the TCE concentration in MW-OU1-01-A decreased considerably suggesting that the source of the TCE at this well was significantly depleted by this time.

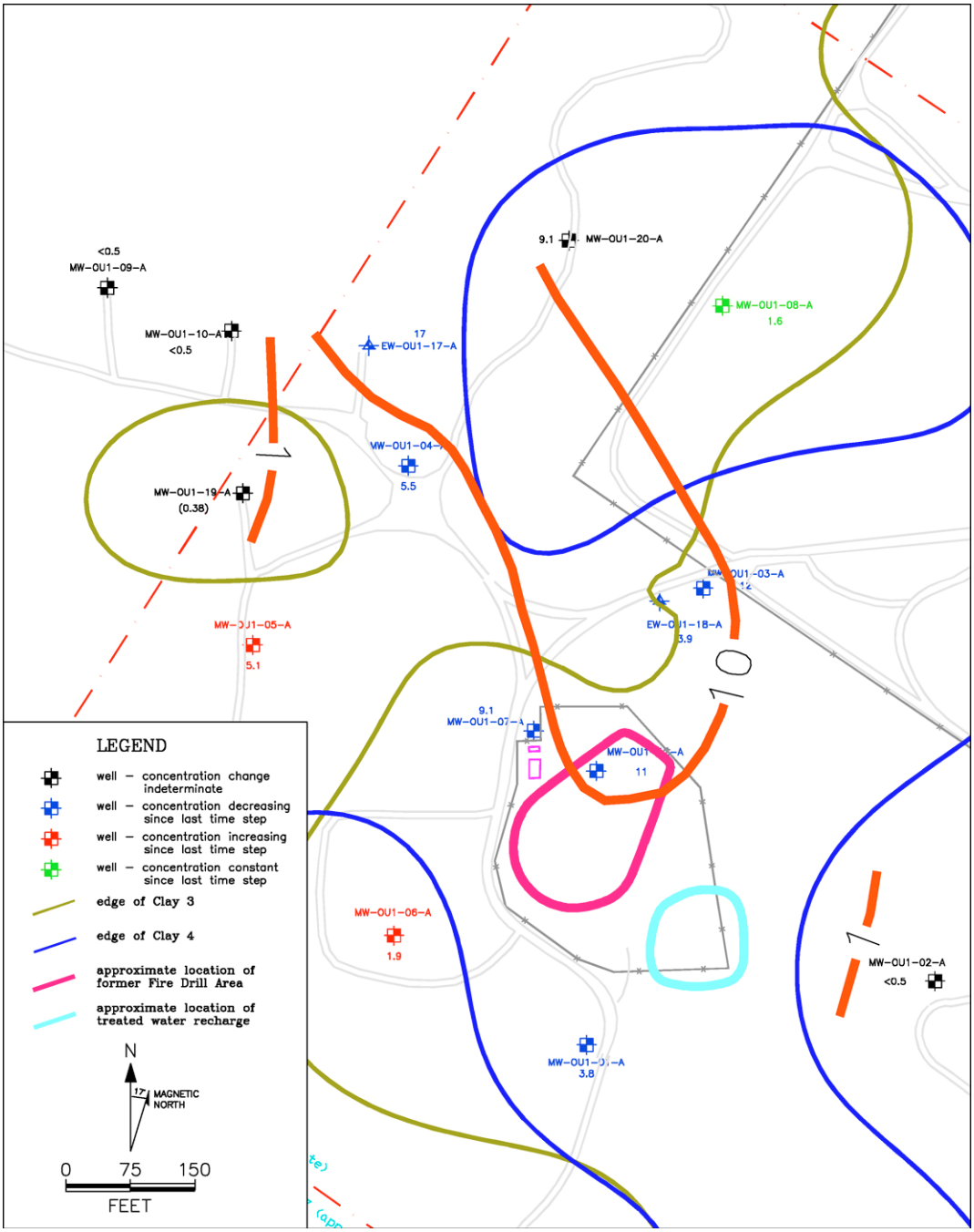

Figure 52. Isoconcentrations of TCE (µg/L) in early 1994 (modified from Oldenburg et al., 2002).

Plume prior to early 1998 recharge

The concentration of TCE in the plume core generally continued to decrease through late 1997 as shown in Figure 53. The concentration in MW-OU1-01-A continued to decrease. The concentration decreased in nearby MW-OU1-06-A as well, probably due to advection along the west side of

the plume of lower concentration groundwater which occurred in 1994 around MW-OU1-01-A. The concentration also decreased in MW-OU1-08-A, probably due to advection of significantly lower concentration groundwater in the vicinity of MW-OU1-03-A along the east side of the plume.

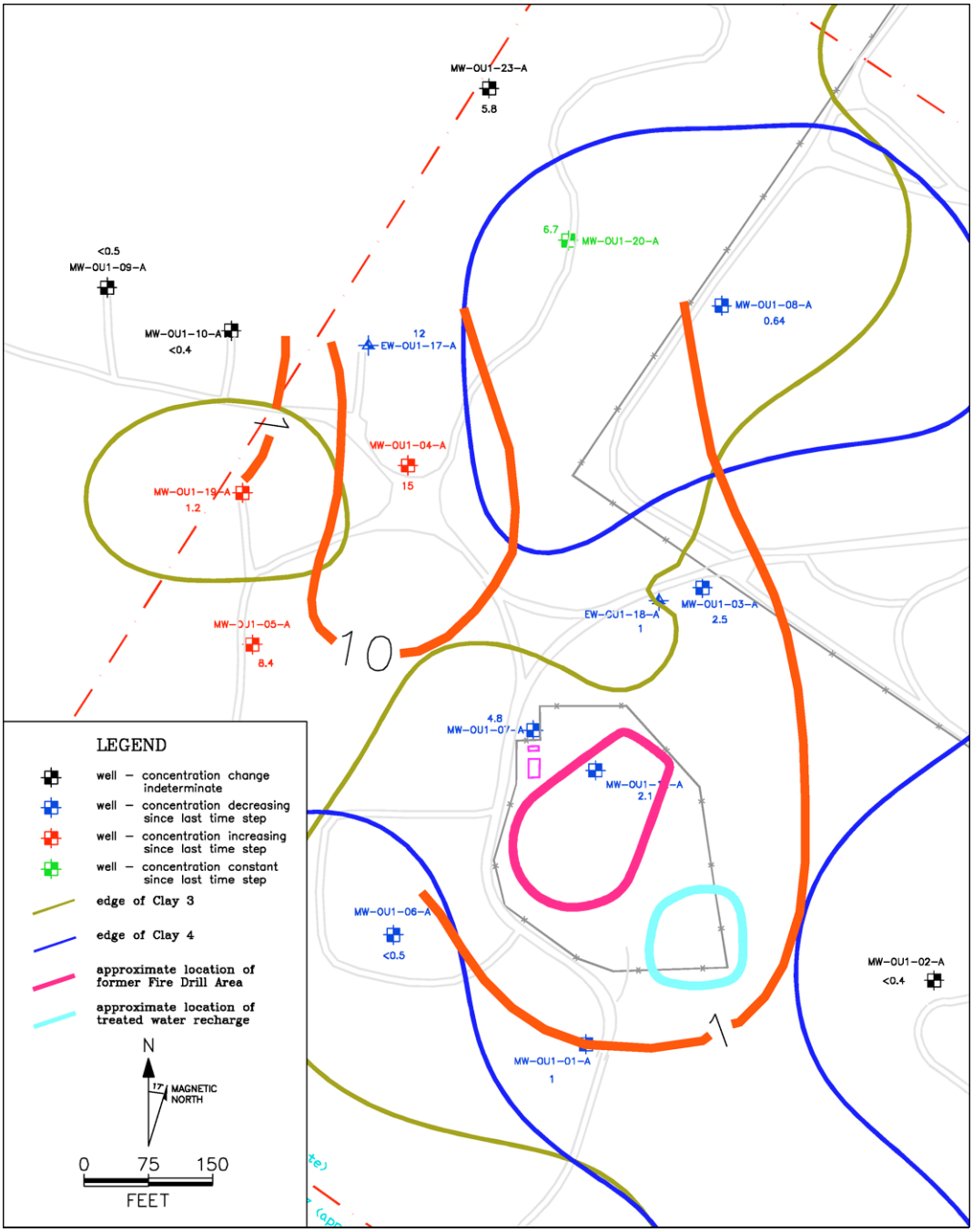

Figure 53. Isoconcentrations of TCE (µg/L) in late 1997 (modified from Oldenburg et al., 2002).

The TCE concentrations in MW-OU1-04-A, -05-A and -19-A increased through late 1997. These increases appear to be due to continued advection along the west side of the plume of the higher-concentration groundwater which occurred in 1990 at MW-OU1-01-A. The distance between MW-OU1-05-A and MW-OU1-06-A is approximately 400 ft (120 m). From Oldenburg et al. (2002), the gradient west of the FDA is 0.011. Using a hydraulic conductivity of 7.5 ft/d (2.6×10^{-5} m s^{-1}) and a porosity of 25% yields a linear velocity of 0.33 ft/d (1.2×10^{-6} m s^{-1}) or a travel time of 3.3 years between the two wells. This matches the apparent travel time of over two years between these two wells based upon a comparison of Figures 52 and 53.

Plume following early 1998 precipitation

Following the historically high precipitation of early 1998, TCE concentrations in EW-OU1-18-A, nearby wells and wells upgradient remained the same as shown on Figure 54. Concentrations in most of the other wells in which TCE had ever been detected increased. One explanation considered in Oldenburg et al. (2002) was that the record high water levels following precipitation caused entrainment of TCE-contaminated water at the base of the unsaturated zone. This water could have been stranded after past water level declines. However, as presented in Oldenburg et al. (2002), the timing of the TCE concentration increases does not match the timing or magnitude of the water level increases. Furthermore, some of the wells that showed concentration increases, such as MW-OU1-06-A and -05-A, do not appear to have been in the vicinity of contaminated groundwater during higher water level periods. Other wells that were in the vicinity of the most contaminated groundwater during higher water level periods, such as MW-OU1-03-A and -07-A, do not show any concentration increase.

Oldenburg et al. (2002) suggested that mobilization of residual contamination west of the FDA could have caused a concentration increase that propagated down gradient. They noted that the concentration increase at MW-OU1-05-A occurred approximately three months after the increase in MW-OU1-06-A, which is too rapid for advection of a single concentration pulse. No other alternative explanations for the concentration increases following the early 1998 precipitation are currently available.

Concentration data from wells installed since early 1997 affords some perspective on the downgradient extent of the TCE plume in 1999 as shown in

Figure 55. While the well field at this time does not characterize the full extent of the plume, the plume axis passes near PZ-OU1-35-A, and MW-OU1-29-A and -34-A at the tip of the plume.

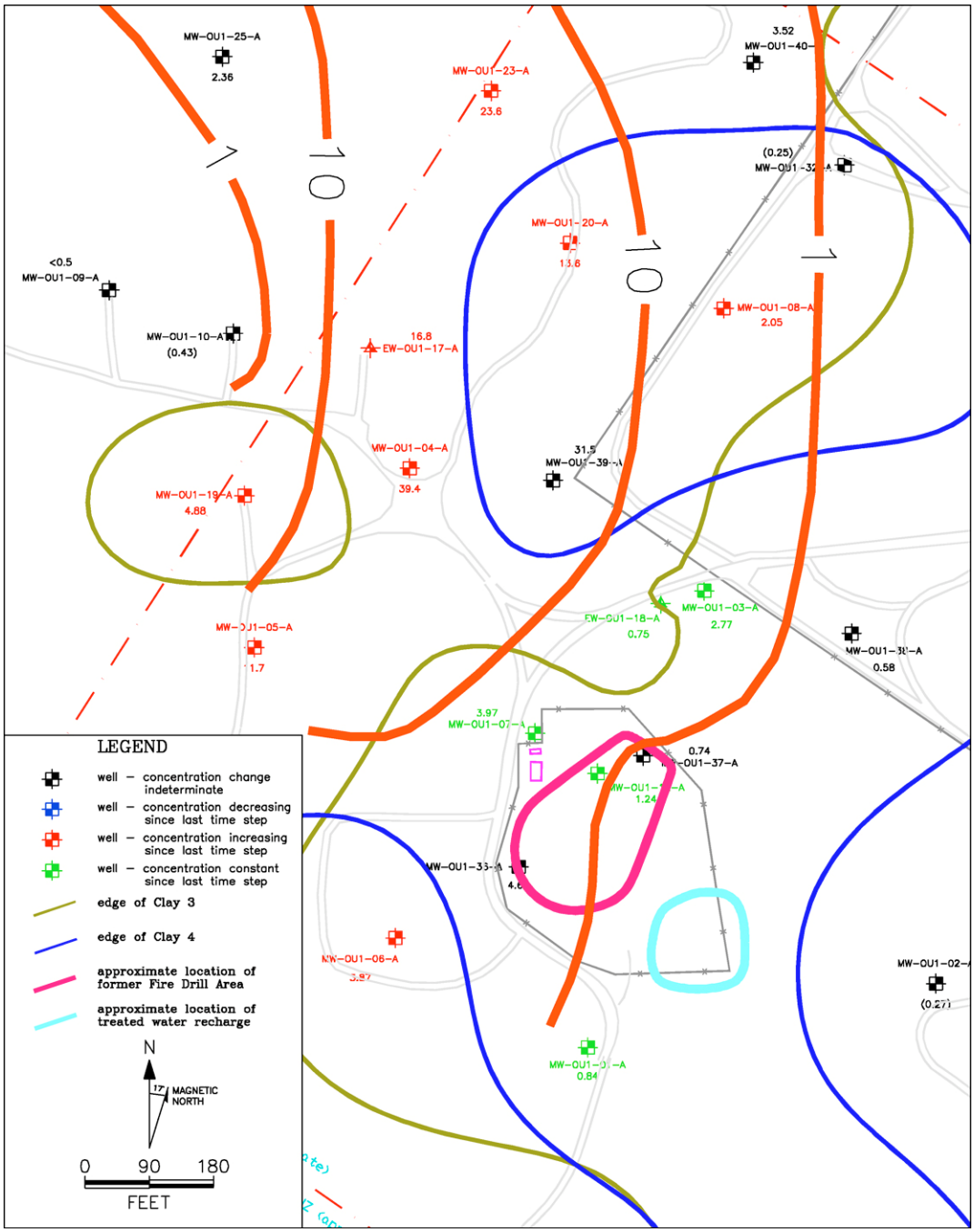

Figure 54. Isoconcentrations (µg/L) in the vicinity of the FDA in late 1999 (modified from Oldenburg et al., 2002).

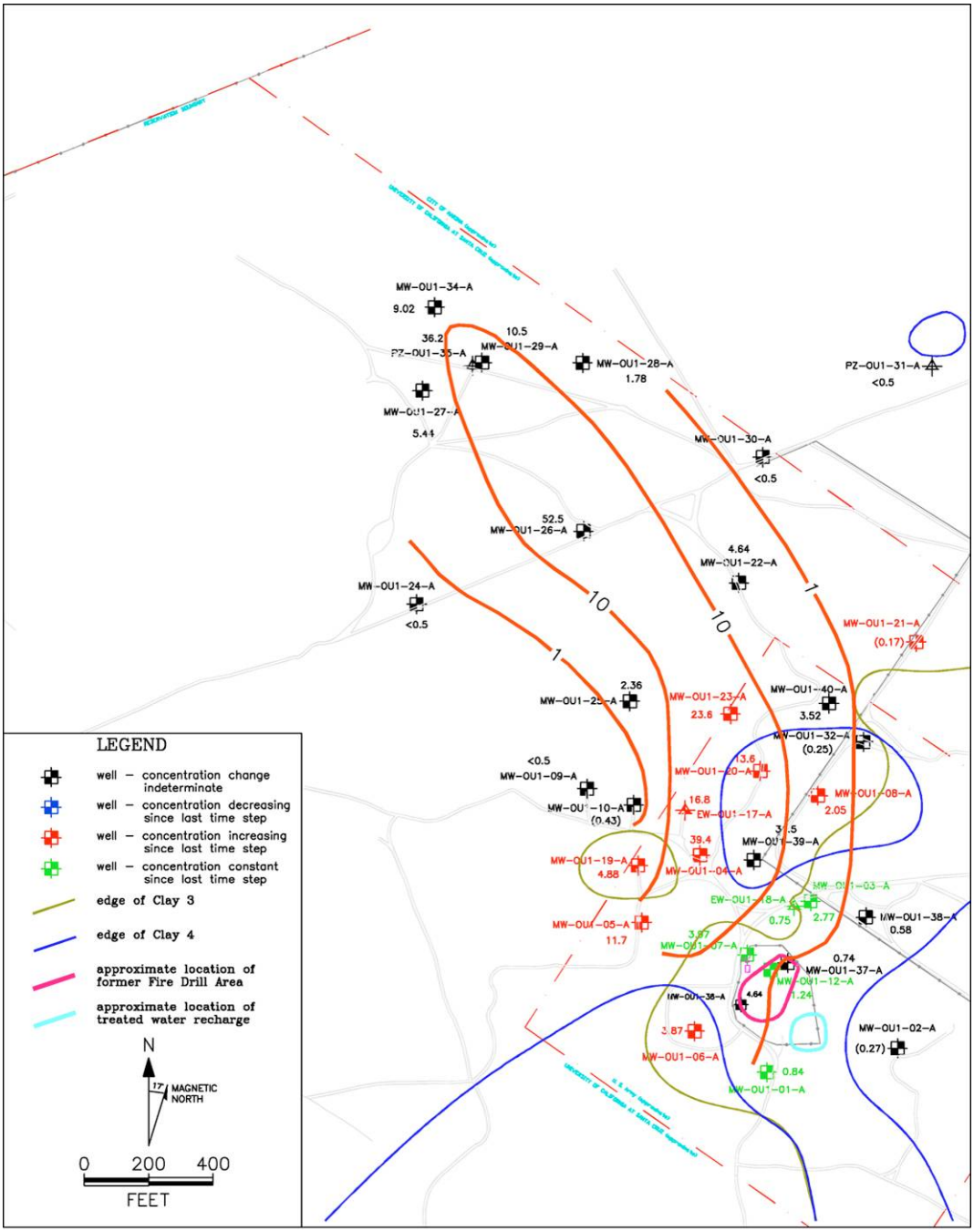

Figure 55. Isoconcentrations of TCE (µg/L) in late 1999 (modified from Oldenburg et al., 2002).

Plume in early 2003

The TCE plume in the vicinity of the extraction wells in early 2003 is shown in Figure 56. Note that the results at MW-OU1-10-A have been anomalously low since the switch to PDS in late 2001. At this time, the plume upgradient of the extraction wells has contracted and the concentrations

have decreased since shortly after the early 1998 precipitation event. In the plume core immediately downgradient from the extraction wells, the concentrations have decreased. This is presumably due to the continued input of uncontaminated water from natural flows and treated water recharge upgradient of the plume.

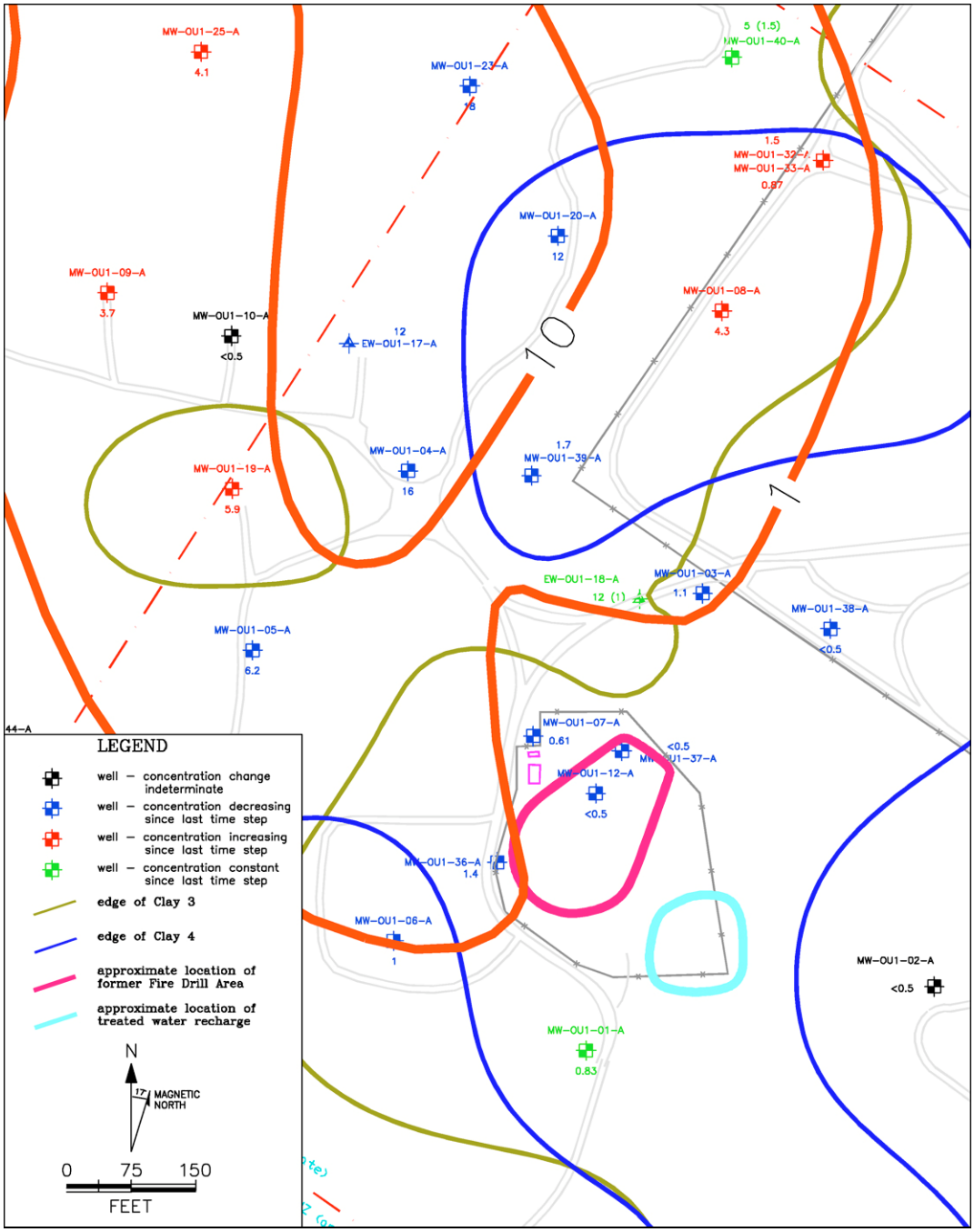

Figure 56. Isoconcentrations of TCE (µg/L) in the vicinity of the FDA in early 2003.

The plume dimension transgradient to EW-OU1-17-A has increased. Concentrations within the areas newly occupied by the plume are at or below the Maximum Contaminant Level (MCL) of 5 parts per billion (ppb) for TCE in drinking water. Trends through late 2003 indicate the TCE concentration will not increase significantly above the MCL in the future.

The concentration increases to the northwest, west, and southwest of EW-OU1-17-A are most likely due to narrowing of the capture zone as indicated in Oldenburg et al. (2002). This narrowing is caused by sustaining the same pumping rate at this well despite the large water level increases following the early 1998 precipitation. The water level in EW-OU1-17-A increased approximately 18 ft (5.5 m), which more than tripled the saturated thickness. The capture zone narrowing allowed the plume to spread in the vicinity of this well.

The plume expansion to the east/northeast of EW-OU1-17-A is likely due to a combination of factors. The capture zone around EW-OU1-18-A also narrowed after the early 1998 precipitation, although not as much as the narrowing at EW-OU1-17-A. The water level in EW-OU1-18-A increased approximately 7 ft (2.1 m), which increased the saturated thickness by approximately one-third. Extraction from EW-OU1-18-A was shut down in mid-2001. Concentrations at MW-OU1-32-A were slightly higher after the switch to PDS.

The downgradient extent of the plume is shown in Figure 57. This figure shows the plume axis has shifted west/southwest and the tip of the plume has moved west from its position in late 1999 as shown in Figure 55. This is in accord with the gradient rotation following the early 1998 precipitation in the vicinity of the downgradient portion of the plume previously discussed. This gradient rotation can be seen by comparing Figures 25 and 26.

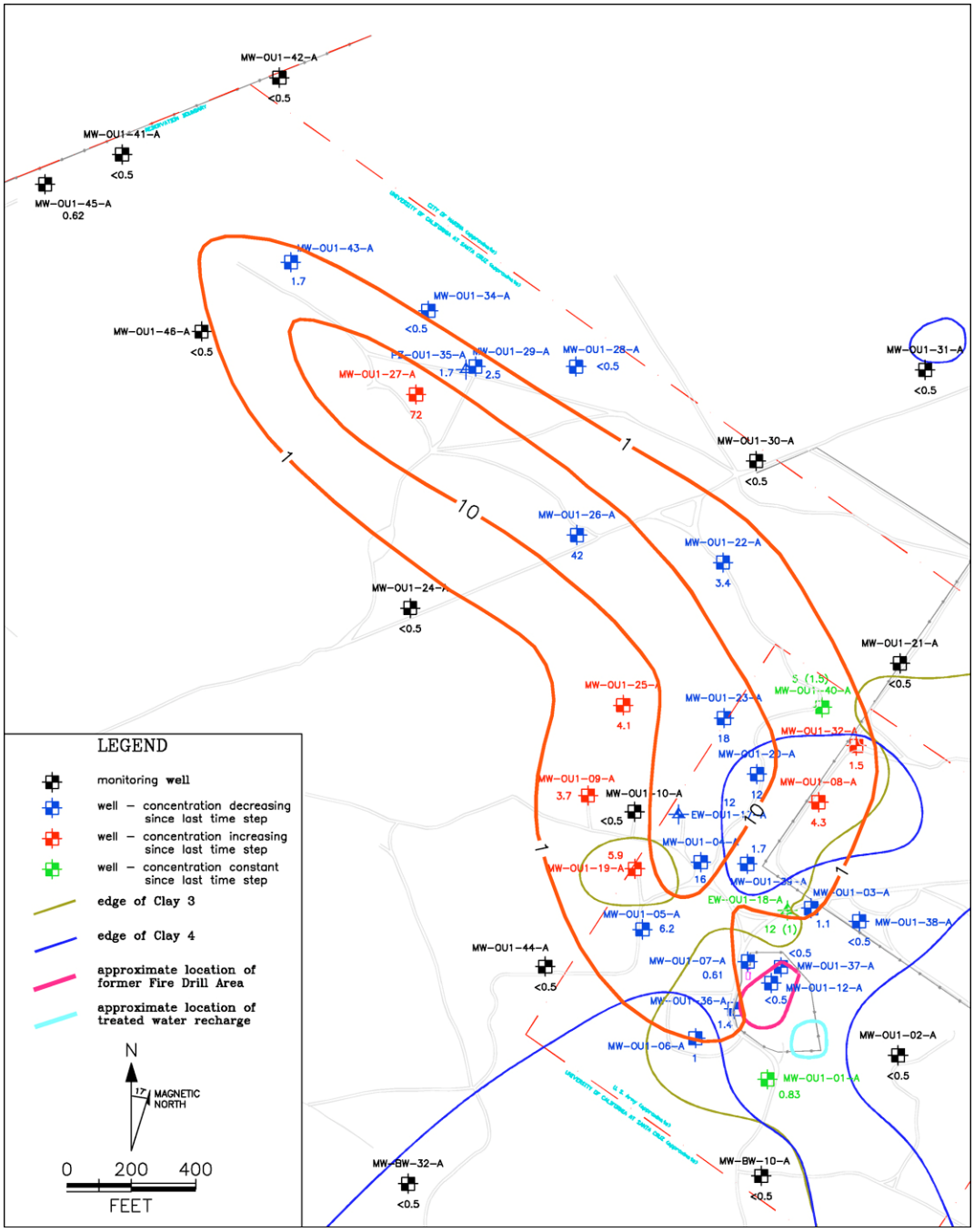

Figure 57. Isoconcentrations of TCE (µg/L) in early 2003.

Simulation of in-situ permeable flow sensors for measuring groundwater velocity

A plot of the steady-state streamlines near the sensor along a horizontal (x-y) plane is shown in Figure 58. Perturbation of the uniform flow field occurs near the sensor, where flow is diverted around it. The streamlines

follow the sensor circumference in the vicinity of the sensor, demonstrating that the shape of the grid did not influence the flow direction.

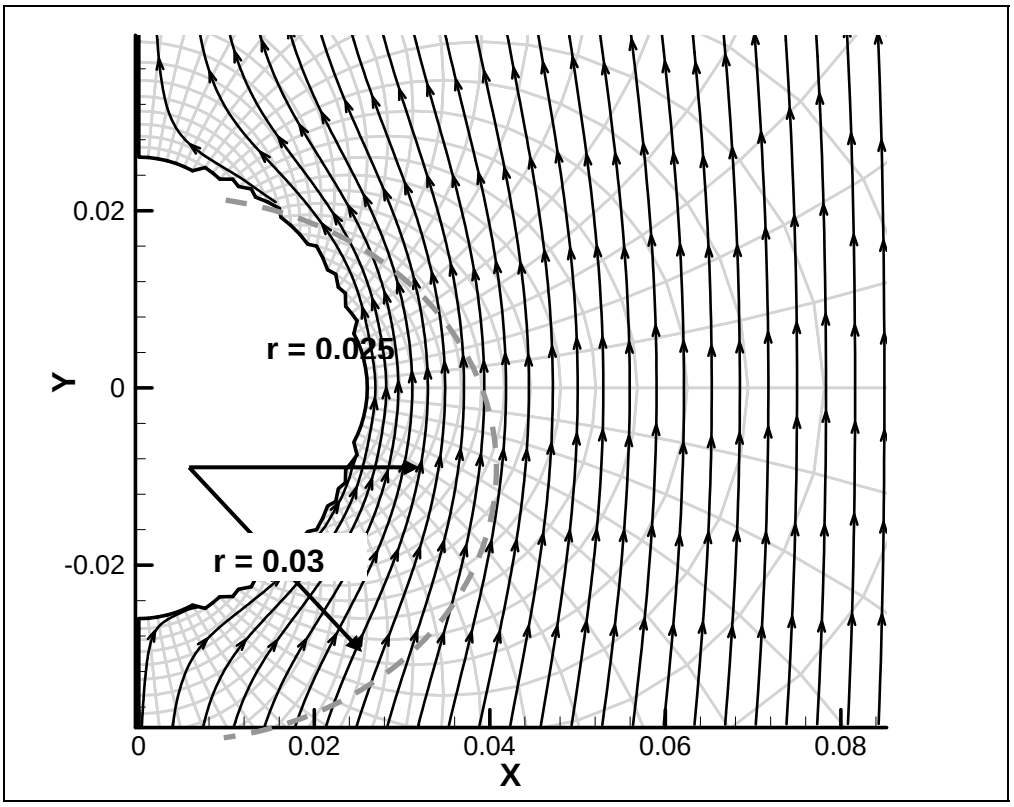

Figure 58. Steady-state streamlines near the sensor along a horizontal plane.

An "unrolled" two-dimensional plot of the simulated temperature at a radial distance of 0.03 m is shown in Figure 59 for Scenario 1. The downstream side of the sensor (azimuth = 0°) is shown on the right side of the plot. The center of the sensor is warmer than the top and bottom, and the upstream side (180°) of the sensor is cooler compared to the downstream side (0°) because of horizontal flow across it. The temperature distribution above and below the center of the instrument is symmetric because the thermal conductivity and permeability are the same in all the layers in this simulation. The vertical symmetry of the temperature distribution also indicates that buoyancy flow is negligible.

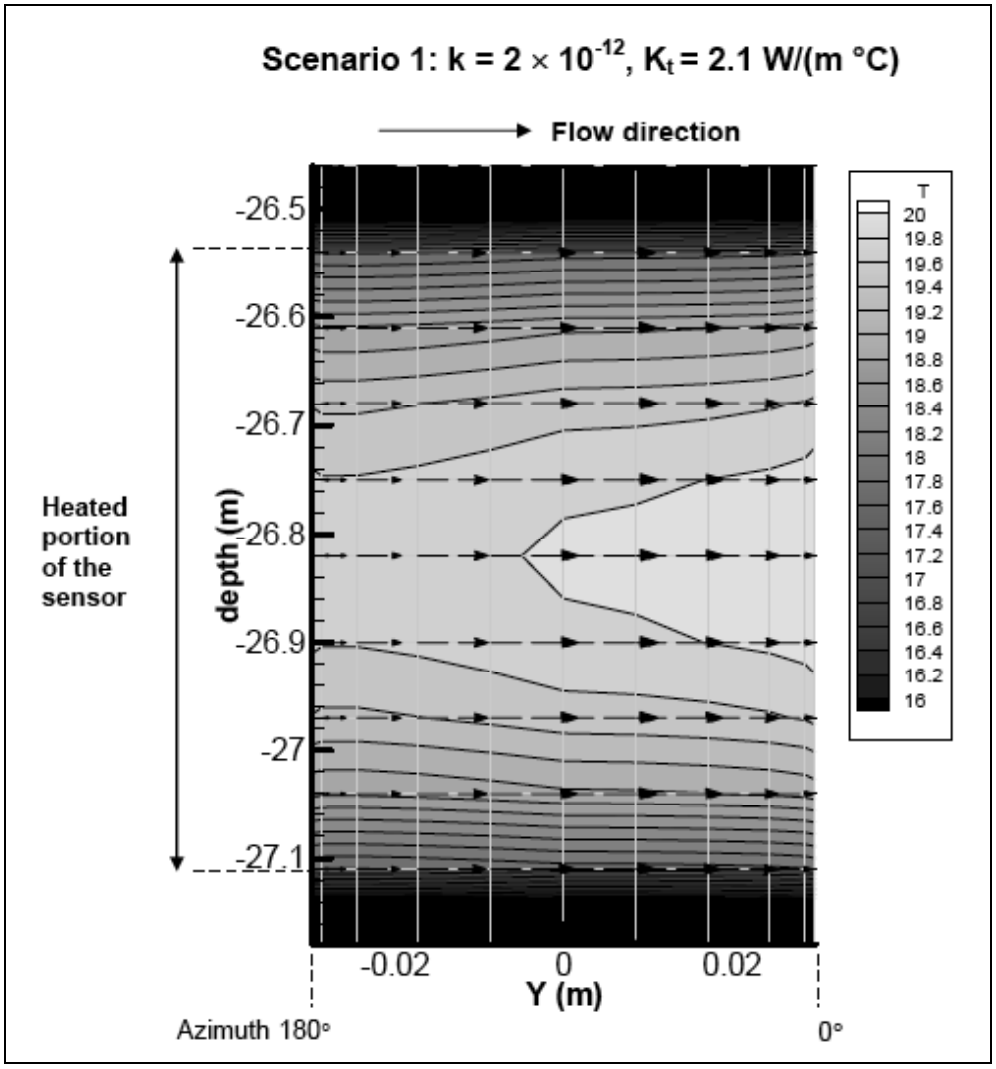

Figure 59. "Unrolled" temperature distribution with depth at a radial distance of 0.03 m (near the sensor surface).

A plot of the temperature profile with depth on the downstream side of the sensor (azimuth = 0°) is shown in Figure 60 for Scenarios 1 through 4. Scenario 1 has a temperature profile that is symmetric over the nine layers representing the heated sensor. In Scenario 2, where the thermal conductivity of layers 14-17 are lowered to 1.0 and 1.8 W/m°C while the thermal conductivity of remaining layers remain at 2.1 W/m°C, the temperatures are higher at the bottom of the sensor compared to the top. The temperatures toward the bottom of the sensor are considerably higher when the thermal conductivity is 1.0 W/m°C compared to 1.8 W/m°C, but the temperature increase is still considerable even when the thermal conductivity is 1.8 W/m°C. The Hydrotechnics® data analysis software would interpret such a temperature profile as having a downward vertical flow component. The simulated temperature profiles could not be analyzed by the Hydro-

technics® software to determine the downward flow velocity associated with these profiles because the program is written to analyze input provided in millivolts (output from the thermistors on the Hydrotechnics® sensors is in these units).

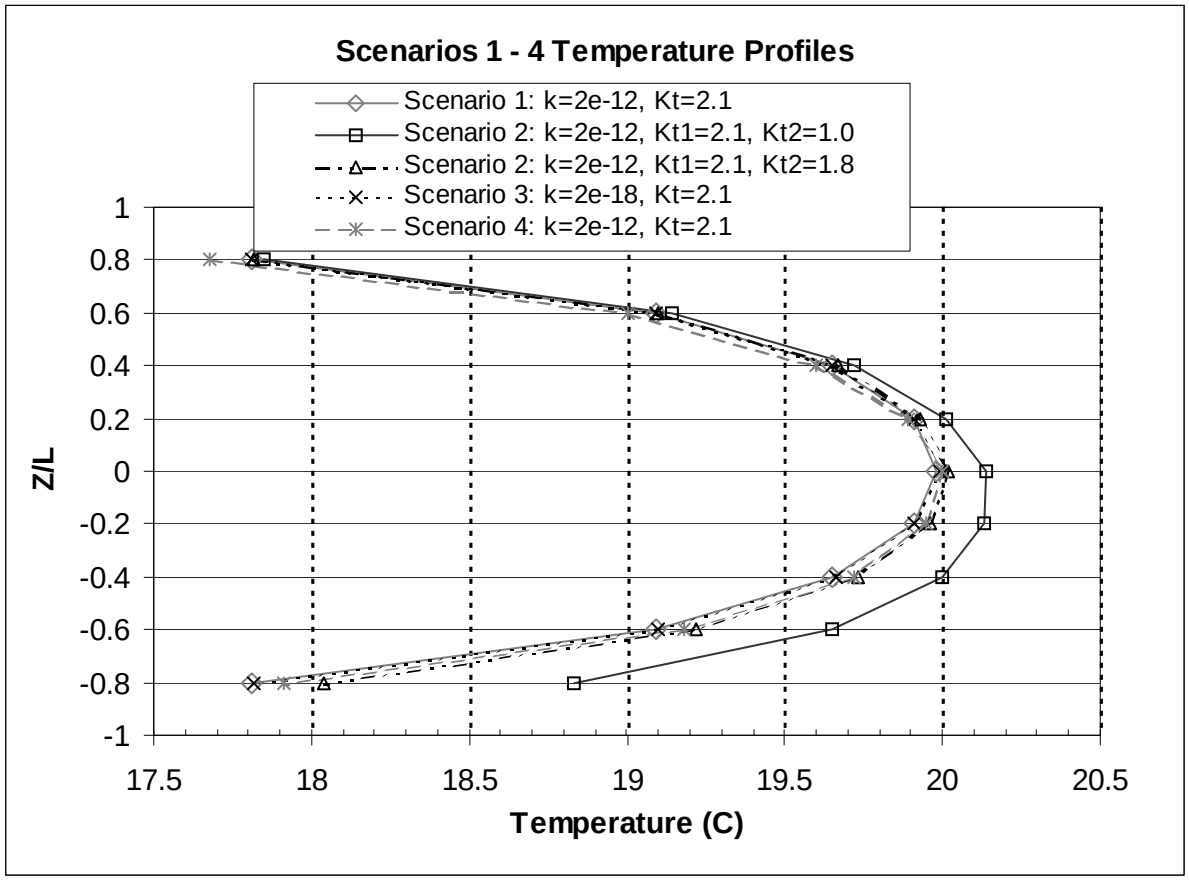

Figure 60. Temperature depth profile along the sensor for Scenarios 1–4.

In Scenario 3, the permeability of the layers below the sensor was lowered to 2×10^{-18} m^2 while the other layers remained at 2×10^{-12} m^2. The temperature profile remains essentially the same as in Scenario 1, indicating that the temperature profile along the heated portion of the sensor is not sensitive to permeability changes below the sensor.

In Scenario 4, a vertical pressure gradient was applied such that it produced downward flow velocities in the range of the vertical velocities estimated at Fort Ord. As expected, the temperature profile from this simulation is not symmetric, but has higher temperatures at the bottom compared to the top. To determine if a similar change in the temperature profiles occurred because of vertical layers of different thermal conductivi-

ties, the magnitude of the temperature shift from the vertical flow case was compared to the results from Scenario 2. A similar temperature shift occurred in Scenario 2 when the bottom layer had a thermal conductivity of 1.8 W/m°C. Therefore, a relatively small decrease in the thermal conductivity of the layer immediately below the sensor can alter the temperature profile enough such that it could be interpreted as having a downward flow velocity with a magnitude similar to the ones estimated at Fort Ord.

At Fort Ord, two of the three flow sensors had a layer of sand separating the bottom of the flow sensor from the top of the clay layer. Simulations were run in Scenario 5 to investigate whether the temperature profile was still altered by the presence of the clay layer when a sand layer separated it from the sensor bottom. With $K_{t,sand}$ = 2.1 W/m°C and $K_{t,clay}$ = 1.0 W/m°C, the simulated temperatures are higher towards the bottom when the sand layer is 0.07 m thick, and then to a much lesser extent when the thickness is 0.144 m, as shown in Figure 61. At a thickness of 0.288 m, the profile is once again nearly symmetric. Therefore, a sand layer with a minimum thickness of around 0.3 m is necessary to prevent the clay layer from altering the temperature profile at the bottom of the sensor. The thicknesses of the sand layer separating two of the sensors from the clay layer at Fort Ord were 0.45 m and 1.3 m (OU1-39 and OU1-36, respectively). Based on the simulated results, the thermal conductivity of the clay layer probably had a minimal impact on the temperature profile recorded by these two flow sensors.

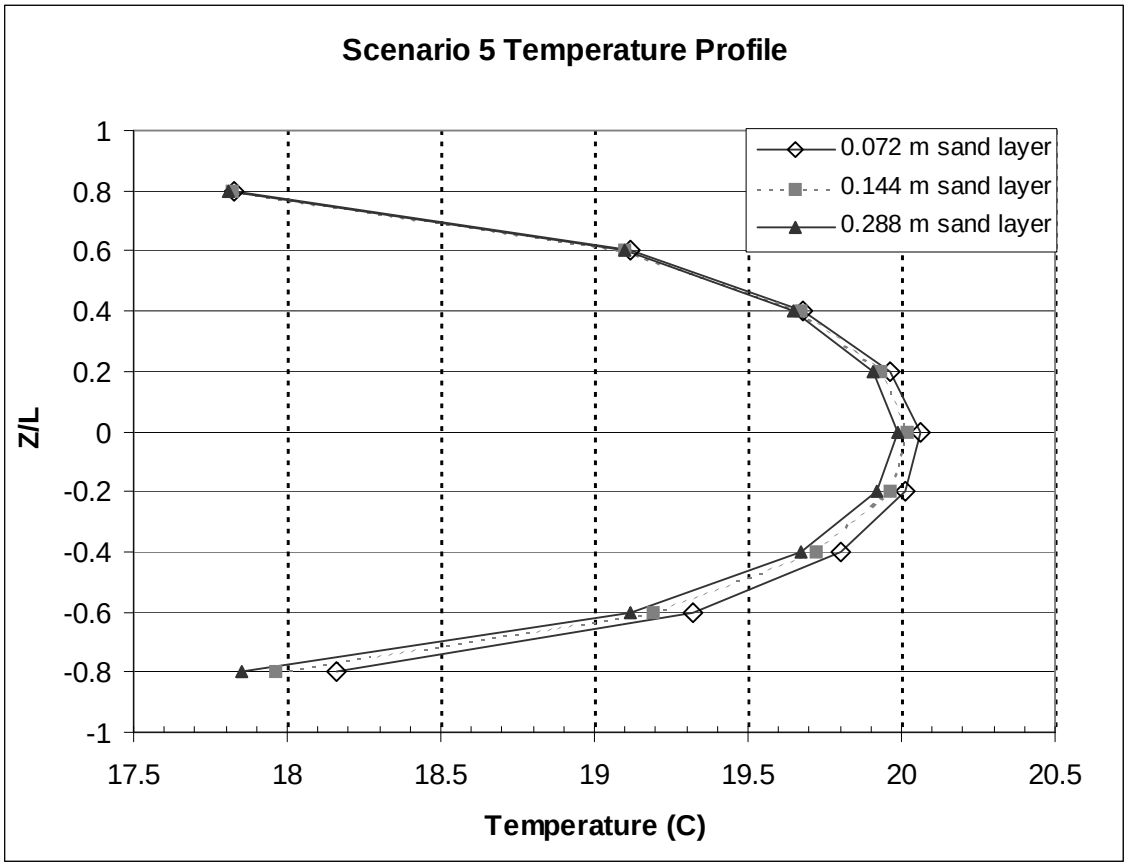

Figure 61. Temperature depth profile along the sensor for Scenario 5.

Scenarios 6 and 7 were conducted to investigate how permeability changes over the length of the sensor affect the temperature profile. Figure 62 shows the temperature profile with depth as the permeability in layers 12 - 17 increases and decreases by a factor of two relative to the layers above. The temperatures towards the bottom of the sensor decrease with increasing permeability and increase with decreasing permeability. Therefore, a decrease in the permeability near the sensor bottom could also produce temperature profiles that when inverted would result in estimates of apparent downward flow velocities. For a permeability decrease of two in layers 12-17 relative to the layers above, the temperature at the sensor bottom is around 0.05°C higher than the top. In order to reproduce the downward flow velocities estimated at Fort Ord, a temperature increase of nearly 0.25°C at the sensor bottom is necessary (Scenario 4). Since the aquifer at Fort Ord is nearly homogeneous, permeability changes over the length of the flow sensors are probably small and cannot entirely account for the shift in the temperature profiles.

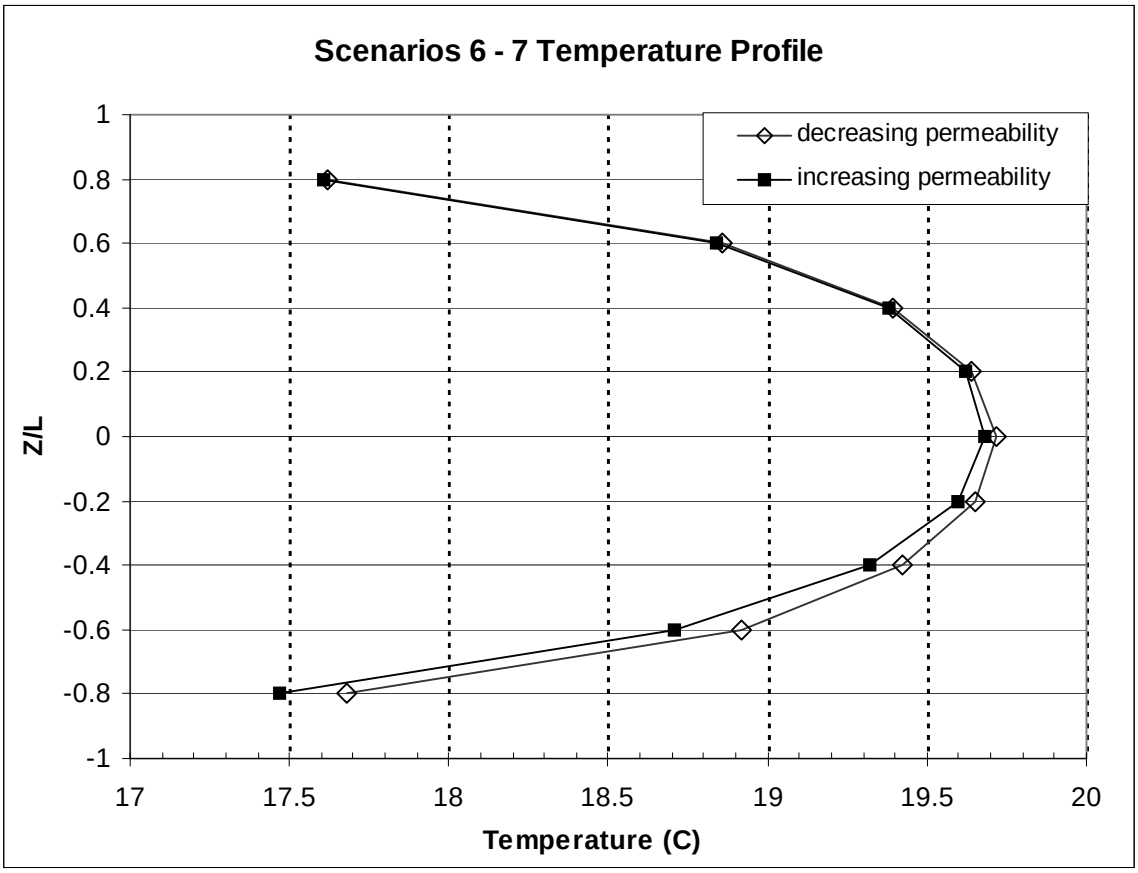

Figure 62. Temperature depth profile along the sensor for Scenarios 6-7.

The temperature profile from Scenario 8, where layers 12 and 13 were modeled with a thermal conductivity of 2.0 W/m°C while the thermal conductivity in the remaining layers was 2.1 W/m°C, is presented in Figure 63. The small decrease in the thermal conductivity towards the bottom of the sensor was enough to produce a similar temperature shift as observed in the vertical flow case. Therefore, a subtle decrease in the thermal conductivity with depth along the flow sensor with or without the presence of a clay layer below the sensor could also give rise to temperature profiles that when inverted could be interpreted as having a downward flow velocity. Finer textured media has a lower thermal conductivity compared to coarser textured ones (Jury 1991). Therefore, if the sand becomes finer with depth, the thermal conductivity could decrease and cause a shift in the temperature profile along the sensor. Even though the temperature profiles recorded by the OU1-36 and OU1-39 flow sensors at Fort Ord were probably not affected by the underlying clay layer, the measured temperature shift may have been because the thermal conductivity of the sand decreased slightly with depth along the flow sensors.

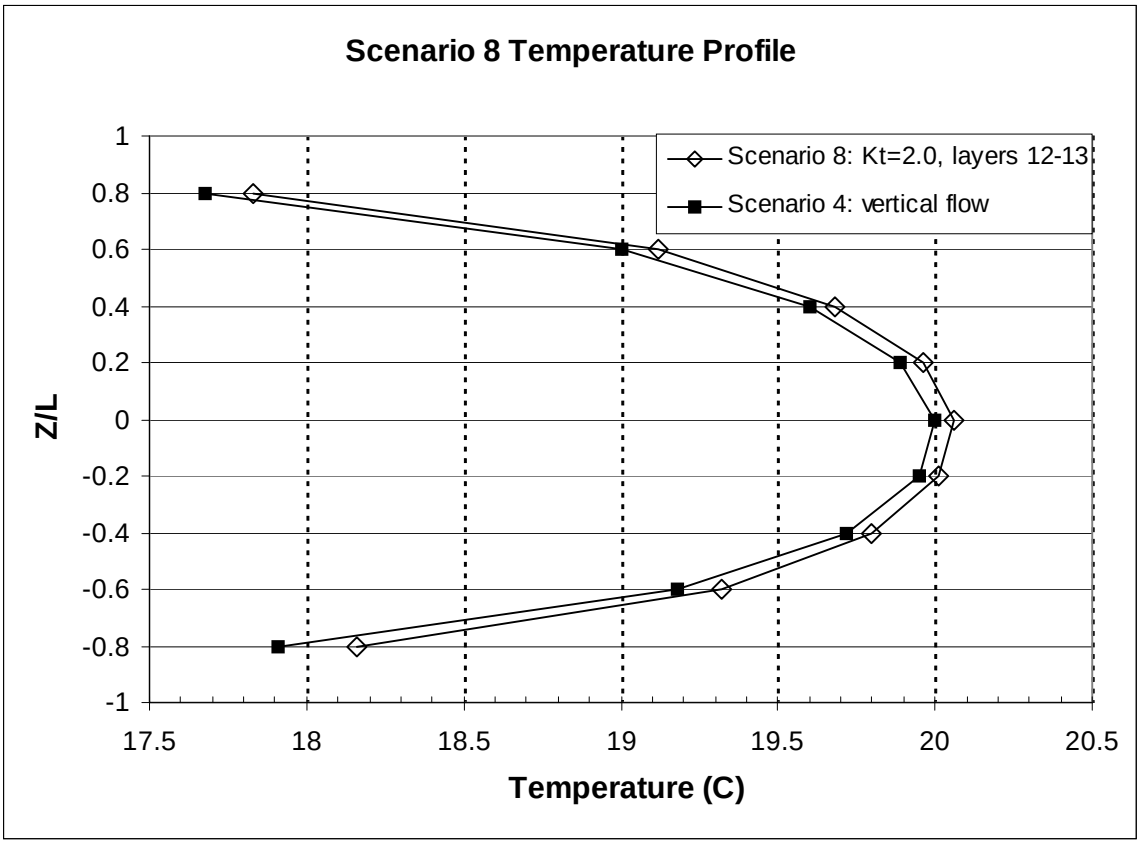

Figure 63. Temperature depth profile along the sensor for Scenario 8.

Inorganic contaminant sampling and analyses

Chromium

Concentrations (µg/L) of chromium in samples collected from wells at OU 1 are listed in Table 18. Also listed in the table are the concurrently measured concentrations (18.36 µg/L) and certified value (18.53 ± 0.2 µg/L) concentrations of chromium in National Institute of Standards and Technology (NIST) certified reference material for trace elements in water (1643d). Comparisons of those two values shows the recoveries for chromium were essentially quantitative (~100%), which attests to the accuracy of the groundwater measurements.

Table 18. Chromium concentrations (µg/L) of groundwater samples collected at OU 1 in August, 2003.

Well	Analysis date	Cr (µg/L)
MWOU1-7-A	04 Sept. 2003	0.9
MWOU1-19-A	28 Aug. 2003	1.8
MWOU1-36-A	28 Aug. 2003	2.0
MWOU1-37-A	04 Sept. 2003	1.6
MWOU1-38-A	28 Aug. 2003	1.5
MWOU1-39-A	28 Aug. 2003	1.0

Chromium concentrations measured in the six different samples ranged from 0.9 to 2.0 µg/L, and averaged (± 1 sd) 1.5 ± 0.4 µg/L. This relatively consistent range contrasts with the range of previously measured chromium concentrations in over 300 groundwater samples collected from wells at OU 1 between 1987 and 1993 (unpublished data). All of those concentrations were reported as Not Detected (ND), with the exception of seven samples from different wells, which had concentrations ranging from 2.9 – 5.4 µg/L, and fifteen samples from one well (MW-OU1-11-SVA), which had concentrations ranging from 0.02 to 10.4 µg/L. Since all but one of those latter values was ≤ 0.1 µg/L, the one high outlier (10.4 µg/L), which was the last reported concentration (April 1992) from the well and the principal cause for concern with chromium contamination in the A-aquifer, is tentatively considered to be a sampling and/or artifact. Moreover, those other data are also circumspect because of the variation in sensitivity (MDL), the absence of concurrent measurements of an appropriate SRM, and concerns with sampling artifacts.

However, the chromium concentrations measured for this study are readily comparable with contemporary measurements of chromium measured in the Aromas Red Sands and Purisima aquifers that also occur in Monterey County, California (Gonzalez et al., 2005). Both sets of measurements were made with the same sampling and analytical protocols. Moreover, the levels of chromium in the surface aquifer at OU 1 are intermediate to the average values for the other two aquifers, which are both attributed to natural processes.

Other trace elements

Concentrations of other trace elements (Cd, Co, Cu, Fe, Mn, Ni, Pb, Zn) sampled from wells at OU 1, along with those of a field blank, are listed in Table 19. These measurements show similarly reproducible (relatively pre-

cise) ranges as observed with the chromium measurements, with one exception. Concentrations collected with a bailer, using trace metal clean techniques, from OU 1—36-A were consistently higher than those collected directly from that site, and both were often orders of magnitude higher than concentrations collected at other sites.

Table 19. Trace metal concentrations in groundwater at OU 1(Fort Ord 2003)

		Cd (µg/L)	Co (µg/L)	Cu (µg/L)	Fe (mg/L)	Mn (mg/L)	Ni (µg/L)	Pb (µg/L)	Zn (µg/L)
Sample ID	Matrix	Value	Value	Value	Value	Value	Value	Value	Value
04A	water	0.0189	0.0179	0.1061	0.0039	0.0003	0.7272	0.0033	0.0135
05A	water	0.0127	0.0360	0.0921	0.0059	0.0002	0.5752	ND	0.0389
07A	water	0.0168	0.0099	0.0906	0.0016	0.0006	1.5584	0.0043	0.2676
07A	water	0.0184	0.0184	0.1046	0.0015	0.0007	1.5655	0.0086	0.3343
07A-average	water	0.0176	0.0142	0.0976	0.0016	0.0006	1.5619	0.0064	0.3009
07A-rpd	water	9%	60%	14%	9%	5%	0%	66%	22%
19A	water	0.0121	0.0164	0.0795	0.0052	0.0004	0.5399	0.0007	ND
20A	water	0.0159	0.0143	0.0808	0.0024	0.0003	1.3536	0.0007	0.0377
36A	water	0.5090	1.0575	1.0665	0.7563	0.0522	4.8065	1.0308	5.2448
36A-BAILER	water	0.1674	1.8017	1.3462	1.6462	0.0854	7.8955	1.9286	4.4845
36-Field Blank	water	0.0013	ND	0.0673	0.0055	0.0001	ND	ND	ND
37A	water	0.0209	0.0248	0.1649	0.0028	0.0010	2.3871	0.0056	0.0792
38A	water	0.0224	0.0278	0.1276	0.0084	0.0012	1.8217	0.0047	0.4124
39A	water	0.0210	0.2634	0.1022	0.0023	0.0008	2.4874	0.0011	0.0719
40A	water	0.0136	0.0177	0.0859	0.0020	0.0002	0.8202	ND	0.3480

ND = non-detected

Values measured at the other sites were not readily comparable to those previously measured at OU 1 between 1987 and 1993 (unpublished data) for the same reasons the chromium data were not comparable: high and variable MDLs, most concentrations were reported as ND, anomalously high outliers, lack of reported QA/QC, and concerns with sampling and analytical protocols. However, the iron and manganese concentrations measured for this study were consistent with data reported by Gonzalez et al. (2005) for the Aromas Red Sands and Purisima aquifers, as they were for chromium; and the all of the trace metal concentrations were comparabale to those measured in a surface aquifer in adjacent Santa Cruz County by Creasey and Flegal (1999), who also used comparable sampling and analytical protocols. Consequently, all trace metal concentrations measured at OU 1 in this study are comparable to those considered natural values in adjacent aquifers.

Automated remote sampling

The relatively high trace element concentrations obtained with the bailer in this study, as well as the highly variable concentrations previously reported for the site for samples that were collected and analyzed with standard procedures, evidence the need for rigorous sampling protocols that do not perturb the aquifer and yield erroneously high values. In contrast the relatively low and precise measurements obtained in this study demonstrate that accurate trace metal data may be remotely collected from aquifers using remote, automatic sampling systems like the one installed at OU 1.

Automated remote sampling devices are extremely beneficial especially for small watersheds and isolated areas, like the Fort Ord site, where manual sampling is difficult and expensive. The combination of VOC contamination together with the low levels of trace metals makes the Fort Ord site a good location to investigate variations in trace metal concentration associated with groundwater recharge after precipitation. The use of automated sampling equipment in a closed flow system greatly reduces the potential for contamination, allowing precise and accurate sample collection under trace metal clean environment.

This automated sampling system offers several advantages over conventional methods. The equipment is both modular and portable making it relatively easy to transport and assemble in the field. The current setup allows up to seven samples to be collected before they must be manually removed and new columns installed. This multiplicity enables not only time series sampling of wells but also discrete sampling of up to seven different wells during one storm event. Sample thorough-put can also be easily increased by using additional multi-position valves.

The automated remote sampling system can accommodate simultaneous sampling of multiple wells. All the plumbing from each wellhead converges at the research weather station, which localizes the site of sampling and allows the pump setup to collect one sample from each well. The use of columns packed with iminodiacetate resin eliminates the need to use sampling bottles. This reduces the time and cost involved in the sampling process by eliminating the use of expensive trace metal grade mineral acids and time required to clean bottles for collection of trace clean water samples. It also eliminates the subsequent acidification of those samples which is required to prevent adsorptive loss of trace metals on bottle walls.

The loaded columns can remain on site until it is convenient for them to be collected for analysis.

4 Conclusions

Groundwater flow monitoring technologies

The feasibility of real-time monitoring of subsurface contaminants during pump-and-treat has been demonstrated. This project produced a working facility for experimentation and demonstration of concepts, and includes field installation of an on-line real-time instrumentation (gas chromatograph, meteorological station). Connection by a wireless link of the site to the Internet enables real-time access to information from the site. Results of this work strongly suggest that, with real-time instrumentation of the water sampling and rainfall, more dynamic control of pumping could result in significant reduction in pumping costs and simultaneously reduce the migration of the toxic plume. Results also support the hypothesis that this approach could be used to pinpoint the contaminant source zone thus enabling localized secondary treatment possibilities. Though the focus of this particular work was the TCE contamination at the former Fort Ord, the design of this system can be adapted to address other contaminant issues such as perchlorate and explosives.

Though it was not the main focus of this project, work was also done on automated trace metal clean sampling and on-line field processing. This was based on our previous experience at other sites in the Santa Cruz area, which demonstrated that standardized sampling protocols may yield erroneously high values for heavy metal concentrations in groundwater, as well as being labor intensive and expensive. Consequently, the applicability of an automated remote sampling system designed to collect groundwater samples under trace metal clean conditions in response to ephemeral events was demonstrated at OU 1. This system was coupled with a rainwater gauge to enable the collection of groundwater samples after an initial volume of rainfall is detected and additional samples in a user defined time series to trace contaminant responses precipitation.

Analysis of aquifer response, groundwater flow and plume evolution

Water-table evolution

At of the end of 2003, the water table at OU 1 was still responding to the high quantity of precipitation that occurred 5 years earlier in early 1998. Water levels in all the wells analyzed in this report had peaked by this

time. The water levels in the portion of the TCE plume downgradient of the extraction wells peaked the latest. The gradient in this area rotated approximately 20° counterclockwise from north- to northwest-directed in 2000, and northwest-directed in 2002. Outside of the plume, water levels toward the center and edge of the FO-SVA peaked earlier than the water levels in the areas midway between. All of these responses can be understood conceptually as resulting from an instantaneous, uniform addition of water on top of the previously equilibrated water table of the A-aquifer, the extent of which is defined by the edge of the FO-SVA.

Porosity

Water level responses to the early 1998 precipitation event in A-aquifer/deeper aquifer well pairs allow estimation of the porosity of the A-aquifer. The estimate of 30-37% total porosity suggests that the effective porosity estimate of 30% used in Oldenburg et al. (2002) is perhaps 5% too high.

Recharge

The water level increases in the A aquifer resulting from the early 1998 precipitation event allow estimation of the fraction of this precipitation that recharged to the water table. The estimate of a 38 to 51% recharge fraction for this precipitation event is higher than the 27% recharge fraction derived from an analysis of water level changes during more typical rain years in Oldenburg et al. (2002). The former should be higher than the latter primarily due to the lack drainages in the OU-1 area and greater relative ground saturation (causing higher vadose zone relative permeabilities). Therefore, the estimated recharge fraction from the early 1998 precipitation is consistent with the recharge fraction estimate for typical rain years.

ISPFS results

The groundwater flow azimuths measured by the ISPFSs were rotated counterclockwise relative to the gradients from water level contouring for unknown reasons. The shifts in gradient azimuth measured by the ISPFSs readily correlate to pumping rate changes from the extraction wells and the water table response to the early 1998 precipitation event. The horizontal flow velocities measured by the ISPFSs match the regional velocities suggested by the water table gradient and hydraulic conductivities from

short term pump tests. The changes in horizontal velocity readily correlate to pumping rate changes from the extraction wells. Based upon instrument installation records and numerical modeling, the large, downward-directed vertical velocities measured by the ISPFSs could be due to either in-situ or drilling induced thermal conductivity heterogeneities possibly in combination with drilling induced permeability heterogeneity.

PDS results

The PDS results from a given well were generally similar to the P&S results. With the exception of MW-OU1-10-A, PDS resulted in slightly higher TCE and 1,2 DCE concentrations in a few wells. In MW-OU1-10-A, PDS resulted in significantly lower concentrations. In general, the PDS and P&S results were more similar for TCE and 1,2 DCE than for CT and Chloroform.

Depth profiling of contaminant concentrations was performed with PDS in many wells. This profiling typically indicated that concentrations are uniform with depth or increased with depth as might be expected due to contaminant off-gassing at the water surface.

A-aquifer hydraulic conductivity

The A-aquifer horizontal hydraulic conductivity estimates from the ISPFSs, short duration pumping tests, drawdowns due to long term extraction, and the entire TCE plume matched remarkably well, indicating unusual uniformity across scales. These estimates indicate the aquifer-scale hydraulic conductivities are likely between 7 and 10 ft/d ($2.5–3.5 \times 10^{-5}$ m s^{-1}). The results of the PDS depth profiling also qualitatively indicate little variation in the horizontal conductivity with depth through the A-aquifer. Vertical conductivities in the vadose zone estimated from water level responses to surficial recharge changes matched the horizontal conductivity estimates well. Finally, flow information from the ISPFSs and the TCE plume shape indicates there is no significant anisotropy in the A-aquifer.

TCE plume evolution

Oldenburg et al. (2002) concluded high recharge rates had mobilized residual TCE in the vicinity of the FDA causing concentrations to increase in various locations transgradient to the plume. This conclusion was favored

over changes in the groundwater flow field due to the treated water recharge because the available water level data did not suggest that extraction and treated water recharge had altered the flow field sufficiently to explain the changes. The conclusions of Oldenburg et al. (2002) were based upon chemistry data from mid-1992. The inclusion of earlier chemistry data in the analysis of the present report has altered the earlier conclusion. Now the likely cause of the transgradient concentration increases is mobilization of residual contamination south of the FDA combined with slight alteration of the flow of contaminated water northeast of the FDA. The earlier chemistry data indicate that the treated water recharge area partially overlay the TCE groundwater plume, thus causing the plume to spread. This stated, the transgradient increases as of 2003 are typically at or below MCLs. The pump-and-treat operation at the head of the OU-1 plume, which commenced in 1988, has significantly reduced contaminant concentrations and dissolved mass.

In the downgradient portion of the TCE plume, concentration data indicate the counterclockwise gradient rotation caused by the early 1998 precipitation is causing the contaminant advection to shift direction. The TCE plume is now advecting west/northwest, that is more westward than its pre-1998 axis. Therefore, any remedial effort based upon capturing or treating the plume as it advects through a transect, will have to change position and take place over a larger transect relative to the pre-1998 conditions. Furthermore, the slow return of groundwater flow to the pre-1998 conditions should also be taken into account when designing remedial systems.

Due to the gradient change at the tail of the plume, the plume is shifting off of the well network to some extent. This shift should be tracked carefully and new monitoring wells installed if necessary. Otherwise there might be a tendency to conclude that the plume is dissipating. The change in gradient direction may also have implications for the design of the remedial system for this portion of the plume. Whether a barrier or volumetric system is designed, the appropriate position for this installation appears to be shifting. In particular, note that in late 1999, the TCE concentration at MW-OU1-27-A was approximately the MCL (5 µg/L). As of early 2003, the TCE concentration is approximately 15 times the MCL, apparently due to a shift of the plume axis.

Simulation of in-situ permeable flow sensors for measuring

groundwater velocity

Three-dimensional flow and heat transport simulations near a Hydrotechnics® flow sensor were conducted to investigate possible reasons for the apparent downward flow velocities estimated at the former Fort Ord Army Base. Under conditions of horizontal flow only, the temperature profile along the length of the sensor can be perturbed by changes in the thermal conductivity and permeability in such a manner that the Hydrotechnics® data analysis software could interpret the shift in temperature as downward flow. This occurs when the thermal conductivity of the porous media decreases towards the bottom of the sensor, and/or when a layer of lower thermal conductivity soil is located close to the bottom of the flow sensor. A decrease in the permeability towards the bottom of the sensor also can result in temperature profiles that could be interpreted as downward flow, but permeability changes have a less significant effect on the temperature profiles compared to changes in thermal conductivity. Our simulations demonstrate that the temperature profiles recorded by the flow sensors are sensitive to changes in the thermal and hydraulic properties of the soil. The vertical velocity estimates obtained by Hydrotechnics® flow sensors should be evaluated carefully and compared with estimates from other methods if possible, such as using groundwater temperature profiles to estimate vertical velocities (e.g., Reiter 2001) and measuring pressures at different depths to determine if a vertical flow gradient exists.

Inorganic contaminant sampling and analyses

Automated remote sampling

As previously noted, automated remote sampling devices are extremely beneficial especially for small watersheds and isolated areas, like the Fort Ord site, where manual sampling is difficult and expensive. The combination of VOC contamination together with the low levels of trace metals makes the Fort Ord site a good location to investigate variations in trace metal concentration associated with groundwater recharge after precipitation. The use of automated sampling equipment in a closed flow system greatly reduces the potential for contamination, allowing precise and accurate sample collection under trace metal clean environment.

This automated sampling system offers several advantages over conventional methods. The equipment is both modular and portable making it relatively easy to transport and assemble in the field. The current setup

allows up to seven samples to be collected before they must be manually removed and new columns installed. This multiplicity enables not only time series sampling of wells but also discrete sampling of up to seven different wells during one storm event. Sample thorough-put can also be easily increased by using additional multi-position valves.

In addition, the system can accommodate simultaneous sampling of multiple wells. All the plumbing from each well head converges at the research weather station, which localizes the site of sampling and allows the pump setup to collect one sample from each well. The use of columns packed with iminodiacetate resin eliminates the need to use sampling bottles. This reduces the time and cost involved in the sampling process by eliminating the use of expensive trace metal grade mineral acids and time required to clean bottles for collection of trace clean water samples. It also eliminates the subsequent acidification of those samples which is required to prevent adsorptive loss of trace metals on bottle walls. The loaded columns can remain on site until it is convenient for them to be collected for analysis.

Trace element concentrations

The capability of the on-line system to collect samples for trace metal concentration measurements was evaluated by comparing elemental concentrations of groundwater samples collected at the site with the remote sampling system to data from previous collections at the site using established protocols. The latter were obtained by different commercial laboratories using U.S. EPA protocols for sampling and analyzing trace metal concentrations in groundwater between 1986 and 1992. During that period they sampled 13 different wells between 6 and 15 times to collect samples for trace element concentration measurements, including the 7 trace elements (Cd, Co, Cr, Cu, Ni, Pb, Zn) we measured in our calibration.

A comparison of data collected with our on-line system and those previous data is provided in Table 1. It shows the analytical detection limits (DL) of our measurements were 2 to 1200 times lower than the reported by other laboratories, which made all of their measurements of some elements (Cd, Co, Pb) below the DL (i.e., all = ND) and most of those of other elements below the DL (Cr = 202/214; Cu = 200/202; Ni = 201/202; Zn = 185/202). In contrast all of our measurements were above the DL, with the exception of some of those of Pb (6/10) and Zn (5/10), and reportable values for those NDs could have been obtained by adjusting the analytical parameters (Ndung'u et al. 2003). Consequently, the initial calibration of the

on-line sampling system provided with 10 samples collected at the study site provided more data than had previously been obtained from hundreds of analyses of samples collected at that site over the previous decade.

Moreover, the few measurable (> ND) trace element concentrations of samples in those previous collection are circumspect. They indicate that concentrations of Cr, Cu, Ni, and Pb in the shallow aquifer vary by ~1 to 2 orders of magnitude (i.e., 3 to 360-fold), although there is no evidence of localized elemental contamination in the small study site. Moreover, those measurable concentrations are as much as 5 to 90-fold higher than the highest concentrations obtained in our preliminary sampling and analyses.

These disparities in sensitivity, precision, and range are consistent with those we observed in a previous comparison of trace element concentrations in groundwater (Creasey and Flegal 1999). In that study it was determined that concentrations of the same elements (Ag, Cd, Cr, Cu, Ni, Pb, Zn) in samples collected with both (1) low-flow purging and sampling, comparable to the on-line collections employed in this study and (2) trace-metal clean techniques were markedly lower by 1 to 3 orders of magnitude than those obtained by another laboratory using conventional sampling and analytical techniques. Consequently, the results of the preliminary calibration of the on-line sampling system (1) substantiate the conclusion of our previous study that the use of low-flow and trace metal clean techniques may preclude reports of erroneously high trace element concentrations in groundwater and (2) attest to the applicability of the on-line sampling system to obtain more representative samples for trace element analyses of groundwater than those obtained with conventional sampling systems.

Table 20. Comparison of elemental concentration (µg/L) analyses of groundwater at OU1 reported by UCSC and other laboratories: including number of samples measured, analytical detection limits (DL), number of samples below the detection limit or non-detected (ND), and range of concentrations.

Element	Laboratory	Samples (#)	DL (µg/L)	ND (#)	Range (µg/L)
Cd	UCSC	10	0.013	0	0.012 - 0.021
	Other	202	0.1 - 2.7	202	ND
Co	UCSC	10	0.0019	0	0.014 - 0.26*
	Other	157	1.0	157	ND
Cr	UCSC	6	0.005	0	0.9 - 2.0
	Other	214	0.1 - 2.7	202	ND - 10.4
Cu	UCSC	10	0.027	0	0.080 - 0.107

	Other	202	0.1 - 7.3	200	ND - 0.34
Ni	UCSC	10	0.024	0	0.54 - 2.49
	Other	202	0.1 - 28.8	201	ND - 33.4
Pb	UCSC	10	0.0022	6	ND - 0.0086
	Other	202	0.1 - 1.6	202	ND
Zn	UCSC	10	0.044	5	ND - 0.412
	Other	202	0.1	185	ND - 36.3

* The upper value of 0.26 µg/L is anomalously high, compared to the other 9 values for Co; and that statistical outlier is considered to be erroneous.

5 Recommendations

Three groundwater flow sensing systems were deployed in the spring of 2004 at the source area of a TCE plume at the Operable Unit 1 of the former Fort Ord Army Base, Monterey County, California. The three systems employ entirely different modes of operation, but all three produce estimates of groundwater flow rate, and two produce estimates of the direction of groundwater flow. The Hydrotechnics® ISPFS system is a permanently installed device that utilizes high precision temperature sensing over the surface of a heated cylindrical probe to measure heat displaced by groundwater flow. Inversion algorithms produce estimates of both horizontal and vertical flow vectors, as well as an azimuth for groundwater flow direction. The device is buried directly in the formation without casing or sandpack, and appears to produce data that are in good agreement with standard analysis of aquifer conductivity generated by pumping tests, combined with gradient analysis. It is designed to provide long-term logging of flow parameters with essentially no operator intervention or maintenance. *Therefore, it is strongly recommended that the system be maintained and upgraded to capitalize on the substantial investment in the project to date and on the demonstrated success of the system.*

The other two tools examined are designed to vertically scan through the water standing in the borehole, and log data that can be used to calculate flow rates, and in one case, flow direction. The RAS HPL system utilizes displacement of groundwater from the well by introduced low electrical conductivity water. As horizontal flow of formation water pushes this low conductivity "tracer" from the well, continuous vertical recordings of conductivity recovery are made, from which influx rates are calculated. The equipment is highly portable; in the present case one well was logged with this system on each day. While not producing flow direction data, this system produced estimates of flow velocity that were in close agreement with the ISPFS data, without addition of any correction for presumed acceleration of groundwater velocity induced by the borehole itself. *Therefore, it is recommended that this RAS HPL system also be employed in subsequent studies.*

The last tool examined, the LLNL scanning colloidal borescope, is also a portable logging tool that can be operated readily by a single worker, log-

ging at a rate roughly equal to that of the RAS HPL system. Its operating principle is the video recording of back-lit particles by a down-hole CCD camera, illuminated from below by a high intensity lamp. Computer software digitizes the video recordings, detects and identifies particles between adjacent image "frames," and calculates horizontal displacement and direction. Many particles are monitored for each data record, which can then be reduced for plotting or statistical analysis. In this study, SCBFM data tended to over-report borehole velocities when compared with the other two tools, but the disagreement was not as great as reported in other comparative efforts. However, flow direction did not correlate with data produced by the ISPFS, even though the experiment was performed in what has heretofore been considered a nearly ideal, homogeneous sand aquifer. The reasons for this disparity are not understood at this time. *Further detailed experimentation with this SCBFM device is warranted, as its speed of deployment and reasonable agreement with the overall magnitude of flow velocities generated by the other two tools appear to be positive results.*

Finally, it is recommended that trace metal clean sampling and analytical protocols become required for measurements of trace metal concentrations in groundwater to preclude the generation of erroneously high and variable data. It is also recommended that automated, remote sampling, processing, and analytical instrumentation be developed to measure inorganic contaminants in groundwater that is comparable to the system developed to measure organic contaminants at OU 1.

References

Appel P.L., P. F. Hudak, 2001. Automated sampling of stormwater runoff in an urban watershed, north-central Texas. *Journal of Environmental Science and Health Part A – Toxic/Hazardous Substances & Environmental Engineering* 36 (6): 897-907.

Ballard, S., 1996. The *in situ* permeable flow sensor: A ground-water flow velocity meter. *Ground Water* 34: 231-240.

Ballard, S., G.T. Barker, and R.L. Nichols, 1996. A test of the *in situ* permeable flow sensor at Savannah River, SC. *Ground Water* 34: 389-396.

Bowles, J. E., 1996. *Foundation Analysis and Design, 5th Edition*, McGraw-Hill, New York, NY.

Bouwer, H., 1978. *Groundwater Hydrology*, McGraw-Hill, New York, NY.

Cohen, A.J.B., 1995. Hydrogeologic characterization of fractured rock formations—A guide for groundwater remediators. *Lawrence Berkeley National Laboratory Report* LBL-38142/UC-800, 144 pp.

Creasey, C.L. and A.R. Flegal. 1999. Elemental analysis of groundwater: demonstrated advantage of low-flow sampling and trace-metal clean techniques over standard techniques. *Hydrogeology Journal* 7: 161-167.

Daley, P.F., J. Jantos, W.H. Pedler and W.A. Mandell. 2005. Intercomparison of Groundwater Flow Monitoring Technologies at Site OU 1, Former Fort Ord, California. Lawrence Livermore National Laboratory.

de Marsily, G. 1986. *Quantitative Hydrogeology: Groundwater Hydrology for Engineers*, Academic Press, San Diego, CA.

Drost, W., D. Klotz, A. Koch, H. Moser, F. Neumaier, and W. Rauert, 1968. *Water Resources Research* 4: 125-146.

Fetter, C. W., 1994. *Applied Hydrogeology, 3rd Edition*, Prentice-Hall, Englewood Cliffs, NJ.

Foster, J.W. and L.J. Fryda, 1990. Ground water azimuth detection. U.S. Patent #4,963019.

Gonzalez, A.R., K. Ndung'u, and A.R. Flegal. 2005. Natural occurrence of hexavalent chromium in the Aromas Red Sands Aquifer, California. *Environmental Science & Technology* (ms. in press).

Harding Lawson Associates (HLA), 1986. Remedial Investigation/Feasibility Study of Soil Contamination, Fritzsche Army Airfield, Fire Drill Area, Fort Ord, California, Harding Lawson Associates, Novato, California, April 14.

Harmel, R.D., K.W. King, J.E. Wolfe and H.A.Torbert. 2002 Minimum Flow Considerations for Automated Storm Sampling on Small Watersheds. *Texas Journal of Science* 54: 177-188.

Harmel, R.D., K.W. King and R.M. Slade. 2003. Automated Storm Water Sampling on Small Watersheds. *Applied Engineering in Agriculture* 19: 667-674.

Hess, A.E. 1986. Identifying hydraulically conductive fractures with a slow-velocity borehole flowmeter: *Canadian Geotechnical Journal*, v. 23, no. 1: 69–78.

Johnson, B., K. Ndung'u, J. Rybczynski, P. Mantey, A. Gonzalez, G. Scelfo and A. Flegal. 2005. Automated Water Sampling for Trace Metals in Response to Ephemeral Events. University of California, Santa Cruz.

Jordan, P.D., C.M. Oldenburg, and G.W. Su, 2005. Analysis of aquifer response, groundwater flow, and plume evolution at Site OU 1, former Fort Ord, California. *Lawrence Berkeley National Laboratory Report* LBNL-57251.

Jury, W.A. 1991. *Soil Physics*, 5th ed, New York: John Wiley and Sons.

Kearl, P.M., 1997. Obervations of particle movement in a monitoring well using the colloidal borescope. *Journal of Hydrology* 200: 323-344.

Kearl, P.M. and C.M. Case, 1992. Direct field measurement of groundwater velocities. *Interdisciplinary Approaches in Hydrology and Hydrogeology,* American Institute of Hydrology, pp. 91-102.

Kearl, P.M., N.E. Korte, and T.A. Cronk, 1992. Suggested modifications to groundwater sampling procedures based on observations from the colloidal borescope. *Groundwater Monitoring Reviews* 12: 155-161.

Kearl, P.M., and Roemer, K. 1998. Evaluation of groundwater flow directions in a heterogeneous aquifer using the colloidal borescope: *Advances in Environmental Research*, v. 2, no. 1: 12–23.

Kearl, P.M. and K. Roemer, 1998. Evaluation of groundwater flow in a heterogeneous aquifer using the colloidal borescope. *Advances in Environmental Research* 3: 49-57.

Kerfoot, W.B., 1988. Monitoring well construction, and recommended procedures for direct ground-water flow measurements using a heat-pulsing flowmeter, In: *Ground water contamination—Field methods*. ASTM Special Technical Publication 963, American Society for Testing and Materials, Philadelphia, PA, pp 146-161.

Kerfoot, W.B., 1995. Independent verification of heatpulse groundwater flowmeter results through long term observation and tracer tests on Superfund sites. In: *Hydrocarbon Contaminated Soils*, Amherst Scientific Publishers, Amherst, MA, pp 37-49.

Lopez, E., B. Soto, D. Rubinos, F. Diaz-Fierros. 2000. Flow-variation-paced sampling: a method for automatic sampling of stream flow during peak runoff periods. *Journal of Hydrology* 229: 255-264.

Lu, N. and S. Ge. 1996. Effect of horizontal heat and fluid flow on the vertical temperature distribution in a semiconfining layer, *Water Resources Research,* v. 32, no. 5: 1449-1453.

Malcus, F., N.K. Djane, L. Mathiasson, L. and G. Johansson. 1996. Automated trace enrichment and determination of metals using a combination of supported liquid membrane for sample pretreatment and graphite furnace atomic absorption spectrometry for the determination. *Analytica Chimica Acta* 327: 295-300.

Mansure, A.J. and M Reiter. 1979. A vertical ground-water movement correction for heat flow, *J. Geophysical Research*, vol. 84: 3490-3496.

Molz, F.J., R.H. Morin, A.E. Hess, J.G. Melville, and O. Guven, 1989. The impeller meter for measuring aquifer permeability variations—Evaluation and comparison with other tests. *Water Resources Research* 25: 1677-1683.

Molz, F.J., and S.C. Young. 1993. Development and application of borehole flowmeters for environmental assessment, *The Log Analyst*, v. 34, no. 1: 13–23.

Momii, K., K. Jinno, and F. Hirano, 1993. Laboratory studies on a new laser Doppler velocimeter system for hirizontal groundwater velocity measurements in a borehole. *Water Resources Research* 29: 283-291.

Ndung'u, K., R.P. Franks, K.W. Bruland and A.R. Flegal. 2003. Organic complexation and total dissolved trace metal analysis in estuarine waters: comparison of solvent-extraction graphite furnace atomic absorption spectrometric and chelating resin flow injection inductively coupled plasma-mass spectrometric analysis. *Analytica Chimica Acta* 481: 127-138.

Oldenburg, C. M., P. F. Daley, B. M. Freifeld, J. Hinds, and P. D. Jordan, 2002. Three-Dimensional Groundwater Flow, Aquifer Response, and Treatment System Monitoring at Site OU 1, Fort Ord, California, *Lawrence Berkeley National Laboratory Report*, *LBNL-49586*, Lawrence Berkeley National Laboratory, February.

Pedler, W.H., R.E. Crowder, J.M. Seracuse, N.J. Myers, J. Daniel, and L. Haines, 1995. Vertical profiling of aquifer flow characteristics and water quality parameters using hydrophysical logging™. In: *Proceedings of the Symposium on the Application of Geophysics to engineering and Environmental Problems*, April 23-26, Environmental and Engineering Geophysical Society, Orlando, FL pp. 311-318.

Pedler, W.H., C.L. Head, and L.L Williams, Hydrophysical logging—A new wellbore technology for hydrogeologic and contaminant characterization of aquifers. 1992. *in* Proceedings, *The Sixth National Outdoor Action Conference on Aquifer Restoration, Ground Water Monitoring, and Geophysical Methods*, National Ground Water Association, May 11–13, 1992, Las Vegas, Nev.: p. 701–71.

Pedler, W.H. and D.W. Urish, 1988. Detection and characterization of hydraulically conductive fractures in a borehole—the emplacement method. *EOS, Transactions of the American Geophysical Union* v. 69, no. 44, pp.1, 186.

Pruess, K., C. Oldenburg, and G. Moridis. 1999. *TOUGH2 user's guide, Version 2*, Lawrence Berkeley National Laboratory Report, LBNL-43134.

Reiter, M. 2001. Using precision temperature logs to estimate horizontal and vertical groundwater flow components, *Water Resources Research*, v. 37, no. 3: 663-674.

Rosen, E.C., T.R. Haining, D.D.E. Long, P.E. Mantey, 1998. "REINAS: A Real-time System for Managing Environmental Data," Journal of Software Engineering and *Knowledge Engineering,* Vol. 8, No. 1, 35-53.

Scelfo, G. 2005. Personal Communication. WIGS Laboratory, University of California, Santa Cruz. 1156 High Street, Santa Cruz, Ca 95064.

SonTek, Inc., 1996. Modified ADV for 3D velocity measurements in boreholes—Final project report. U.S. Geological Survey Contract Number 1434-95-C-40232, 29 pp.

Su, G.W., B.M. Freifeld, C.M. Oldenburg, P.D. Jordan, and P.F. Daley, 2005. Data analysis and simulation of in-situ permeable flow sensors for measuring groundwater velocity, *Lawrence Berkeley National Laboratory Report*, *LBNL-57084*, and *Groundwater*, in press.

Tsang, C.F. and C. Doughty. 2003. Multirate flowing fluid electric conductivity logging method, *Water Resources Research*, v. 39, no. 12: 1354, doi:10.1029/2003WR002308.

Tsang, C.F., P. Hufschmied, and F.V. Hale. 1990. Determination of fracture inflow parameters with a borehole fluid conductivity logging method, *Water Resources Research*, v. 26, no. 4: 561–578.

van Genuchten, M. Th., 1980. A closed-form equation for predicting the hydraulic conductivity of unsaturated

Van Wijk, W.R. and D.A. de Vries. 1966. The atmosphere and the soil, in van Wijk, W.R., ed., *Physics of Plant Environment*, 2nd ed. Amsterdam: North-Holland Publishing Co.

Wilson, J. T., W.A. Mandell, F.L. Paillet, E.R. Bayless, R. T. Hanson, P. M. Kearl, W. B. Kerfoot, M.W. Newhouse, and W. H. Pedler, 2001. *An Evaluation of Borehole Flowmeters Used to Measure Horizontal Ground-Water Flow in Limestones of Indiana, Kentucky, and Tennessee, 1999.* U.S. Geological Survey Water-Resources Investigations Report 01-4139.

Yamartino, R.J., 1984. A comparison of several “single-pass” estimators of the standard deviation of wind direction. *Journal of Climate and Applied Meteorology* 23: 1362-1366.

Young, S.C., H.S. Pearson, G.K. Moore, and R.B. Clapp. 1991. *Application of the electromagnetic borehole flowmeter technique at the Oak Ridge Laboratory: Tennessee Valley Authority*, Report WR28-1-900-247, Norris, Tenn.

Acronyms

DCE	dichloroethylene
DL	detection limits
DOC	dissolved organic carbon
EPA	Environmental Protection Agency
FDA	fire drill area
FEC	fluid electrical conductivity
FO	Fort Ord
GC	gas chromatograph
GFAAS	graphite atomic absorption spectrometer
HPL	hydrophysical logging tool
ISPFS	in-situ permeable flow sensor
LBNL	Lawrence Berkeley National Laboratory
LLNL	Lawrence Livermore National Laboratory
MEK	methylethylketone
MCL	maximum contaminant level
MDL	maximum detectable limits
ND	non-detected
NRCC	National Research Council of Canada

OU	operable unit
P&S	purge and sample
PDS	permeable diffusion sampling
QA/QC	quality assurance/quality control
SCBFM	scanning colloidal borescope flow meter
SRM	standard reference material
SVA	Salinas Valley Aquitard
TCE	trichloroethylene
UCSC	University of California, Santa Cruz
VOC	volatile organic compound

REPORT DOCUMENTATION PAGE

Form Approved
OMB No. 0704-0188

1. REPORT DATE *(DD-MM-YYYY)*	2. REPORT TYPE	3. DATES COVERED *(From - To)*
August 2006	Final	

4. TITLE AND SUBTITLE

Fort Ord Groundwater Remediation Studies, 2002 – 2006

5a. CONTRACT NUMBER
DACA42-02-2-0056

5b. GRANT NUMBER

5c. PROGRAM ELEMENT NUMBER

6. AUTHOR(S)

A. Russell Flegal, Patrick Mantey, Curt Oldenburg, Paul Daley

5d. PROJECT NUMBER

5e. TASK NUMBER

5f. WORK UNIT NUMBER

7. PERFORMING ORGANIZATION NAME(S) AND ADDRESS(ES)

U.S. Army Engineer Research and Development Center
Construction Engineering Research Laboratory
P.O. Box 9005
Champaign, IL 61826

8. PERFORMING ORGANIZATION REPORT NUMBER
ERDC/CERL CR-06-2

9. SPONSORING / MONITORING AGENCY NAME(S) AND ADDRESS(ES)

Office of the Assistant Secretary of the Army
(Installations and Environment (ASA I&E))
110 Army Pentagon Room 3E464
Washington, DC 20310-0110

10. SPONSOR/MONITOR'S ACRONYM(S)

11. SPONSOR/MONITOR'S REPORT NUMBER(S)

12. DISTRIBUTION / AVAILABILITY STATEMENT

Approved for public release; distribution is unlimited.

13. SUPPLEMENTARY NOTES

14. ABSTRACT

This report presents the results of collaborative studies of groundwater contamination, remediation, and monitoring at the former Fort Ord Army Base in northern Monterey County, California. These complementary, integrated studies were conducted at the site by principal investigators from three different institutions: the Lawrence Livermore National Laboratory; Environmental Restoration Division, Physical and Biological Sciences Division at the University of California – Santa Cruz; and Earth Sciences Division, Lawrence Berkeley National Laboratory.

These collaborative studies resulted in assessments of groundwater flow monitoring technologies; analyses of aquifer response, groundwater flow, and plume evolution; simulation of in-situ permeable flow sensors for measuring groundwater velocity; and remote sampling and analyses of inorganic contaminants in the groundwater.

The first three assessments addressed concerns with organic contaminants previously detected at the site, while the fourth was designed to determine the applicability of the remote sampling system developed to monitor organic contaminants to the monitoring of inorganic contaminants that had also been detected at elevated levels in the general study area. Four separate reports were developed from this project and the results are combined in this integrated summary report.

15. SUBJECT TERMS

groundwater remediation
environmental management
simulation modeling
Fort Ord

16. SECURITY CLASSIFICATION OF:			17. LIMITATION OF ABSTRACT	18. NUMBER OF PAGES	19a. NAME OF RESPONSIBLE PERSON
a. REPORT	b. ABSTRACT	c. THIS PAGE			R. Lampo
Unclassified	Unclassified	Unclassified		150	19b. TELEPHONE NUMBER *(include area code)* 217-352-6511